# A NUMERICAL MODEL FOR A ROTARY ACTIVE MAGNETIC REGENERATIVE REFRIGERATOR

by

Ian Gregory Spearing
B.A.Sc., University of Toronto, 1990

A Thesis Submitted in Partial Fulfilment of the
Requirements for the Degree Of

MASTER OF APPLIED SCIENCE

in the Department of
Mechanical Engineering

We accept this thesis as conforming
to the required standard

[redacted]

Dr. J.A. Barclay, Supervisor (Department of Mechanical Engineering)

[redacted]

Dr. H.-H. Rogner, Member (Department of Mechanical Engineering)

[redacted]

Dr. M. Danard, Outside Member (Department of Computer Science)

[redacted]

Dr. J.D. Jones, External Examiner (Simon Fraser University)



University of Victoria

Supervisor: Dr. John A. Barclay

## ABSTRACT

Magnetic refrigeration employing the magnetocaloric effect of ferromagnetic materials has been identified as potentially more efficient and cost-effective than conventional refrigeration systems. One magnetic cycle that shows promise for efficiently achieving cooling over large temperature spans is active magnetic regenerative refrigeration (AMRR). In this cycle the magnetic material serves the dual functions of work input and thermal regeneration. The operation of an AMRR is complex, having coupled thermal and magnetic phenomena. This complexity means that a detailed numerical model is required for optimized design purposes. This thesis describes a numerical modelling approach and a solution of the complete 2-dimensional, quasi-steady-state energy equations describing the operation of rotary active magnetic regenerative refrigerators. Effects of solid-fluid heat transfer, conduction in the solid and fluid, fluid entrainment in the solid, electrical eddy current generation, and material magnetocaloric effects are included in the model. Three different solution algorithms are described and the relative benefits and drawbacks of each are compared. One algorithm is selected as the best candidate for future modelling exploration. Selected AMRR results are presented and compared with model results for a rotary passive regenerator.

Examiners:

[redacted]

Dr. J.A. Barclay, Supervisor (Department of Mechanical Engineering)

[redacted]

Dr. H.-H. Rogner, Member (Department of Mechanical Engineering)

[redacted]

Dr. M. Danard, Outside Member (Department of Computer Science)

[redacted]

Dr. J.D. Jones, External Examiner (Simon Fraser University)

# Table of Contents

# List of Tables

# List of Figures

# Nomenclature

| | |
|---|---|
| $A$ | • regenerator matrix surface area per unit length $[m^2 \cdot m^{-1}]$ |
| $A_x$ | • area enclosed by the largest possible eddy current loop $[m^2]$ |
| $A'''$ | • regenerator matrix surface area per unit volume $[m^2 \cdot m^{-3}]$ |
| $A_c$ | • heat transfer fluid free flow area $[m^2]$ |
| $B$ | • magnetic field [Tesla] |
| $C_H$ | • active regenerator solid heat capacity per unit mass at constant applied field $[J \cdot kg^{-1} \cdot K^{-1}]$ |
| $C_P$ | • heat transfer fluid heat capacity at constant pressure $[J \cdot kg^{-1} \cdot K^{-1}]$ |
| $\bar{C}_P$ | • average fluid heat capacity at constant pressure at which a cooling load is absorbed or rejected $[J \cdot kg^{-1} \cdot K^{-1}]$ |
| $C_s$ | • regenerator solid heat capacity $[J \cdot kg^{-1} \cdot K^{-1}]$ |
| $COP$ | • coefficient of performance [dimensionless] |
| $COP_{ideal}$ | • coefficient of performance for a Carnot cycle [dimensionless] |
| $D_p$ | • packed particle regenerator bed particle diameter [m] |
| $G$ | • heat transfer fluid mass flow rate per unit free flow area $[kg \cdot s^{-1} \cdot m^{-2}]$ |
| $h$ | • heat transfer coefficient between fluid and regenerator solid $[W \cdot m^{-2} \cdot K^{-1}]$ |

- $H$ • applied magnetic field [$A \cdot m^{-1}$]
- $H_f$ • heat transfer fluid enthalpy [$J \cdot kg^{-1}$]
- $H^*$ • dimensionless applied field [dimensionless]
- $H_{max}$ • maximum value of applied magnetic field [$A \cdot m^{-1}$]
- $i$ • index in the radial direction
- $j$ • index in the azimuthal direction
- $k_{fr}$ • effective thermal conductivity of the fluid in the radial direction [$W \cdot m^{-1} \cdot K^{-1}$]
- $k_{f\theta}$ • effective thermal conductivity of the fluid in the azimuthal direction [$W \cdot m^{-1} \cdot K^{-1}$]
- $k_{sr}$ • effective thermal conductivity of the solid in the radial direction [$W \cdot m^{-1} \cdot K^{-1}$]
- $k_{s\theta}$ • effective thermal conductivity of the solid in the azimuthal direction [$W \cdot m^{-1} \cdot K^{-1}$]
- $L$ • regenerator bed length [m]
- $M$ • magnetization of magnetic material [$A \cdot m^{-1} \cdot K^{-1}$]
- $M^*$ • dimensionless magnetization of magnetic material [dimensionless]
- $M_s$ • mass of the regenerator solid material [kg]
- $\dot{m}_f$ • regenerator sector fluid mass flow rate [$kg \cdot s^{-1}$]
- $P$ • regenerator blow time [s]
- $P_e$ • eddy current dissipation power [W]
- $P_f$ • heat transfer fluid pressure [$N \cdot m^{-2}$]
- $\dot{Q}_{load}$ • cooling load [W]
- $\dot{Q}_{in}$ • rate of heat entering the system [W]

$\dot{Q}_{out}$ • rate of heat leaving the system [W]

$\dot{Q}_{rejected}$ • heat rejection load [W]

$\delta Q_v$ • infinitesimal heat transferred per unit volume [$J \cdot m^{-3}$]

$\Delta \dot{Q}_V$ • heat transfer rate per unit volume [$W \cdot m^{-3}$]

r • radial regenerator bed position [m]

$\Delta r$ • radial width of the regenerator control volume [m]

$r^*$ • dimensionless regenerator radial position [dimensionless]

$r_i$ • regenerator bed inner radius [m]

$r_o$ • regenerator bed outer radius [m]

s • entropy [$J \cdot kg^{-1} \cdot K^{-1}$]

t • time [s]

T • temperature [K]

$T_c$ • Regenerators: inlet heat transfer fluid temperature to the regenerator magnetized region [K]

$T_c$ • Carnot cycle: heat source temperature [K] (refrigeration)

$T_f$ • heat transfer fluid temperature [K]

$T_f^*$ • heat transfer fluid dimensionless temperature [dimensionless]

$T_h$ • Regenerators: inlet heat transfer fluid temperature to the regenerator demagnetized region [K]

$T_h$ • Carnot cycle: heat sink temperature [K] (refrigeration)

$T_s$ • regenerator solid temperature [K]

$T_{s*}$ • regenerator solid dimensionless temperature [dimensionless]

- $U$ • regenerator utilization factor [dimensionless]
- $u_{i,j}$ • property "u" evaluated at mesh point *i,j*
- $V$ • volume [$m^3$]
- $V_f$ • heat transfer fluid volume flow rate [$m^3 \cdot s^{-1}$]
- $\dot{W}_{in}$ • total input power required to rotate the AMRR [W]
- $x$ • linear regenerator bed position [m]
- $z$ • regenerator bed axial thickness [m]

Greek:

- $\alpha$ • regenerator bed porosity [dimensionless]
- $\beta$ • dimensionless fluid entrainment [dimensionless]
- $\gamma$ • radial bed regenerator length factor [dimensionless]
- $\Gamma$ • eddy current geometrical shape factor [dimensionless]
- $\Delta\theta$ • angular width of the control volume [radians]
- $\zeta$ • dimensionless parameter, magnetocaloric factor [dimensionless]
- $\eta_{rel}$ • relative efficiency [dimensionless]
- $\eta_{th}$ • thermal efficiency [dimensionless]
- $\Lambda$ • dimensionless parameter, reduced length [dimensionless]
- $\lambda_{f\theta}$ • dimensionless parameter, fluid azimuthal conduction [dimensionless]
- $\lambda_{fr}$ • dimensionless parameter, fluid radial conduction [dimensionless]
- $\lambda_{s\theta}$ • dimensionless parameter, solid azimuthal conduction [dimensionless]
- $\lambda_{sr}$ • dimensionless parameter, solid radial conduction [dimensionless]

$\mu_0$ • permeability of free space [$4\pi \times 10^{-7}$ H·m$^{-1}$]

$\xi$ • regenerator flow regime factor [dimensionless]

$\Pi$ • dimensionless parameter, reduced period [dimensionless]

$\rho_e$ • material electrical resistivity [Ω·m]

$\rho_f$ • heat transfer fluid density [kg·m$^{-3}$]

$\rho_s$ • magnetic material density [kg·m$^{-3}$]

$\phi_i$ • total angular width of the flow regime *i* [radians]

$\omega$ • rotational frequency [radians·s$^{-1}$]

$\Omega$ • dimensionless parameter, eddy current factor [dimensionless]

# Acknowledgements

My work at the Institute for Integrated Energy Systems with the Cryofuel Systems Group at the University of Victoria was exciting and quite rewarding. I would like to thank those who helped make this work possible:

- My Supervisor, Dr. John Barclay, for trusting that progress was steadily being made despite missed deadlines and little materialization of nifty looking plots and charts;
- Dr. Sunil Sarangi, whose philosophy was as inspiring and instrumental as his help;
- Research Associate, Jeff Hall, whose "just get the core of the problem done and fill in the details later" advice wisely kept me from modelling the kitchen sink (but not the faucet);
- Sue and Dolores, administrative assistants with gusto;
- All of the other members of IES*Vic*, each having contributed help at one time or another; and
- Finally, and most of all, my wife, Moira, for helping to get some of the pesky diagrams together and for putting up with all my late nights and cranky mornings.

I would like to acknowledge Natural Sciences and Engineering Research Council of Canada (NSERC) and Centra Gas Inc., a division of Westcoast Energy, for their support of projects of which this work forms but a modest part.

# Chapter 1

# Introduction

## 1.1 Objective

This thesis was performed within the Institute for Integrated Energy Systems (IES*Vic*) at the University of Victoria. IES*Vic* is engaged in the development of energy systems that simultaneously:

- Offer a foundation for economic growth and industrial diversification;
- Cause minimal environmental intrusion, and especially, reduce climate destabilizing emissions; and
- Provide flexibility and resilience in response to technical, geopolitical and environmental change.

Towards these goals, IES*Vic*'s activities are divided into three synergistic research groups. The first group, Systems Analysis, analyzes energy system evolution. The other two groups, Electrochemical Systems and Cryofuel Systems, focus on hardware development. Currently, Cryofuel Systems is developing new liquefiers and cryogenic fuel handling systems, with a major emphasis on magnetic refrigeration. Following the goals of Cryofuel Systems, this thesis had the following statement of purpose:

> *The objective of this study was to develop a versatile quasi-steady-state computer model of a rotary active magnetic regenerative refrigerator (AMRR) that could be used to help design energy efficient AMRR's comprised of multiple refrigerant materials by predicting performance under design variations.*

## 1.2 Motivation

Rapid and convenient transportation has become a mainstay of our developed societies, using vehicles powered primarily by high carbon content fuels. Several researchers [33], [34], [35], [36], [37], [41] have identified economic, geo-political, and environmental benefits to a society that shifts its energy currencies to low carbon content fuels, such as natural gas (NG), and ultimately to carbon-free fuels, such as hydrogen ($H_2$). Natural gas, as provided by pipeline distribution systems, is composed primarily of methane, which has four atoms of hydrogen for each atom of carbon, the highest ratio of hydrogen to carbon of the hydrocarbon fuels. The exact composition of pipeline natural gas varies, but it has been measured to contain 82.2 - 97.8 % methane, with ethane, nitrogen, carbon dioxide, heavier hydrocarbons, and other trace gases and odourants making up the remainder [38].

Recent efforts to introduce NG fuelled vehicles have been hampered, in part, by the limited range of these vehicles due primarily to the low volumetric storage capacity of compressed gas fuel storage tanks. Fuel storage, and hence vehicle range, can be increased by storing the fuel as a liquid rather than as a compressed gas. Liquefied natural gas (LNG) at atmospheric pressure has 2.6 times the volumetric energy density of compressed natural gas (CNG) at 3000 psig. At atmospheric pressure natural gas liquefies at 112 K, considerably below room temperature of 293 K. Liquids below 123 K are known as cryogens, and LNG is thus a cryogenic fuel.

To supply LNG to a vehicular fuel market, a supply of natural gas and an inexpensive and efficient refrigeration system for liquefaction are required. Natural gas distribution systems exist in most major North American cities; however, current refrigeration systems in the LNG temperature range are expensive or inefficient, or both. New liquefaction technologies that are less expensive and more efficient are required to reduce the refuelling system cost component of LNG. The Cryofuel Systems Group at the University of Victoria has identified active magnetic regenerative refrigeration (AMRR) as a viable technique to achieve refrigeration at high efficiencies and competitive capital expense compared to current technologies.

## 1.3 Refrigeration Cycles

Many different thermodynamic cycles have been exploited to achieve refrigeration, that is, the pumping of heat from a low temperature source to a higher temperature sink. Venturing to thermodynamics or refrigeration texts ([9], [10], and [49], for example) would reveal the intricacies of regenerative cycles such as Stirling, Ericsson, and Gifford McMahon, recuperative cycles such as Claude and Linde-Hampson, and non-regenerative/non-recuperative cycles such as absorption, vapour-compression and Carnot cycles. The Carnot cycle merits special mention, but for this discussion the intricacies of the other cycles, some employing expansion and compression of gases, some employing mixtures of liquids, and some employing liquid/vapour phase change, and the many cycles not referenced, are beyond the scope of this introduction. What is important to note is that every refrigeration cycle is achieved by the directed changes in entropy and temperature of the working material according to its thermodynamic processes. Each cycle has its own comparative advantages and disadvantages, with practical limits to achievable temperature span, operating temperature, cooling capacity, and efficiency dictated by the working materials and the thermodynamics concerned.

Figure 1.1 shows the domain of operation of several commercially available refrigeration systems. Some domains have been drawn using solid lines suggesting a sharp transition from one domain to another; however, technology improvements continually expand and merge these domains into one another. It should also be noted that the domain of refrigeration capacity is not specifically limited to that shown by the diagram. Indeed, vapour compression devices and turbo expander Brayton-Claude cycle devices are available in capacities extending beyond the upper limit of the diagram, for example.

### 1.3.1 Carnot Cycle

The Carnot cycle merits special mention because it is often used as the standard for comparison of refrigeration and power cycles. The Carnot power cycle is shown in Figure 1.2 and is made up of two internally reversible isothermal (constant temperature) processes and two internally reversible adiabatic (constant entropy or *isentropic*) processes. The cycle is shown on temperature-entropy (*T-s*) coordinates so that the nature of the working material need not be specified; the shape of each process line is specified by the process alone.

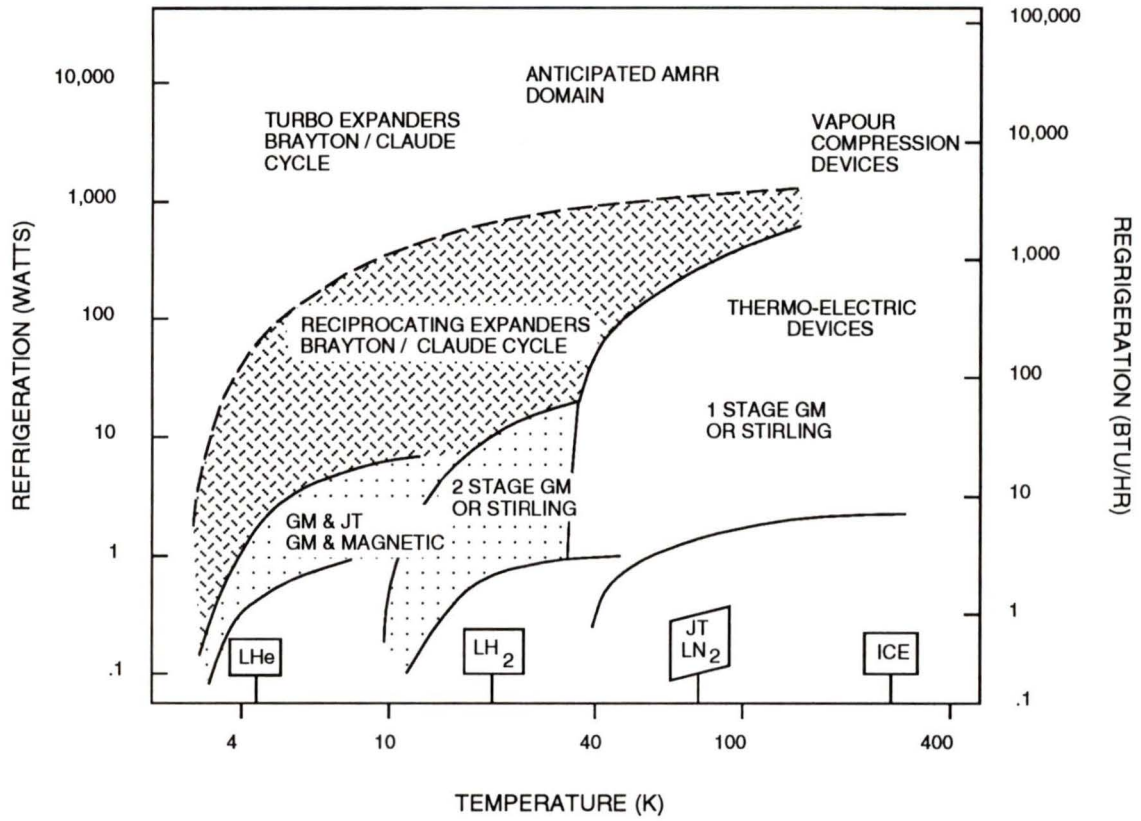


**Figure 1.1** Cooling Power - Load Temperature for commercial refrigeration systems (after Kral *et. al.* [56]).

For any power cycle, thermal efficiency, $\eta_{th}$, is the ratio of the useful work output of the cycle to the energy that must be supplied to the cycle for that output:

$$\eta_{th} = \frac{\textit{Useful work output}}{\textit{Energy supplied}} \tag{1.1}$$

and for a Carnot power cycle thermal efficiency is given by:

$$\eta_{th} = \frac{T_H - T_L}{T_H} \tag{1.2}$$

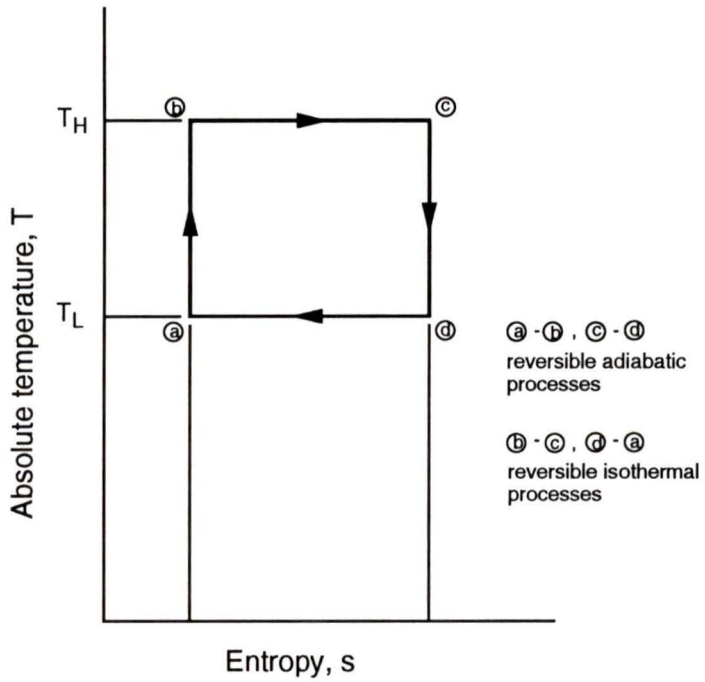


**Figure 1.2** *T-s* diagram of the Carnot power cycle.

where $T_H$ and $T_L$ are the high and low isothermal heat transfer temperatures, respectively, of the cycle.

It is a corollary of the second law of thermodynamics that no cycle can be more efficient than a reversible cycle operating between the same temperature limits; also, any two *reversible* cycles receiving heat at one particular temperature and rejecting it at another particular temperature must have identical values of thermal efficiency. Thus, it is often useful to compare the thermal efficiency of the cycle being considered with the thermal efficiency of a reversible cycle operating between the same two temperatures.

The term *thermal efficiency* is not easily applicable to a refrigeration machine. For a power cycle, the thermal efficiency must always be equal to or less than unity, but following the definition above, thermal efficiency for a refrigeration device could be greater than one. To avoid confusion,

the term coefficient of performance or COP is used instead. For a Carnot refrigeration cycle, the coefficient of performance is given by:

$$COP = \frac{T_L}{T_H - T_L} \tag{1.3}$$

## 1.4 Magnetic Refrigeration

### 1.4.1 Brief History

The magnetocaloric effect, which is the basis for all magnetic refrigerators, was discovered in ferromagnets by A. Piccard and P. Weiss in 1918 [50]. They experimentally observed the reversible heating and cooling of ferromagnetic nickel near its Curie temperature of 631 K upon

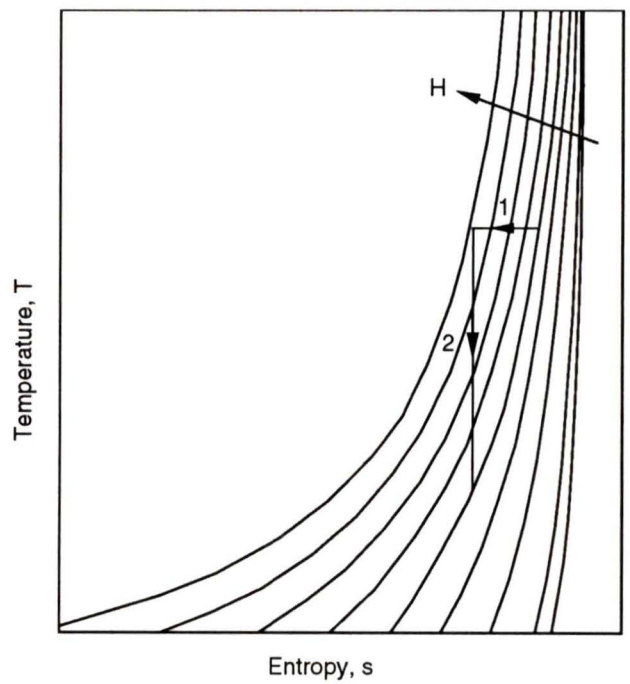


**Figure 1.3** *T-s* diagram of a one-shot magnetic cooling process, where *H* gives the applied magnetic field.

application and removal of a magnetic field. In 1933 Giauque [51] and his graduate student were able to use the magnetocaloric effect of paramagnetic materials in a practical device to achieve a cooling temperature of 0.5 K. His method was to isothermally magnetize a paramagnetic salt at 3.5 K and then to adiabatically demagnetize it to achieve 0.5 K. Figure 1.3 illustrates this process on a low-temperature *T-s* diagram, with process 1 being the isothermal magnetization, and process 2 being the adiabatic demagnetization. This one-shot technique is still in use today to temporarily create ultra-low temperatures for physics experiments.

The method of Giauque is a one-shot process, and any cooling effect produced is short term. In 1949 Daunt and Heer [52] suggested combining two isothermal and two adiabatic magnetization

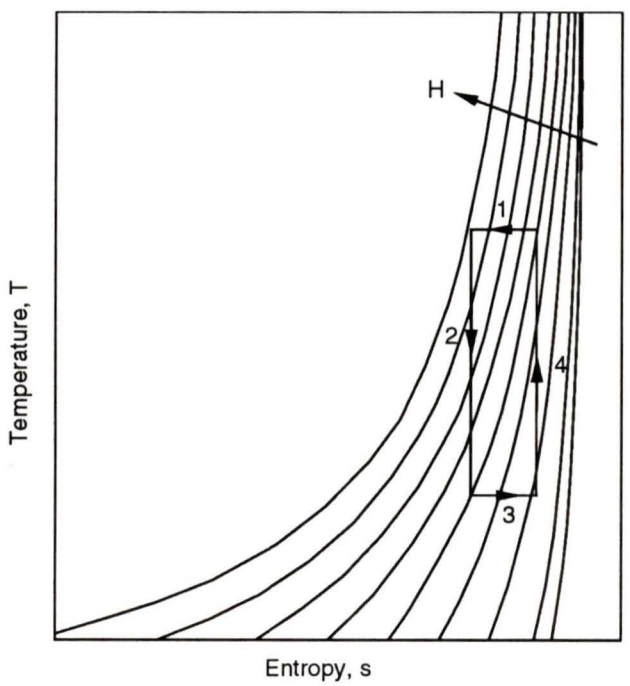


**Figure 1.4** *T-s* diagram of a magnetic Carnot cycle.

and demagnetization processes to form a magnetic Carnot heat pump cycle for continuous operation. The magnetic Carnot cycle using a paramagnetic salt is illustrated in Figure 1.4. The process begins by the isothermal magnetization of the working material, thereby rejecting heat from the material and decreasing the material's entropy. The material is then adiabatically

demagnetized, decreasing its temperature. Heat is absorbed by the material in the next process, isothermal demagnetization, increasing the material's entropy. Finally, the material is raised to its initial temperature by adiabatic magnetization. In 1954 Heer et. al [53] built a continuous magnetic refrigerator approximating the Carnot cycle and achieved temperatures below 0.2 K.

### 1.4.2 Thermodynamics of the Magnetocaloric Effect

Altering the thermodynamic state of a magnetic material by performing heat and magnetic work processes is known as the *magnetocaloric effect.* The magnetocaloric effect is essentially the

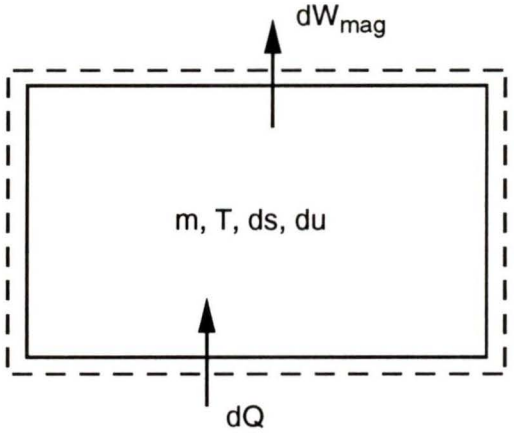


**Figure 1.5** Magnetic material undergoing differential work and heat processes.

application of the first and second laws of thermodynamics to a magnetic system. Consider the magnetic system in Figure 1.5. It consists of a mass $m$ of magnetic material undergoing a differential magnetic work process and differential reversible heat process. Drawing a control volume around the system and performing an energy balance gives:

$$dU + dW_{mag} = dQ \tag{1.4}$$

where $dU$ is the differential change in the internal energy of the material, $dW_{mag}$ is the work performed by the material, and $dQ$ is the heat transferred into the material at temperature $T$. If an entropy balance on the control volume is performed for the reversible process, the result is:

$$m\,ds = \frac{dQ}{T} \tag{1.5}$$

where $m \cdot ds$ is the differential change in the total entropy of the material at temperature $T$. Substituting Equation (1.4) into Equation (1.5) and dividing by the mass of the system gives:

$$du = T\,ds - dw_{mag} \tag{1.6}$$

The specific differential magnetic work performed by a magnetic material is given by:

$$dw_{mag} = -\mu_0 v H\,dM \tag{1.7}$$

where $\mu_0$ is the permeability of free space, $v$ is the specific volume of the magnetic material, $H$ is the applied field, and $dM$ is the differential change in magnetization. Substituting Equation (1.6) into Equation (1.7), gives the combined first and second law for a magnetic system:

$$du = T\,ds + \mu_0 v H\,dM \tag{1.8}$$

Equation (1.8) is very similar to the corresponding equation in a $p$-$v$ system, given by:

$$du = T\,ds - p\,dv \tag{1.9}$$

where $p \cdot dv$ is analogous to $-\mu_0 \cdot v \cdot H \cdot dM$. It is the method by which work enters and exits the system that forms the fundamental difference between Equations (1.8) and (1.9), in the first case being magnetic work, and the second being $p \cdot dv$ work. To further illustrate the similarities of the

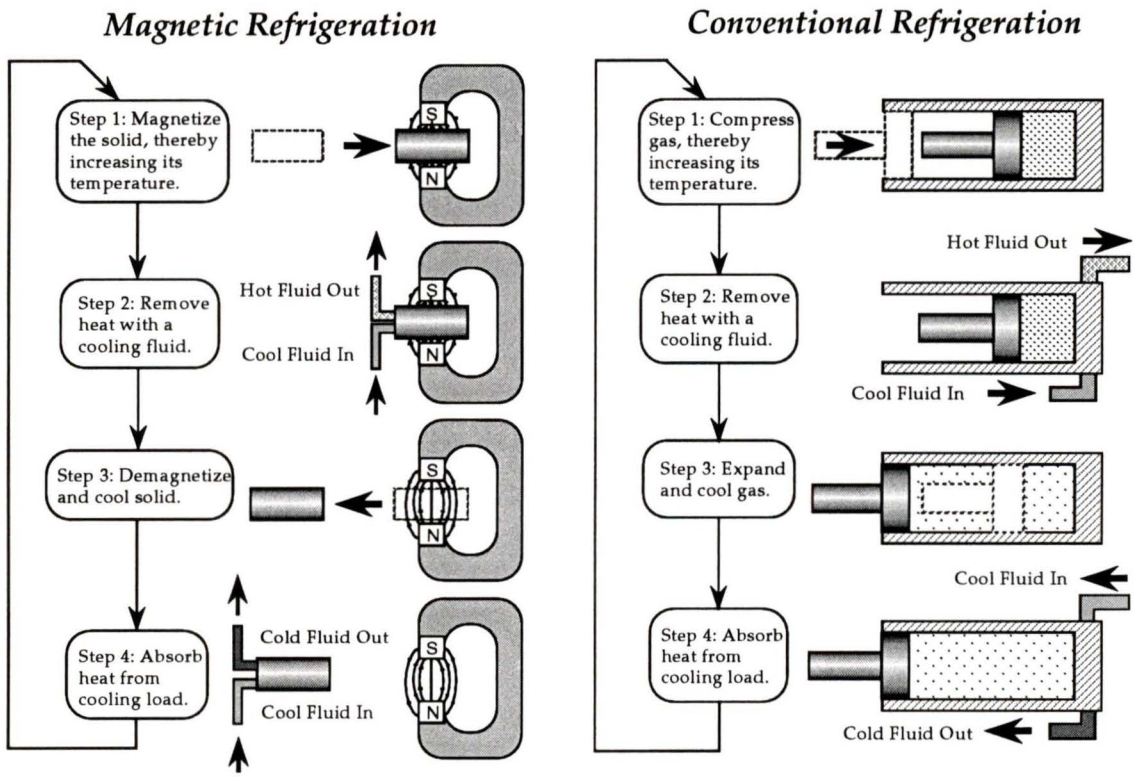


**Figure 1.6** Comparison of magnetic refrigeration and conventional gas compression refrigeration.

magnetic system and the $p \cdot dv$ system, Figure 1.6 shows schematically the steps of a possible magnetic refrigeration cycle, and for comparison, the corresponding steps of a gas compression refrigeration cycle.

### 1.4.3 Comparison of Gas and Magnetic Systems

The process of decreasing a magnetic material's entropy state by isothermal application of a magnetic field, and then restoring the material's entropy state by removal of the field is analogous to the more commonly understood isothermal compression and re-expansion of a gas. When a gas is isothermally compressed its entropy is decreased with heat transferred at constant temperature. When the gas is isothermally re-expanded to its original volume, its entropy is increased to its original value. Alternatively, a gas can be isentropically compressed, keeping its

entropy constant and raising its temperature with no heat transfer. It can then be isentropically re-expanded, lowering its temperature.

Neither of the reversible isothermal and isentropic compression and re-expansion processes cause a net creation of entropy. Isothermal compression requires perfect heat transfer with no temperature gradients, while isentropic compression requires perfect thermal insulation. In practice, a compression or expansion process is polytropic, lying somewhere between the extremes of isothermal or isentropic compression and expansion, with an accompanying net increase in entropy of the entire system, simply because perfect heat transfer or perfect insulation of the gas during the compression or expansion process is difficult to achieve in a practical gas device. The entropy production is associated with a deviation from the minimum work required to perform the complete process, and so is indicative of inefficiency.

It is the compression and expansion stages in a gas compression refrigeration cycle that causes the majority of the entropy production; therefore, a more efficient cycle can be created if more efficient means of creating the material entropy changes needed for refrigeration can be used. For a magnetic substance in a practical device, it is easier to approach isentropic and reversible isothermal processes than in the compression process. This makes it possible to achieve a more efficient refrigeration process with a magnetic cycle than with a compression (or other) cycle in a practical device. The magnetic cycle allows a transformation whereby the largest source of inefficiency is no longer from the introduction of work into the cycle via the working material but from the heat flows within the other components of the system. This shift allows a net gain in overall efficiency.

### 1.4.4 Adiabatic Temperature Change

The adiabatic temperature change caused by the magnetocaloric effect ($\Delta T_{adiabatic}$) is not only a function of the material used, but is a function of the applied field and absolute temperature of the material itself. For practical continuous refrigeration devices, material adiabatic temperature changes on the order of several degrees are necessary, which requires the use of strong magnetic fields. Superconducting magnets are preferred to create these strong fields which, due to their relative complexity and historically high expense, might help explain the lack of commercial

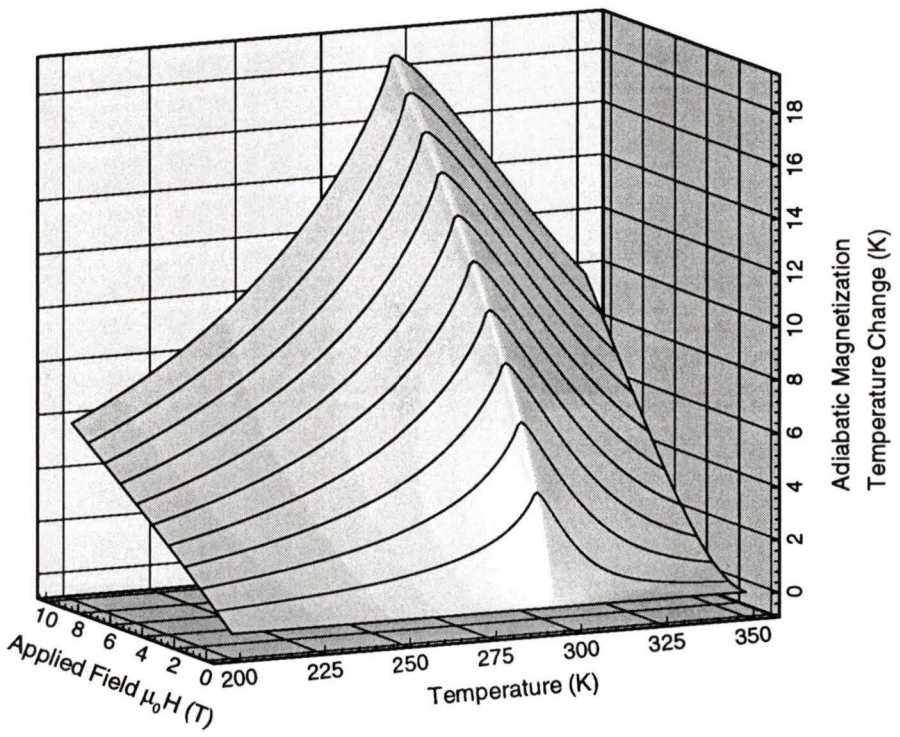


**Figure 1.7** $\Delta T_{adiabatic}$ of gadolinium as a function of temperature and applied field.

magnetic refrigeration devices. Figure 1.7 gives the adiabatic magnetization temperature change of gadolinium as a function of initial material temperature for fields ranging from 0 to 10 Tesla, as calculated using a molecular field model. From this diagram, the temperature dependence of the magnetocaloric effect is easily discernible, with the peak temperature change corresponding to the material's Curie point.

## 1.5 Temperature Span

The adiabatic temperature change in a magnetic material is relatively small, about 1 - 2 K per Tesla field change. For a refrigeration cycle to span a temperature range exceeding the magnitude of the magnetocaloric temperature change of the working material, the cycle must include recuperative or regenerative heat exchange. A recuperative heat exchanger is a device where

separate flow passages are provided for hot and cold fluid streams, and heat is transferred between streams via conduction through the passage walls. In contrast, a regenerative heat exchanger has a single set of flow passages where hot and cold fluids flow alternately and periodically through a porous matrix.

## 1.6 Regenerators

A regenerator can be thought of as a "thermal flywheel", accepting heat during the first half and then supplying heat during the second half of its cycle. During the *hot blow*, when hot fluid is passing through the matrix, heat is transferred from the fluid to the matrix. The matrix is heated and the fluid is cooled. Subsequently, the flow is switched to the *cold blow*, wherein the flow of hot fluid is replaced by a flow of cold fluid. Heat is now transferred from the matrix to the fluid, cooling the matrix and warming the fluid.

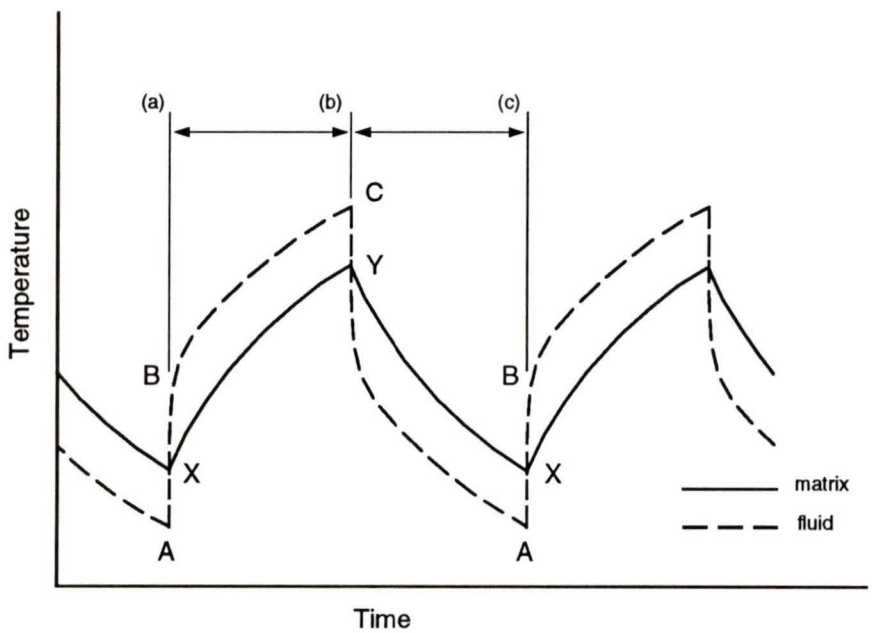


**Figure 1.8** Time-temperature variation of fluid and matrix in a passive thermal regenerator.

Figure 1.8 shows the variation with time of the matrix temperature and fluid temperature at any station in a passive regenerator bed. Figure 1.9 shows the variation with position of the matrix

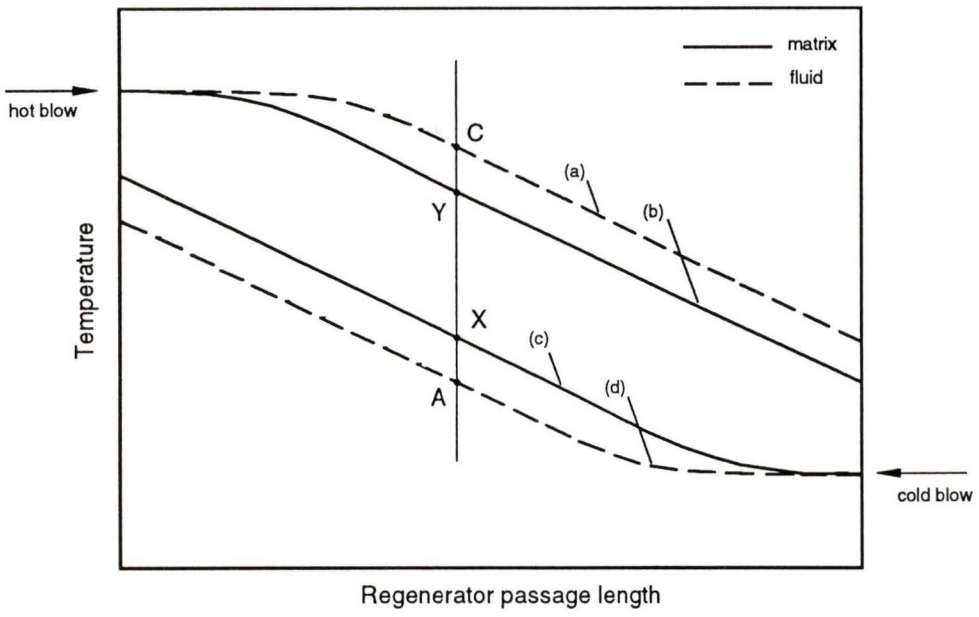


**Figure 1.9** Spatial temperature variation of fluid and matrix in a passive thermal regenerator.

and fluid temperature at the instants of flow reversal. The upper curves represent the temperature of the fluid and matrix at the end of hot blow and the start of cold blow, while the lower curves represent the end of cold blow and the start of hot blow. Each station in the matrix fluctuates between these two sets of curves in time dependent manner similar to that shown in Figure 1.8.

A regenerator's function is fairly straightforward; however, its operation is cited as one of the most difficult to analyze mathematically [10]. A complete description of the operation of a regenerator is a complex function of many coupled parameters, including:

- matrix geometry (particles, wire screens, thin plates, tubes, as well as macroscopic shape);
- mass and heat capacities of matrix material and heat transfer fluid;
- matrix porosity;
- matrix material and fluid thermal conductivities;

- parasitic heat leaks to the regenerator from the environment;
- effective heat transfer between fluid and solid matrix;
- enhancement of fluid thermal conductivity due to eddy diffusion of fluid;
- flow channel pressure drops; and
- variations of properties with position or time.

To make a regenerator analysis tractable, several simplifying assumptions are often made, including:

a) The thermal conductivity of the matrix is zero parallel to the fluid flow, and infinitely large normal to the fluid flow.

b) The thermal conductivity of the matrix is zero parallel to the fluid flow, and finite normal to the fluid flow.

c) The specific heats of the fluids and of the matrix material do not change with the temperature.

d) The fluids flow in opposite directions, and have inlet temperatures that are constant both over the flow section and with time.

e) The heat transfer coefficients and fluid velocities are constant with time and space, (though they may be different for the hot and cold blow fluids).

f) The rate of mass flow of either fluid is constant during the blow period, though it may be different for the two fluids, and the blow periods may be different.

Walker [10] gives a complete summary of common simplifications in regenerator analysis. In the simplest case, properties are assumed constant with temperature and position, momentum effects are ignored, mass conservation is solved trivially, and only an energy balance for the fluid and solid is considered. This gives two partial differential equations describing the solid and fluid temperatures as a function of time and position:

Fluid:

$$\frac{\partial T_f}{\partial x} = \frac{hA}{V_f C_P}\left(T_s - T_f\right) \tag{1.10}$$

Solid:

$$\frac{\partial T_s}{\partial t} = \frac{hA}{M_s C_s}\left(T_f - T_s\right) \tag{1.11}$$

where $h$ is the heat transfer coefficient between fluid and matrix, per unit surface area, $A$ is the matrix surface area per unit length, $V_f$ is the fluid volume flow rate, $C_P$ is the heat capacity of the fluid, $M_s$ is the mass of the matrix material, and $C_s$ is the heat capacity of the matrix material.

This limited approach provides rudimentary performance data that can be presented in a number of ways, but one of the most common is to express the regenerator effectiveness in terms of two dimensionless parameters (after Hausen [11]) called reduced length, $\Lambda$, and reduced period, $\Pi$. The reduced length (in the flow direction) is defined by:

$$\Lambda = \frac{hAL}{V_f C_P} \tag{1.12}$$

The reduced period is defined by:

$$\Pi = \frac{hAP}{M_s C_s} \tag{1.13}$$

where $L$ is the matrix length, and $P$ is the blow time. With the introduction of dimensionless distance:

$$\xi = \frac{x}{L} \tag{1.14}$$

and dimensionless time:

$$\tau = \frac{t}{P} \tag{1.15}$$

it is possible to describe a large class of problems with two dimensionless fluid and solid energy balance equations:

Fluid:

$$\frac{\partial T_f}{\partial \xi} = \Lambda\left(T_s - T_f\right) \tag{1.16}$$

Solid:

$$\frac{\partial T_s}{\partial \tau} = \Pi\left(T_f - T_s\right) \tag{1.17}$$

Frequently, $\Pi$ and $\Lambda$ are combined by the quotient:

$$\frac{\Pi}{\Lambda} = U = \frac{V C_P}{M_s C_s} \frac{P}{L} \tag{1.18}$$

and called the utilization factor, representing the ratio of the sensible heat capacity of the fluid per blow to the heat storage capacity of the matrix. The greater this ratio, the greater the magnitude of the time variation of the fluid and matrix temperatures for each blow period.

## 1.7 The Magnetic Brayton Cycle

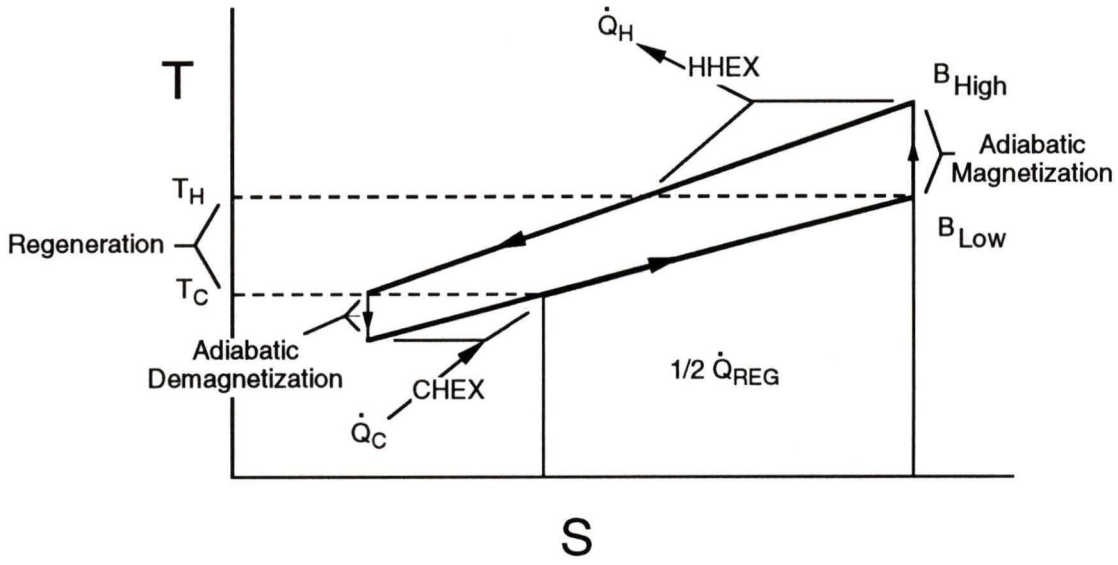


**Figure 1.10** *T-s* diagram for a magnetic Brayton cycle.

The Brayton cycle is a regenerative cycle that lends itself well to magnetic refrigeration. Figure 1.10 gives a temperature-entropy diagram for a magnetic Brayton cycle and Figure 1.11 gives a temperature-entropy diagram for a gas Brayton cycle for comparison. The magnetic process has two isentropic steps and two isofield steps, while the gas cycle has two isentropic steps and two isobaric steps. The isentropic magnetization and demagnetization processes in the magnetic cycle are analogous to the isentropic compression and expansion processes, respectively, in the gas cycle. This isentropic stage is the weak point of the gas cycle and the strong point of the magnetic cycle. In practical gas devices, isentropic compression and expansion of the gas cause large temperature differences between the gas and its surroundings, whereas in magnetic devices isentropic magnetization and demagnetization cause much smaller temperature differences

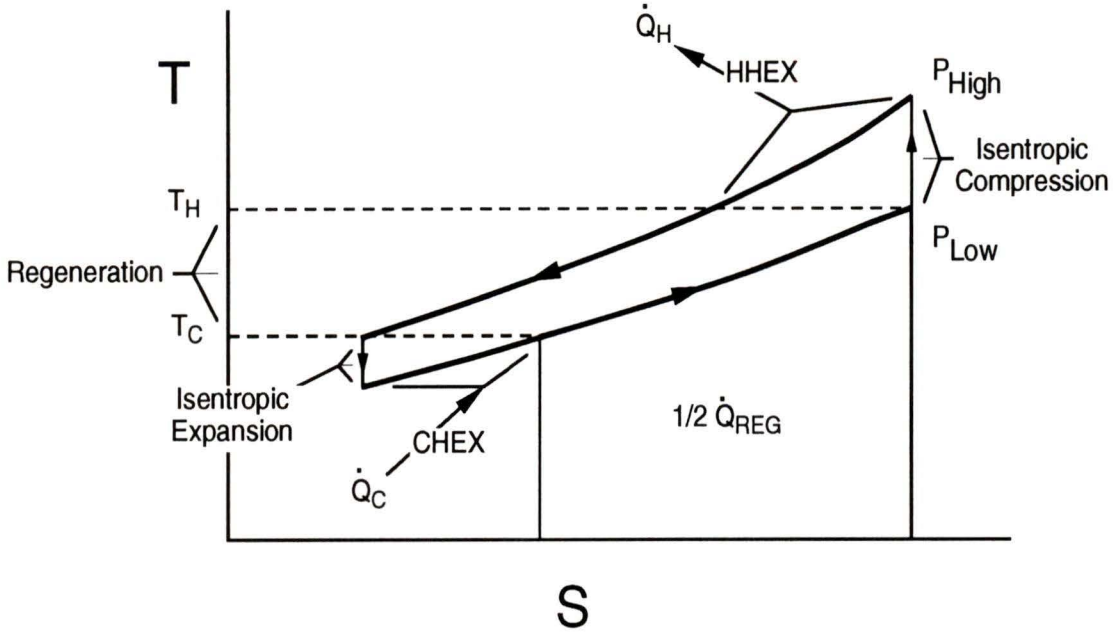


**Figure 1.11** *T-s* diagram for a gas Brayton cycle.

that create entropy. This distinction forms the basis of potentially much higher efficiencies in magnetic refrigeration than gas cycle refrigeration. It also shifts the design problem for magnetic Brayton cycles from applying work to the working material to efficient heat transfer during regeneration. A thorough comparison of magnetic and gas refrigeration from a thermodynamic standpoint has been presented by Barclay [2], [41].

Figure 1.12 gives a process schematic of the magnetic Brayton cycle. The process starts by adiabatically magnetizing the magnetic material to raise its temperature where heat is then rejected to a high temperature sink. The magnetic material is then cooled, transferring its heat to a regenerator, to give a large temperature span in the cycle. Adiabatic demagnetization lowers the material's temperature, where heat is then absorbed from a low temperature source. To complete the cycle, the material is warmed using the heat previously stored in the regenerator. In this description, the regeneration process is separate and distinct from the heat load absorption and rejection stages. Further, all the magnetic material spans the complete temperature range.

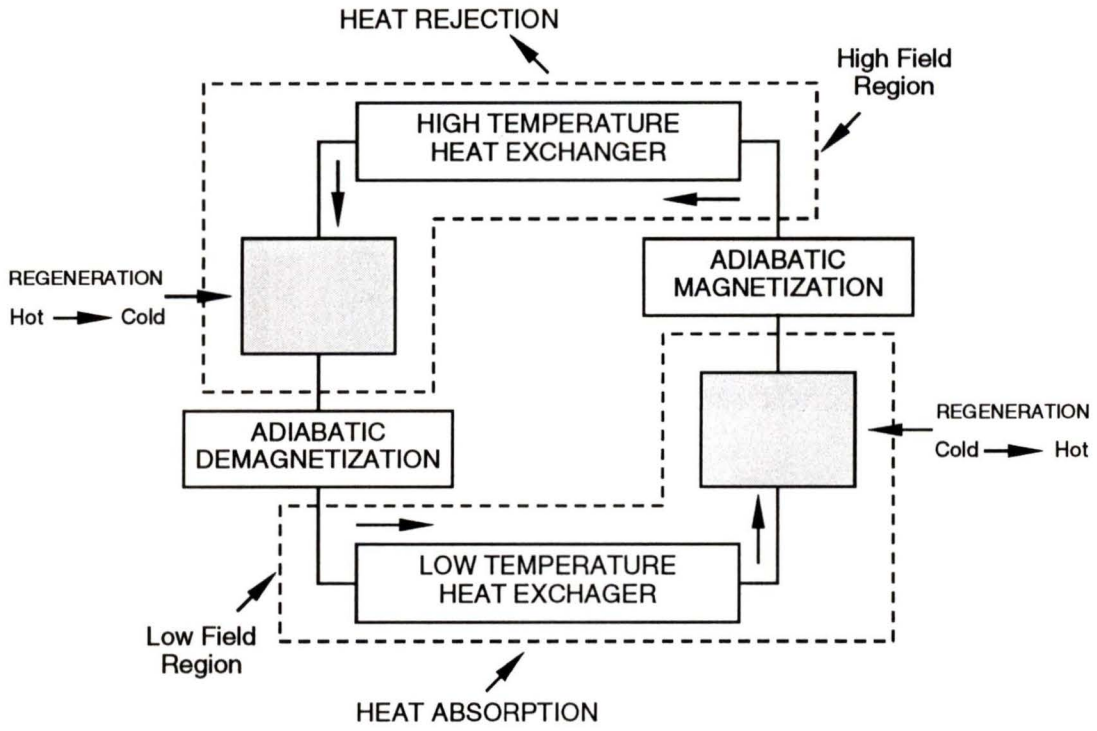


**Figure 1.12** Process diagram of a magnetic Brayton cycle.

## 1.8 Other Magnetic Cycles

The magnetic Brayton cycle is not the only possible magnetic cycle. Indeed, devices employing the magnetic Carnot cycle have already been achieved (see references [53] and [28], for example), as well as a modified magnetic Ericsson cycle (a second regenerative cycle consisting of an isothermal magnetization, two isofield temperature changes, and an isothermal demagnetization; see [26], for example), and recuperative cycles have also been considered [54]. The focus of this work, however, is the magnetic Brayton cycle because of its extension to active magnetic regeneration.

## 1.9 Active Magnetic Regeneration

In a regenerative magnetic cycle, it is possible to integrate the regeneration stages with the heat load absorption and rejection stages. In this configuration, the magnetic material performs the duty of regenerator, as well as of active working material. Because the magnetic material

performs both functions, this configuration is known as an Active Magnetic Regenerator, or *AMR*, and its operation describes a unique cycle. No other cycle has the feature where the working material is also the regenerative material.

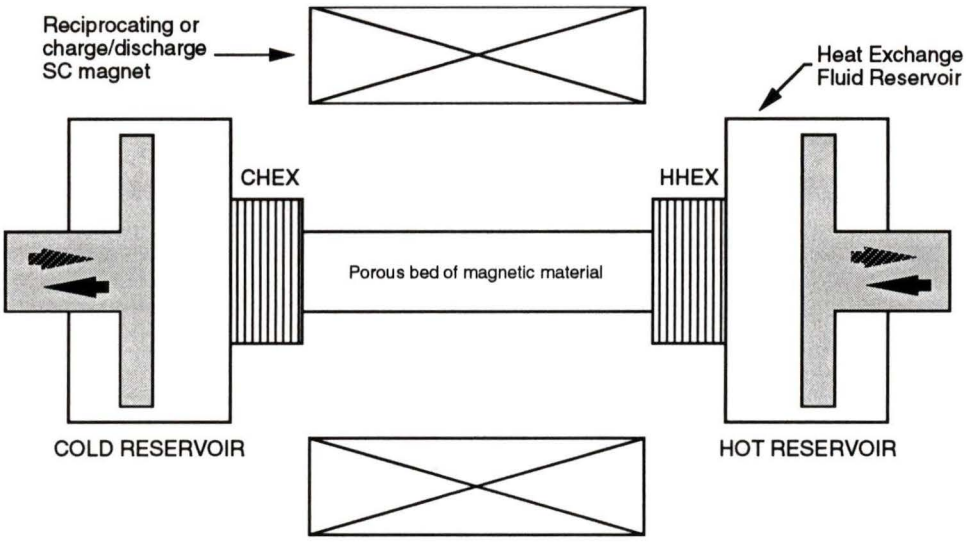


**Figure 1.13** Reciprocating AMRR schematic.

Figure 1.13 gives a schematic of a reciprocating version of an AMR. In the figure, hot and cold heat exchangers sandwich a regenerator bed composed of magnetic material, while pistons shuttle heat transfer fluid periodically and in cooperation with the periodic application of a magnetic field.

The process cycle for the AMR is slightly simpler than the magnetic Brayton cycle described previously. With all the fluid in the cold reservoir, the magnetic material is adiabatically magnetized, causing the temperature everywhere in the bed to increase by some amount as determined by the local value of magnetocaloric effect. The fluid is then passed from the cold reservoir, through the magnetic material thus picking up heat from the material, through the hot heat exchanger (HHEX) where heat is rejected, and into the hot reservoir. With the fluid now in the hot reservoir, the bed is adiabatically demagnetized, causing the temperature everywhere in the material to decrease by some amount as determined by the local value of magnetocaloric effect. The fluid is then passed from the hot reservoir back through the magnetic material thus

depositing heat to the material and itself cooling, through the cold heat exchanger (CHEX) where a load is absorbed, and into the cold reservoir to complete the cycle.

In the AMR, an element of magnetic material merely cycles through a simple non-regenerative Brayton (or Ericsson, for example) cycle about a specific temperature as determined by its position in the regenerator bed. The heat transfer fluid couples the magnetic elements to give a large temperature span. This is a significant advantage for the AMR because no magnetic element has to be active over the entire temperature span; every element can potentially be optimized to operate in its own temperature range.

## 1.10 Rotary Active Magnetic Regeneration

The reciprocating design is not the only possible configuration of an AMR device. The original concept of rotating magnetic refrigerators as conceived by Steyert [55] was taken a step further by the invention of the rotary active magnetic regenerators in 1983 by Barclay [57].

A schematic diagram of a rotary AMR refrigerator (AMRR) is given in Figure 1.14. A ring shaped regenerator of magnetic material is rotated through a high constant magnetic field region. As a radial segment of the regenerator enters the high field region, it responds to the field and experiences warming from the magnetocaloric effect. While in the high field region, heat transfer fluid from the cold heat exchanger flows through the segment, picking up heat to be rejected in the hot heat exchanger. As the segment rotates through the high field region, it is continuously cooled by the fluid flow. Eventually, the segment rotates to the area where fluid flow ends, and the segment rotates out of the high field region. Again it responds to the change in field, this time getting cooler. In the zero field region, heat transfer fluid from the hot heat exchanger flows in the opposite direction through the radial segment, regenerating the magnetic material and thereby cooling the fluid so it can absorb a load at the cold heat exchanger. Eventually, the segment rotates to the area where fluid flow ends, material regeneration is complete, and the segment is ready to undergo another cyclic rotation.

Both the rotary AMRR and reciprocating AMRR undergo the same thermodynamic processes in a periodic manner. The rotary AMRR, however, achieves periodicity by physical rotation of the

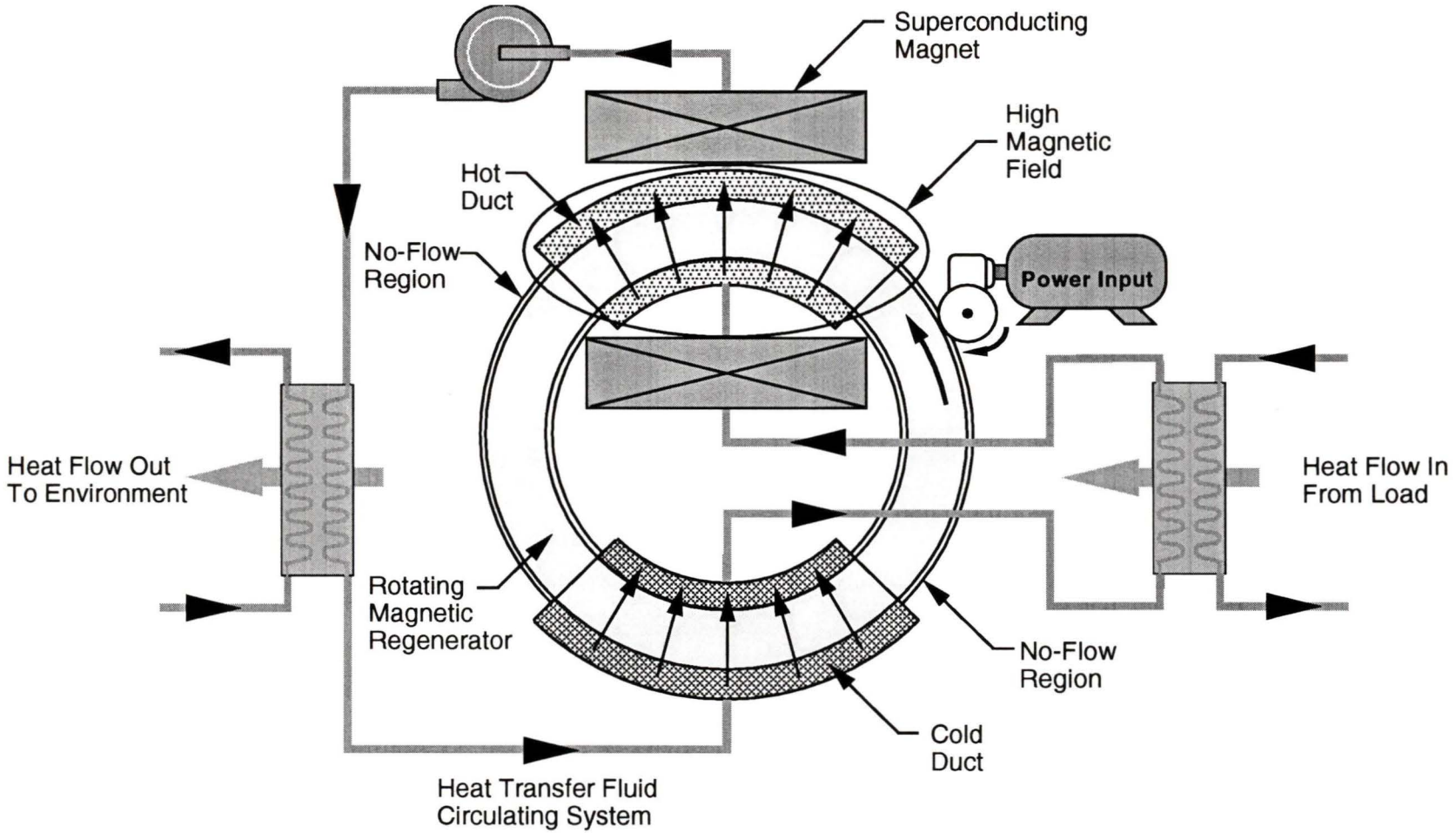


**Figure 1.14** Rotary AMRR schematic showing key system components.

magnetic solid through the various phases of operation, while the reciprocating AMRR achieves periodicity by applying the different phases at different times. At any given time, in the rotary AMRR, every phase of the cycle is being applied to some portion of the magnetic solid, whereas in the reciprocating AMRR only one phase of the cycle is being applied to every portion of the magnetic solid. From the point of view of the cold and hot heat exchangers where the cooling load is absorbed and rejected, respectively, the rotary AMRR has constant loads, whereas the reciprocating AMRR has periodic loads. This provides the rotary device with a distinct advantage for most cooling applications where constant cooling is preferred, as well as certain mechanical advantages from steady forces and constant work input. Before an efficient rotary AMRR can be built, however, a very thorough understanding of the influence of its many design parameters is required. This understanding comes from the study of AMRR models, both mechanical and numerical.

# Chapter 2

# Reported Work in Magnetic Refrigeration

## 2.1 Overview of Magnetic Refrigeration Literature

### 2.1.1 General Overview

Compared to gas cycle refrigeration devices, relatively few results from either mechanical prototypes or numerical models have been published concerning the performance of magnetic refrigeration cycles. Of all the results concerning magnetic devices, only a portion pertain to the AMRR cycle. One means of classifying the results that have been published is according to the span between heat source temperature, $T_c$, and heat sink temperature, $T_h$. The following ranges have been reported in the literature: 0.1-1.5, 1.5-4.2, 4.2-20, 20-77 K, in addition to those in the neighbourhood of 300 K. Zhang [23] provides an excellent summary of reported work on magnetic refrigeration devices for each temperature range. Barclay [45] provides a comprehensive review of researchers studying system analysis, database component development, and engineering prototype development as of 1990.

The above temperature ranges are inspired by the common classes of refrigeration applications. In the lowest temperature range, 0.1-1.5 K, cooling is provided for infrared detection and the study of critical phenomena in quantum fluids. References [18], [22], [19], and [21] provide examples of work for these applications. The next temperature range, 1.5-4.2 K, focuses on the production of superfluid liquid helium [23], which is commonly used to more effectively cool large superconducting magnets. Barclay [26] describes work on a reciprocating Carnot cycle for cooling superconducting transmission lines using superfluid helium.

Helium liquefies at 4.2 K, while hydrogen liquefies at 20 K, setting the limits for the third temperature range. Again, the focus in this range is liquefaction of helium and cooling of superconductors. There have been many devices reported to operate in this range, including rotating devices such as that described by Barclay [3], reciprocating devices such as that described by Johnson [27] and Nakagome [28], and active regenerative devices such as that described by Seyfert [29].

The next temperature range, 20-77 K, is bounded in the upper limit by the boiling point of nitrogen. The use of liquid nitrogen as a readily available and inexpensive heat sink explains why 77 K is the upper temperature. Potential applications in this range include liquefaction of hydrogen or production of hydrogen slush, and more currently, cooling of high temperature superconductors. Some researchers working in this range include [30], [31], and [7].

In 1976, Brown [58] performed magnetic refrigeration in the last temperature range mentioned above, the area of 300 K, using an Ericsson cycle. He succeeded in getting a large temperature difference (50 K) between the top and bottom of a regenerator column using gadolinium as the working material and an applied magnetic field change of 7 Tesla. A refrigerator operating near room temperature has also been reported by Steyert and Barclay [24], [25]. Green and Patton have also reported a device operating in this temperature range [8]. Devices operating near room temperature have many potential applications, including food handling and air conditioning. A feasibility study of magnetic air conditioning applications was conducted by Barclay [32].

### 2.1.2 Active Magnetic Regenerative Refrigeration

The extent of research in magnetic refrigeration is modest, and a focus on active magnetic regenerative refrigeration cycles narrows the available literature to a limited number of papers covering prototype test results and mathematical models. Following is a brief review of AMRR computer modelling efforts.

In "The Theory of an Active Magnetic Regenerative Refrigerator", Barclay, [4], identifies the heat transfer in the regenerative stages as the dominant inefficiency in a magnetic cycle, and notes that excellent regenerator designs with respect to heat transfer, viscous flow dissipation, and

longitudinal conduction are required. For regenerator design, he presents previously developed one-dimensional energy balance equations for passive regenerators. He extends these to include one-dimensional continuity, momentum, and solid, fluid and container wall energy balance equations for the prediction of the thermal-wavefront propagation in a porous bed with a large temperature gradient when all properties are temperature dependent. The equations include lumped energy source and sink terms of which Barclay cites magnetocaloric effect, eddy currents, and heat leak from the surrounding as examples. Modelling efforts accounted for the magnetocaloric effect by adding (subtracting) the adiabatic temperature change as the magnetic material was subjected to a step field increase (decrease), and also included the effects of longitudinal conduction of the solid and fluid. Preliminary modelling of multiple materials was performed [48].

In "Evaluation of Industrial Magnetic Heat Pump/Refrigerator Concepts that Utilize Superconducting Magnets", Waynert *et. al.* [39] present performance curves for a simplified numerical model of a rotary AMRR. In their model, the reduced period, $\Pi$, is assumed to be zero. Because of the low temperature operating regime, 20 - 77 K, effects of temperature dependent properties were considered. Pressure drop and conduction were calculated by the use of empirical expressions, though fluid properties were evaluated at constant pressure. Graphs of cooling power, efficiency, and pressure drop are given as a function of fluid mass flow and regenerator bed particle diameter. There is no indication in this paper whether radial geometry effects were considered, however one of the authors [48] has indicated they were not due to the large wheel diameters and short bed lengths considered.

In "Performance predictions of a Magnetocaloric Refrigerator using a Finite Element Model", Schroeder [42] builds upon earlier work at the David Taylor Research Center [43] for a linear pulsed AMRR. Schroeder describes a technique of using the one-dimensional, transient heat transfer analysis capability of a commercial package (NASTRAN) for a single blow operation, then using the results from one blow in an external program to describe the input conditions for a subsequent blow. AMRR operation is then described by several successive cycles. The magnetocaloric effect is accounted for by adding (subtracting) the adiabatic magnetization temperature change of the bed material before the start of the cold (hot) blow period. Each NASTRAN solution used constant material thermal properties, but the properties were varied

based on the progression of the temperature profiles obtained. Results provided include cooling curves under two different assumptions of regenerator material heat capacity and lowest temperatures reached under several heat loads.

In "Modelling the Active Magnetic Regenerator", DeGregoria [6] presents a model for a linear reciprocating AMR. Starting from the basic regenerator fluid and solid energy balance equations (see equations (1.10) and (1.11) in chapter 1), he considers the limit of zero for reduced period, $\Pi$, and gives the resulting simplified model. Conduction and pressure drop are added externally for the performance considerations, but apparently not for the calculation of temperature profiles. The magnetocaloric effect is accounted for by adding (subtracting) the adiabatic magnetization temperature change of the bed material before the start of the cold (hot) blow period. Simulation marches stepwise with time, with results from one time period providing the input to the next. DeGregoria presents temperature profiles for an AMRR composed of Gadolinium nickel working between approximately 60 to 80 K. He also presents cooling power as a function of mass flow for blow periods ranging from 0 to 8 s, using the simplified model for the lower limit of blow period.

In "Numerical Study of Magnetic Refrigeration including Consideration of Magnetic Nanocomposites", Carpetis [40] provides results for several AMRR model cases using gadolinium, gadolinium nickel, holmium nanocomposites, and gadolinium nanocomposites as working materials. He also presents results for magnetic refrigeration with external regeneration. His numerical model of a linear AMRR is described as "the differential equations for the refrigerant and the fluid"; however, in his conclusion he recommends future work should include the addition of all diffusion, convection, and source terms for the system, as well as the addition of terms for heat conduction and convection during the adiabatic process. The magnetocaloric effect is accounted for by adding (subtracting) the adiabatic magnetization temperature change of the bed material before the start of the cold (hot) blow period. Results of temperature profiles are presented and include simulated cool-down profiles, and steady-state temperature profiles for the bed at the end of hot blow and cold blow, and after bed magnetization and demagnetization. Also provided are plots of Quality Factor versus lower temperature for several different heat transfer durations for both passive regenerator magnetic refrigeration and active magnetic regenerative refrigeration cycles.

In "An Assessment of the Efficiency and Refrigeration Power of Magnetic Refrigerators with Ferromagnetic Refrigerants", Carpetis [44] refines his earlier linear regenerator AMRR work [40] (described above) by including conduction and pore fluid heat capacity terms. He gives efficiency and refrigeration per unit mass of working material for gadolinium, erbium, gadolinium nickel, and gadolinium nanocomposite as a function of fluid mass flux, temperature span,and blow period.

The literature cited above focuses on the modelling of single materials in an AMRR. Researchers [1], [47], have presented theoretical arguments for "optimal" material temperature-entropy relationships for AMRR's, and that this relationship can be approximated by layering multiple materials in a regenerator so that each material operates near its optimum temperature range. Schuricht et. al. [46] have modeled a linear AMRR layered with two materials, gadolinium nickel and an erbium alloy, and have presented the effect on performance as a function of the ratio of each material in the matrix. They found that multiple materials can offer improved performance over an active regenerator having a single material.

Numerical modelling to date has centred on simplified solid and fluid energy balance equations using a transient one-dimensional analysis. Effects of thermal conduction and fluid pore heat capacity have been recognized as important factors, but have typically not been included in numerical simulations. Eddy current generation has been analyzed and expressions given [20], yet despite its recognized importance, has not been included in models. All models have been for linear AMRR geometries with the exception of Waynert et. al. [39] who applied a linear geometry model to a large diameter wheel with a small aspect ratio.

The lack of numerical models can be attributed in part to the difficulty of designing an algorithm that will solve the complex equations quickly and easily. The complexity of the task is reflected in a paper by Seyfert [29] who reports that:

> *We have tried to model the real behaviour of the magnetic regenerator. The goal was to establish a calculation which would predict the time dependent temperature profiles for a given set of boundary conditions. The development of a computer program for that purpose turned out to be a long and difficult task.*

*At present, our code works in a way which allows it to be used, with some precaution, for the interpretation of experimental results.*

## 2.2 Research Goals

The objective of this research was to enable further development of expertise in the design of energy efficient AMRR's by the creation of a versatile and comprehensive computer model of a rotary active magnetic regenerative refrigerator with the following attributes:

- 2-dimensional, quasi-steady-state solid and fluid energy balance;
- fluid momentum equations not considered; imposed fluid velocity profile consistent with mass conservation;
- rotating wheel geometry with effects of radial geometry considered;
- effects of axial and radial conduction included in balance equations with the option for each to be included or excluded in solution;
- effects of eddy currents included in balance equations with the option to be included or excluded in solution;
- effects of fluid pore heat capacity included in equations;
- magnetocaloric effect modeled by change of state with local temperature and magnetic field;
- all properties temperature dependent (and magnetic field or pressure dependent as applicable) or constant as specified by input file;
- capacity for multiple working materials layered in any proportions; capacity for multiple geometries using multiple layers (such as packed particles for one layer and wire screens for another);
- all operating and design parameters specified by input file.

# Chapter 3

# AMRR Model Equations

# - System Equations

## 3.1 Conservation Equations

### 3.1.1 Model Assumptions and Simplifications

The operation of the AMRR can be fully described mathematically by considering the conservation of mass, momentum, and energy in the AMRR over time. The model can be simplified without significant loss of generality by focusing on the conservation of mass and energy only, and ignoring the conservation of momentum. In effect, this presupposes that the pressure drop caused by the flow within the AMRR does not significantly affect the temperature distribution in the AMRR. In the case of heat transfer fluids with properties which depend weakly on pressure, such as high pressure helium, this presupposition is valid. Further, the pressure drop can be calculated independently.

The AMRR model can be further simplified by considering only the steady state performance and ignoring the transient performance. While the transient performance could prove quite interesting, it was deemed beyond the scope of this investigation. Some further simplification can be achieved by assuming mass and energy fluxes to be two dimensional rather than fully three dimensional. For a wheel where fluid flow is radial and the rotation is azimuthal, this means mass fluxes are only permitted in radial and azimuthal directions, and not in the axial direction.

## 3.2 Fluid Equations

Using the simplifications above, and a space-fixed control volume as shown in Figure 3.1, the energy balance for the heat transfer fluid and the magnetic solid can be derived in turn. Consider first the fluid energy balance for a control volume $z \cdot r \cdot \Delta\theta \cdot \Delta r$. There are four distinct flow regimes, three of which are unique. These regimes are determined by the direction of the heat transfer fluid flow: 1) flow from the inner radius to the outer radius, 2) flow from the outer radius to the inner radius, and 3) no flow.

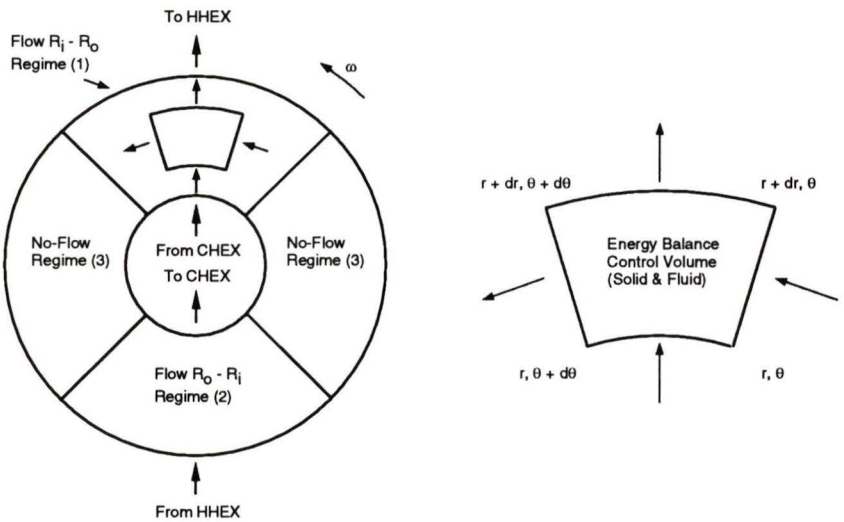


**Figure 3.1** Flow regimes and control volume for AMRR solid and fluid energy balances.

### 3.2.1 Fluid Convection

Following the nomenclature outlined on page x, energy fluxes for the first flow regime can be determined to give the energy balance for the fluid. Consider first the movement of the fluid into and out of the control volume. This provides two components of the fluid convection. The first component is due to the desired radial flow which provides the thermal "washing" of the solid and

the regenerative action of the AMRR bed. The second component is due to fluid entrained in the porous solid being carried with the solid as it rotates. These fluxes are given by:

Fluid Convection:

In:

$$\dot{m}_f \frac{\Delta\theta}{\phi_1} H_f(T_f,P_f) + \alpha\,\omega\, z\, r\, \Delta r\, \rho_f H_f(T_f,P_f) \tag{3.1}$$

Out:

$$\dot{m}_f \frac{\Delta\theta}{\phi_1}\left\{H_f(T_f,P_f) + \frac{\partial H_f}{\partial r}\Delta r\right\} + \alpha\,\omega\, z\, r\, \Delta r\, \rho_f\left\{H_f(T_f,P_f) + \frac{\partial H_f}{\partial \theta}\Delta\theta\right\} \tag{3.2}$$

where $\dot{m}_f$ is the total sector fluid mass flow rate, $\Delta\theta$ is the angular width of the control volume, $\phi_1$ is the total angular width of the flow regime 1 (flow from inner radius to outer radius), $H_f$ is the fluid enthalpy, $T_f$ is the fluid temperature, $P_f$ is the fluid pressure, $\alpha$ is the regenerator bed porosity, $\omega$ is the rotational frequency, $z$ is the axial thickness of the regenerator bed, $r$ is the radial position of the element, $\Delta r$ is the radial width of the control volume, and $\rho_f$ is the fluid density.

### 3.2.2 Fluid-Solid Heat Transfer

Consider next the fluid energy change inside the control volume. As the fluid moves within the porous solid, conduction and convection between the fluid and solid provides energy transfer:

Fluid-Solid Heat Transfer:

In:

$$h A''' z r \Delta\theta \Delta r \left(T_s - T_f\right) \tag{3.3}$$

where $h$ is the heat transfer coefficient, $A'''$ is the heat transfer area per unit volume, and $T_s$ is the solid temperature.

### 3.2.3 Fluid Conduction

Finally, consider the heat conduction due to thermal gradients in the fluid:

Fluid Conduction:

In:

$$- z r \Delta\theta k_{f_r} \frac{\partial T_f}{\partial r} - z \Delta r k_{f_\theta} \frac{\partial T_f}{\partial \theta} \tag{3.4}$$

Out:

$$\begin{aligned} &- z(r+\Delta r)\Delta\theta \left\{ k_{f_r} \frac{\partial T_f}{\partial r} + \frac{\partial}{\partial r}\left( k_{f_r} \frac{\partial T_f}{\partial r} \right) \Delta r \right\} \\ &- z \Delta r \left\{ k_{f_\theta} \frac{\partial T_f}{\partial \theta} + \frac{\partial}{\partial \theta}\left( k_{f_\theta} \frac{\partial T_f}{\partial \theta} \right) \Delta\theta \right\} \end{aligned} \tag{3.5}$$

where $k_{fr}$ is the effective thermal conductivity of the fluid in the radial direction, and $k_{f\theta}$ is the effective thermal conductivity of the fluid in the azimuthal direction. The effective thermal conductivity differs from the "natural" fluid conductivity by including the effects of geometry, such as porosity of the control volume, and perhaps other effects such as eddy diffusion.

### 3.2.4 Fluid Energy Balance Equation

On the basis of energy balance over the volume, steady state, and no fluid work terms, the sum of these terms over the control volume is zero, therefore:

$$\sum Out - \sum In = 0 \tag{3.6}$$

or

$$\begin{aligned} &\dot{m}_f \frac{\Delta\theta}{\phi 1}\frac{\partial H_f}{\partial r}\Delta r + \alpha\omega z r \Delta r \rho_f \frac{\partial H_f}{\partial \theta}\Delta\theta - z r \Delta\theta \Delta r\left(T_s - T_f\right) \\ &- z(r+\Delta r)\Delta\theta \frac{\partial}{\partial r}\left(k_{f_r}\frac{\partial T_f}{\partial r}\right)\Delta r - z\Delta r\Delta\theta k_{f_r}\frac{\partial T_f}{\partial r} - z\Delta r \frac{\partial}{\partial\theta}\left(k_{f_\theta}\frac{\partial T_f}{\partial\theta}\right)\Delta\theta = 0 \end{aligned} \tag{3.7}$$

Some further simplifications of the equation can be made. For a single phase fluid, the change in enthalpy can be represented in terms of its change with respect to pressure and temperature:

$$dH_f = \left(\frac{\partial H_f}{\partial T_f}\right)_{P_f} dT_f + \left(\frac{\partial H_f}{\partial P_f}\right)_{T_f} dP_f \tag{3.8}$$

For liquids and nearly ideal gases, the enthalpy is a strong function of temperature and a very weak function of pressure. Further, by definition, the change in enthalpy with respect to temperature is denoted as heat capacity, giving the following relations:

$$\frac{\partial H_f}{\partial\theta} \approx \left(\frac{\partial H_f}{\partial T_f}\right)_{P_f}\frac{\partial T_f}{\partial\theta} = C_P\frac{\partial T_f}{\partial\theta} \tag{3.9}$$

and

$$\frac{\partial H_f}{\partial r} \approx \left(\frac{\partial H_f}{\partial T_f}\right)_{P_f} \frac{\partial T_f}{\partial r} = C_P \frac{\partial T_f}{\partial r} \tag{3.10}$$

Using these simplifications for enthalpy change, dividing each term in Equation (3.7) by $z \cdot r \cdot \Delta\theta \cdot \Delta r$, and letting the control volume radial and azimuthal dimensions shrink to zero, the following energy balance equation for the fluid results:

$$\frac{\dot{m}_f C_P}{z r \phi_1} \frac{\partial T_f}{\partial r} + \alpha \omega \rho_f C_P \frac{\partial T_f}{\partial \theta} - \frac{1}{r} \frac{\partial}{\partial r}\left(r k_{f_r} \frac{\partial T_f}{\partial r}\right) - \frac{1}{r} \frac{\partial}{\partial \theta}\left(\frac{k_{f_\theta}}{r} \frac{\partial T_f}{\partial \theta}\right) - hA'''\left(T_s - T_f\right) = 0 \tag{3.11}$$

## 3.3 Fluid Dimensionless Groups

Equation (3.11) was derived for the flow zone having fluid flow from the inner radius to the outer radius. A similar analysis will yield similar equations for the other flow zones differing only in the radial convective flux due to the fluid flow direction. All three fluid equations can be represented with one set of dimensionless coefficients consistent with the dimensionless groups outlined for passive regenerators by introducing the following definitions:

Reduced Length:

$$\Lambda = \frac{hA'''\left(r_o - r_i\right)}{\left(\frac{\dot{m}_f}{z r_o \phi_i}\right) C_P}$$

Dimensionless Radial Conduction:

$$\lambda_{f_r} = \frac{k_{f_r} z \phi_i}{\dot{m}_f C_P}$$

Dimensionless Radial Conduction Gradient:

$$\lambda^*_{f_r} = \frac{z \phi_i}{\dot{m}_f C_P} \frac{\partial k_{f_r}}{\partial r^*}$$

Dimensionless Azimuthal Conduction:

$$\lambda_{f_\theta} = \frac{k_{f_\theta} z \phi_i}{\dot{m}_f C_P}$$

Dimensionless Azimuthal Conduction Gradient:

$$\lambda^*_{f_\theta} = \frac{z \phi_i}{\dot{m}_f C_P} \frac{\partial k_{f_\theta}}{\partial \theta}$$

Dimensionless Fluid Entrainment:

$$\beta = \frac{\alpha \omega z r_o^2 \phi_i \rho_f}{\dot{m}_f}$$

Dimensionless Fluid Temperature:

$$T^*_f = \frac{T_f - T_c}{T_h - T_c}$$

Dimensionless Solid Temperature:

$$T_s^* = \frac{T_s - T_c}{T_h - T_c}$$

Dimensionless Position:

$$r^* = \frac{r}{r_o}$$

Length Factor:

$$\gamma = \frac{r_o}{(r_o - r_i)}$$

Flow Regime Factor:

$$\xi = \begin{cases} +1 & \textit{radial flow outward} \\ 0 & \textit{no flow} \\ -1 & \textit{radial flow inward} \end{cases}$$

where $T_h$ and $T_c$ are the inlet fluid temperatures to the regenerator demagnetized and magnetized regions respectively, $r_o$ and $r_i$ are the outer and inner radii of the regenerator bed respectively, and $\phi_i$ is one of $\phi_1$, $\phi_2$, or $\phi_3$ as appropriate for each of the flow regimes.

## 3.4 Fluid Dimensionless Energy Balance Equation

Applying the above definitions for the fluid dimensionless groups to Equation (3.11), the dimensionless energy balance for the fluid becomes:

Fluid Dimensionless Energy Equation:

$$\xi \frac{\partial T_f^*}{\partial r^*} = \Lambda \gamma r^* \left(T_s^* - T_f^*\right) + \lambda_{f_r} r^* \frac{\partial^2 T_f^*}{\partial r^{*2}} + \lambda_{f_r} \frac{\partial T_f^*}{\partial r^*} + \lambda_{f_r}^* r^* \frac{\partial T_f^*}{\partial r^*} + \lambda_{f_\theta} \frac{1}{r^*} \frac{\partial^2 T_f^*}{\partial \theta^2} + \lambda_{f_\theta}^* \frac{1}{r^*} \frac{\partial T_f^*}{\partial \theta} - \beta r^* \frac{\partial T_f^*}{\partial \theta} \tag{3.12}$$

This generalized, non-dimensionalized equation applies to each of the three flow regimes, flow from the inner radius to the outer radius, flow from the outer radius to the inner radius, and no-flow, where each of the coefficients is evaluated for the respective flow zones. In the case of the no-flow regime, the mass flow is defined as the mass flow for the demagnetized region of the AMRR. In effect, this mass flow definition does not alter the balance represented by the equation but merely acts as if to divide the entire equation by a constant rather than divide the entire equation by zero.

## 3.5 Solid Equations

The energy balance equation for the solid can be determined using the same procedure as was used for the fluid, namely, summing the fluxes across the boundaries and energy sources and sinks of the control volume. It is easiest, however, to start with a generalized expression of the heat transfer during an infinitesimal change of state of a magnetic substance in a fixed mass system. On the basis of the regenerator solid being a rigid body, the expression can then be transformed to reflect the applicable AMRR geometry control volume analysis. Finally, it can be further refined after identifying the components of the heat transfer term in that expression. Identifying the heat transfer components for the solid is accomplished by the same procedure as was used for the fluid equation.

### 3.5.1 Magnetic Solid Heat Transfer

For a magnetic solid, the heat transfer per unit volume during an infinitesimal change of state is given by:

Magnetic Solid Heat Transfer:

$$\delta Q_V = \rho_s C_H dT + \mu_o T\left(\frac{\partial M}{\partial T}\right)_H dH \tag{3.13}$$

where $\delta Q_V$ is the heat transferred, $\rho_s$ is the material density, $C_H$ is the heat capacity per unit mass at constant applied field, $\mu_o$ is the permeability of free space, $M$ is the magnetization of the material, and $H$ is the applied field.

In the case of the rotary AMRR, this equation can be written to reflect the porous nature of the solid, and the rotation of the solid by noting the following relations:

$$\Delta \dot{Q}_V = \frac{dQ_v}{dt} \tag{3.14}$$

and

$$\frac{1}{dt} = \omega \frac{1}{d\theta} \tag{3.15}$$

and therefore, for the AMRR:

$$\Delta \dot{Q}_V = (1-\alpha)\omega \rho_s C_H \frac{dT}{d\theta} + (1-\alpha)\omega \mu_o T\left(\frac{\partial M}{\partial T}\right)_H \frac{dH}{d\theta} \tag{3.16}$$

The rate of heat transferred, $\Delta \dot{Q}_V$, can be determined by focusing on the total fluxes across the boundary of the control volume and the sources within the control volume, then representing the sum on a per unit volume basis. In contrast to the fluid equation, the solid equation has a volume energy source term. This source term merits some discussion.

### 3.5.2 Induced Electrical Eddy Currents

The source term in the solid energy balance equation is a result of the electrical eddy current generation in the regenerator bed material as the material rotates into and out of the magnetic field region. Faraday's Law states that a time varying magnetic flux linking an electric circuit induces a voltage in the circuit. If the circuit is closed, a current flows through it. If the AMRR bed is made from electrically conductive material, then it will act like a closed circuit experiencing a time varying magnetic flux. Depending on regenerator material and geometry, very large or negligibly small current loops could be generated upon magnetization and demagnetization of the regenerator bed.

The electrical eddy current source term is proportional to the square of the change in applied field, a geometrical shape factor, and the area enclosed by the generated current loops, and inversely proportional to electrical resistivity of the regenerator material. A comprehensive derivation of eddy current heating and geometry shape factors is given by [20]. For any simple current loop geometries, such as square rods, circular rods, etc., the total eddy current power dissipation is given by:

$$P_e = \frac{\left(\frac{dB}{dt}\right)^2}{32\,\rho_e}\,\Gamma A_x V \tag{3.17}$$

where $B$ is the magnetic field, $\Gamma$ is a geometrical shape factor, $A_x$ is the area enclosed by the largest possible current loop, $V$ is the volume of material, and $\rho_e$ is the material's resistivity.

For complex geometrical shapes, the geometry shape factor $\Gamma$ can be difficult to compute. Further, the exact orientation of the applied field with respect to the orientation of the shape is important and can, for some geometries with large aspect ratios, change the expected power dissipation by several orders of magnitude. Last, the effective current loop area and effective electrical resistivity of the regenerator bed is influenced by the presence of electrically insulating oxide films that form on common AMRR materials. For this reason, the eddy current term is included in the derivation of the solid equation, but forms only a limited part of this study.

The eddy current term can be written to reflect the configuration of the rotary AMRR system. The time dependence can be re-written in terms of the rotation rate and angular position. Further, as porosity increases, one would expect the volumetric power dissipation to decrease, so one needs to account for regenerator porosity. Finally, the change in the field, $B$, is dependent on the material magnetization, $M$, which is dependent on the change in the material's temperature and applied field with position. Incorporating these considerations, the eddy current power dissipation term becomes:

Eddy Current Dissipation:

$$P_e = \frac{(1-\alpha)\mu_o^2 \omega^2 \Gamma A_x V}{32 \rho_e} \left\{ \left[ 1 + \left( \frac{\partial M}{\partial H} \right)_T \right] \frac{dH}{d\theta} + \left( \frac{\partial M}{\partial T} \right)_H \frac{dT}{d\theta} \right\}^2 \tag{3.18}$$

### 3.5.3 Solid-Fluid Heat Transfer

The solid-fluid heat transfer can be calculated in the same manner as the fluid equation:

Solid-Fluid Heat Transfer:

In:

$$h A''' z r \Delta\theta \Delta r \left( T_f - T_s \right) \tag{3.19}$$

Note that the solid-fluid heat transfer is identical to the heat transfer expression previously developed for the fluid energy equation except for sign. This term provides the coupling between the solid and fluid energy equations.

### 3.5.4 Solid Conduction

The conduction due to thermal gradients in the solid can be calculated in the same fashion as the fluid equation:

Solid Conduction:

In:

$$-z\,r\,\Delta\theta\,k_{s_r}\frac{\partial T_s}{\partial r} - z\,\Delta r\,k_{s_\theta}\frac{\partial T_s}{\partial \theta} \tag{3.20}$$

Out:

$$\begin{aligned} &-z(r+\Delta r)\,\Delta\theta\left\{k_{s_r}\frac{\partial T_s}{\partial r} + \frac{\partial}{\partial r}\left(k_{s_r}\frac{\partial T_s}{\partial r}\right)\Delta r\right\} \\ &-z\,\Delta r\left\{k_{s_\theta}\frac{\partial T_s}{\partial \theta} + \frac{\partial}{\partial \theta}\left(k_{s_\theta}\frac{\partial T_s}{\partial \theta}\right)\Delta\theta\right\} \end{aligned} \tag{3.21}$$

where $k_{sr}$ is the effective thermal conductivity of the solid in the radial direction, and $k_{s\theta}$ is the effective thermal conductivity of the solid in the azimuthal direction. The effective thermal conductivity differs from the "natural" solid conductivity by including the effects of geometry, such as regenerator porosity, and perhaps material or geometrical anisotropy.

### 3.5.5 Solid Energy Balance Equation

The sum of the source term and fluxes represents the total heat transfer rate giving the following relation:

$$\Delta\dot{Q} = \sum In - \sum Out \tag{3.22}$$

Summing the eddy current source, and the heat transfer and conduction fluxes yields the total heat transfer rate, $\Delta\dot{Q}$, and further dividing by the volume of the control volume, $z \cdot r \cdot \Delta\theta \cdot \Delta r$, gives the heat transfer rate per unit volume:

$$\Delta \dot{Q}_V = hA'''\left(T_f - T_s\right) + \frac{1}{r}\frac{\partial}{\partial r}\left(r k_{s_r}\frac{\partial T_s}{\partial r}\right) + \frac{1}{r}\frac{\partial}{\partial \theta}\left(\frac{k_{s_\theta}}{r}\frac{\partial T_s}{\partial \theta}\right) \\ \frac{(1-\alpha)\mu_o^2\omega^2\Gamma A_x}{32\rho_e}\left\{\left[1+\left(\frac{\partial M}{\partial H}\right)_T\right]\frac{dH}{d\theta} + \left(\frac{\partial M}{\partial T}\right)_H\frac{dT_s}{d\theta}\right\}^2 \tag{3.23}$$

Setting Equation (3.16) and Equation (3.23) equal, and rearranging, yields the control volume energy balance equation for the solid:

$$(1-\alpha)\omega\rho_s C_H\frac{\partial T_s}{\partial \theta} = hA'''\left(T_f - T_s\right) - (1-\alpha)\omega\mu_o T_s\left(\frac{\partial M}{\partial T}\right)_H\frac{dH}{d\theta} \\ + \frac{1}{r}\frac{\partial}{\partial r}\left(r k_{s_r}\frac{\partial T_s}{\partial r}\right) + \frac{1}{r}\frac{\partial}{\partial \theta}\left(\frac{k_{s_\theta}}{r}\frac{\partial T_s}{\partial \theta}\right) \\ + \frac{(1-\alpha)\mu_o^2\omega^2\Gamma A_x}{32\rho_e}\left\{\left[1+\left(\frac{\partial M}{\partial H}\right)_T\right]\frac{dH}{d\theta} + \left(\frac{\partial M}{\partial T}\right)_H\frac{dT_s}{d\theta}\right\}^2 \tag{3.24}$$

## 3.6 Solid Dimensionless Groups

The solid equation can be represented with dimensionless coefficients consistent with the dimensionless groups outlined previously for passive regenerators by introducing the following definitions:

Reduced Period:

$$\Pi = \frac{hA'''}{(1-\alpha)\omega\rho_s C_H}$$

Dimensionless Radial Conduction:

$$\lambda_{s_r} = \frac{k_{s_r}}{(1-\alpha)\,\omega\,\rho_s r_o^2 C_H}$$

Dimensionless Radial Conduction Gradient:

$$\lambda_{s_r}^* = \frac{1}{(1-\alpha)\,\omega\,\rho_s r_o^2 C_H}\frac{\partial k_{s_r}}{\partial r^*}$$

Dimensionless Azimuthal Conduction:

$$\lambda_{s_\theta} = \frac{k_{s_\theta}}{(1-\alpha)\,\omega\,\rho_s r_o^2 C_H}$$

Dimensionless Azimuthal Conduction Gradient:

$$\lambda_{s_\theta}^* = \frac{1}{(1-\alpha)\,\omega\,\rho_s r_o^2 C_H}\frac{\partial k_{s_\theta}}{\partial \theta}$$

Dimensionless Magnetocaloric Factor:

$$\zeta = \frac{\mu_o H_{max}^2}{\rho_s C_H\left(T_h - T_c\right)}$$

Dimensionless Eddy Current Factor:

$$\Omega = \frac{\mu_o^2 H_{max}^2\,\omega\,\Gamma A_x}{32\,\rho_e\,\rho_s C_H\left(T_h - T_c\right)}$$

Dimensionless Solid Temperature:

$$T_s^* = \frac{T_s - T_c}{T_h - T_c}$$

Dimensionless Fluid Temperature:

$$T_f^* = \frac{T_f - T_c}{T_h - T_c}$$

Dimensionless Applied Field:

$$H^* = \frac{H}{H_{max}}$$

Dimensionless Material Magnetization:

$$M^* = \frac{M}{H_{max}}$$

where $H_{max}$ is the maximum (peak) field applied to the magnetic material.

## 3.7 Solid Dimensionless Energy Balance Equation

Applying the above definitions for the solid dimensionless groups to Equation (3.24), the dimensionless energy balance equation for the solid becomes:

Solid Dimensionless Energy Equation:

$$\begin{aligned}\frac{\partial T_s^*}{\partial \theta} &= \Pi\left(T_f^* - T_s^*\right) - \zeta\left(T_s^* + \frac{T_c}{T_h - T_c}\right)\left(\frac{\partial M^*}{\partial T^*}\right)_{H^*}\frac{dH^*}{d\theta} \\ &+ \lambda_{s_r}\frac{\partial^2 T_s^*}{\partial r^{*2}} + \frac{\lambda_{s_r}}{r^*}\frac{\partial T_s^*}{\partial r^*} + \lambda_{s_r}^*\frac{\partial T_s^*}{\partial r^*} \\ &+ \frac{\lambda_{s_\theta}}{r^{*2}}\frac{\partial^2 T_s^*}{\partial \theta^2} + \frac{\lambda_{s_\theta}^*}{r^{*2}}\frac{\partial T_s^*}{\partial \theta} \\ &+ \Omega\left\{\left[1 + \left(\frac{\partial M^*}{\partial H^*}\right)_{T^*}\right]\frac{dH^*}{d\theta} + \left(\frac{\partial M^*}{\partial T^*}\right)_{H^*}\frac{dT_s^*}{d\theta}\right\}^2\end{aligned} \tag{3.25}$$

This generalized, non-dimensionalized equation applies to the entire AMRR solid, and does not change form with the local fluid flow regime. The dimensionless period, $\Pi$, does, however, reflect the differing flow regimes through that group's dependence on the local heat transfer coefficient, which is a function of local fluid flow conditions.

# Chapter 4

# AMRR Model Equations

## - Performance Equations

---

### 4.1 Motivation

The dimensionless solid and fluid energy balance equations, when solved, yield the solid and fluid temperature profiles in the AMRR. Once the temperature profiles are known, other expressions which characterize the AMRR performance can be calculated. A development of some of these expressions follows.

### 4.2 Cooling Power

An AMRR is designed to provide refrigeration; therefore, some measure of its cooling capacity is required. Typically, two values are given to denote the cooling capacity of a device, namely, the temperature at which the cooling is provided and the rate at which heat can be transported from the cooling load. The temperature at which cooling is provided is given directly by the solution of the fluid and solid energy equations. The cooling rate is given by the ability of the fluid from the outlet of the demagnetized region of the AMRR to absorb some load before being re-injected into the AMRR at the inlet of the magnetized region. Considering this, the cooling load is given by:

$$\dot{Q}_{load} = \dot{m}_f\left(H_f(T_c,P_c) - H_f(T_l,P_l)\right) \tag{4.1}$$

where $\dot{m}_f$ is the fluid mass flow rate, $H_f$ is the fluid enthalpy, $T$ and $P$ are the fluid temperature and pressure respectively, and the subscripts $c$ and $l$ denote that the properties are to be evaluated at the magnetized region fluid inlet, and the demagnetized region fluid outlet, respectively. Using the approximation for fluid enthalpy outlined in the previous chapter, the cooling load can also be expressed as:

$$\dot{Q}_{load} = \dot{m}_f \bar{C}_P \left(T_c - T_l\right) \tag{4.2}$$

where $\bar{C}_P$ is the average fluid heat capacity at which the load is absorbed.

## 4.3 Heat Rejection Rate

The AMRR acts to move a heat load from a low temperature source to a higher temperature sink. The heat rejection rate of the fluid to the high temperature sink is given by the rejection of heat between the fluid outlet of the magnetized region of the AMRR and the fluid inlet of the demagnetized region. Considering this, the heat rejection rate is given by:

$$\dot{Q}_{rejected} = \dot{m}_f \left(H_f\left(T_r, P_r\right) - H_f\left(T_h, P_h\right)\right) \tag{4.3}$$

where the subscripts $r$ and $h$ denote that the properties are to be evaluated at the magnetized region fluid outlet, and the demagnetized region fluid inlet respectively. Again, using the approximation for fluid enthalpy outlined in the previous chapter, the heat rejection rate can also be expressed as:

$$\dot{Q}_{rejected} = \dot{m}_f \bar{C}_P \left(T_r - T_h\right) \tag{4.4}$$

where $\bar{C}_P$ is the average fluid heat capacity at which the load is rejected.

## 4.4 Input Power

### 4.4.1 Magnetic Work

To provide refrigeration, the input of power is required. There can be several power input loads for a complete refrigeration system, including, for example, control systems, fluid pumps, and the power to achieve the refrigeration cycle. In this study, the input power of interest is that which is required to perform the thermodynamic refrigeration cycle, which is the power required to continuously move the AMRR bed through the magnetic field. The input power for rotation can be calculated by summing the power input upon magnetizing the solid and subtracting the power output upon demagnetizing the solid. For any infinitesimal magnetic work interaction for some volume of material, the work is given by [16], [17]:

$$\delta W_V = -\mu_o H \, dM \tag{4.5}$$

where $\delta W_V$ is the infinitesimal magnetic work interaction for the volume, $\mu_0$ is the permeability of free space, $H$ is the magnetic field intensity, and $dM$ is the change in magnetization of the material.

### 4.4.2 Rotary AMRR Input Power

For the rotary AMRR, the infinitesimal power per unit volume for any small volume undergoing magnetization or demagnetization as it rotates into or out of the magnetic field at a frequency ω can be expressed as:

$$\frac{\delta W_V}{\Delta t} = -\mu_o H \, \omega \, \frac{dM}{d\theta} \tag{4.6}$$

The total input power required to rotate the AMRR is given by summing all the infinitesimal volumes, therefore:

$$\dot{W}_{in} = -\mu_o \omega \int_{vol} H \frac{dM}{d\theta} dV \tag{4.7}$$

The input power to rotate the AMRR can also be independently calculated by a global energy balance over the entire AMRR. From a global energy balance, the input power is given by:

$$\dot{W}_{in} = \sum \dot{Q}_{out} - \sum \dot{Q}_{in} \tag{4.8}$$

where $\dot{Q}_{out}$ is the rate of heat leaving the system and $\dot{Q}_{in}$ is the rate of heat entering the system. If the heat loads in and out of the AMRR are solely as a result of the fluid transport into and out of the regenerator (as opposed to including some parasitic heat leaks into the solid from the environment, for example), then the input power can also be expressed as:

$$\dot{W}_{in} = \dot{Q}_{reject} - \dot{Q}_{load} \tag{4.9}$$

## 4.5 Coefficient of Performance

For refrigeration systems, a measure of performance is given by the ratio of the cooling provided to the work required to achieve that cooling. This ratio is commonly named the "Coefficient of Performance", or "COP". For the AMRR operating as a refrigerator, ignoring the power to run any auxiliary equipment such as the pump to move the heat transfer fluid, etc., the COP is given by:

$$COP = \frac{\dot{Q}_{load}}{\dot{W}_{in}} \tag{4.10}$$

Note that the work input in the above equation can be determined by any of Equations (4.7), (4.8), or (4.9).

The AMRR's COP can vary widely, depending on the temperatures being spanned by the refrigerator. This makes it difficult to immediately see whether a given COP represents an AMRR cycle performing at its best or at its worst. To provide some measure of how well the cycle is performing, the AMRR COP can be compared to the COP for a Carnot cycle, thus giving a measure of the AMRR's performance relative to the best that could be achieved for an ideal refrigeration system under the same refrigeration conditions. The COP of a Carnot cycle refrigerator is given by:

$$COP_{ideal} = \frac{T_c}{T_h - T_c} \tag{4.11}$$

## 4.6 Relative Efficiency

The relative efficiency of the AMRR cycle compared to the Carnot cycle is given by the ratio of the AMRR's COP to the Carnot cycle's COP:

$$\eta_{rel} = \frac{COP_{AMRR}}{COP_{ideal}} = \frac{(T_h - T_c)}{T_c} \frac{\dot{Q}_{load}}{\dot{W}_{in}} \tag{4.12}$$

The relative efficiency is a number between zero and one; the closer the relative efficiency is to one, the more efficient the cycle, and the closer the cycle is to being ideal. Some works denote this quantity as the figure of merit (FOM).

# Chapter 5

# AMRR Model Solution Techniques

## 5.1 Solution Approach

### 5.1.1 General Considerations

In order to understand the influence on performance of the many parameters of an AMRR, the dimensionless energy balance equations for the AMRR solid and fluid must be solved, then performance expressions compared. Solving the energy balance equations cannot simply be done analytically, since the two equations are coupled and have several non-linear terms. Thus, in order to solve these equations, some computer numerical methods are required.

The simplest approach to solve these partial differential equations (PDE's) is to use a commercial package designed for basic computational fluid dynamics linked with external code to account for the influence of the magnetocaloric effect, eddy currents, regenerator bed porosity, and other effects unique to the AMRR. At the time of this effort, however, there is no suitable commercial package available with sufficient flexibility. A custom program employing some numerical solution technique is therefore required to solve the energy balance equations.

### 5.1.2 Numerical Solution

There are many possible approaches described in the literature for numerically solving non-linear partial differential equations, including representing the problem with finite elements, finite differences, or finite volumes. Thorough examinations of many of the more common approaches are given by [12], [13], [14], and [15], for example. Each solution approach has its own benefits and drawbacks. Usually, there are two aspects of the approach to consider. The first

consideration is the means of transforming a partial differential equation, which is valid over the entire domain, into a set of simultaneous algebraic equations, each of which is assumed valid over its own small portion of the entire domain. The second consideration is the method of actually solving the resultant set of algebraic equations and making adjustments to the set of algebraic equations to account for any non-linearities.

### 5.1.3 Finite Difference Technique

Because of its relative simplicity, the energy balance PDE's were solved using finite difference techniques. In the finite difference approach, the continuous problem domain is "discretized" so that the dependent variables are considered to exist only at discrete points. Derivatives are approximated by differences, reducing a calculus problem to an algebraic problem.

The first step in establishing a finite difference procedure for a problem is to replace the continuous problem domain by a finite difference mesh. Because of the circular geometry of the AMRR wheel, a polar mesh was chosen. Further, for simplicity, the mesh was chosen to be of uniformly spaced elements, and, for all solutions, the total number of azimuthal mesh divisions chosen to be integrally divisible in proportion to the angular widths of the four flow regimes. This last restriction ensured that all nodes on the boundaries of the flow regimes were wholly representative of one flow regime, and not "straddling" two different regimes.

The second step in the finite difference procedure is to represent the derivative terms by difference terms. The difference approximations can be generated using Taylor series expansions about a mesh point, $u_{i,j}$, for each adjacent mesh point, $u_{i+1,j}$, $u_{i-1,j}$, $u_{i,j+1}$, $u_{i,j-1}$, and rearranging for the derivative. This yields an exact expression for the derivative, but has an infinite number of terms to be evaluated. The derivative is then approximated by retaining only a finite number of terms of the expansion, and noting that the terms dropped represent truncation error. For a complete description of the process of generating the finite difference expressions, the reader is referred to any standard numerical methods text, including those listed above.

### 5.1.4 General Finite Difference Expressions

An infinite number of difference representations can be found for the derivatives. The simplest and most common expressions for the first derivative are given by forward, backward, and central difference approximations, which, for a constant grid size are given by:

Forward Difference:

$$\left(\frac{\partial u}{\partial x}\right)_{i,j} = \frac{u_{i+1,j} - u_{i,j}}{\Delta x} + O(\Delta x) \tag{5.1}$$

where the notation $O(\Delta x)$ represents the truncation error, where the truncation error scales with the mesh size, i.e., $|\text{T.E.}| \leq K|\Delta x|$ for sufficiently small $\Delta x$.

Backward Difference:

$$\left(\frac{\partial u}{\partial x}\right)_{i,j} = \frac{u_{i,j} - u_{i-1,j}}{\Delta x} + O(\Delta x) \tag{5.2}$$

Central Difference:

$$\left(\frac{\partial u}{\partial x}\right)_{i,j} = \frac{u_{i+1,j} - u_{i-1,j}}{2\Delta x} + O(\Delta x)^2 \tag{5.3}$$

Note that the truncation error for the central difference derivative approximation scales with the square of the mesh size, rather than linearly with mesh size as it does for both forward and backward difference approximations.

The Taylor series expansion technique also applies to give higher order derivatives, and forward, backward, and central difference representations are possible. Commonly, the central difference representation for second derivative is used:

Central Difference:

$$\left.\frac{\partial^2 u}{\partial x^2}\right)_{i,j} = \frac{u_{i+1,j} - 2u_{i,j} + u_{i-1,j}}{(\Delta x)^2} + O(\Delta x)^2 \qquad (5.4)$$

Once again, the reader is directed to texts on numerical methods, for examples of the derivations of these and higher order expressions.

With the infinite number of difference approximations possible, some criteria must be available to select which approximations should be used to discretize the PDE's. One usually balances simplicity with accuracy, selecting the difference approximation with the fewest number of terms while having an acceptable truncation error. Another criterion is stability. Not all PDE's are stable with all difference approximations and solution techniques. It turns out that the AMRR equations, being much like the two-dimensional time dependent heat conduction equation, are unconditionally unstable if discretized using central difference in both azimuthal and radial coordinate directions [12], [15].

### 5.1.5 Finite Difference Expressions Employed

Using the above selection criteria for discretization difference schemes, the following finite difference formulations were used to discretize the AMRR energy balance equation temperature derivatives for interior nodes:

$$\left.\frac{\partial T}{\partial r}\right)_{i,j} = \frac{T_{i+1,j} - T_{i-1,j}}{2\Delta r} + O(\Delta r)^2 \qquad (5.5)$$

$$\left.\frac{\partial T}{\partial \theta}\right)_{i,j} = \frac{T_{i,j} - T_{i,j-1}}{\Delta \theta} + O(\Delta \theta) \qquad (5.6)$$

$$\left.\frac{\partial^2 T}{\partial r^2}\right)_{i,j} = \frac{T_{i+1,j} - 2\,T_{i,j} + T_{i-1,j}}{(\Delta r)^2} + O(\Delta r)^2 \qquad (5.7)$$

and,

$$\left.\frac{\partial^2 T}{\partial \theta^2}\right)_{i,j} = \frac{T_{i,j+1} - 2\,T_{i,j} + T_{i,j-1}}{(\Delta \theta)^2} + O(\Delta \theta)^2 \qquad (5.8)$$

where the nodal subscript $i$ is associated with the radial direction, the $j$ subscript is associated with the azimuthal direction, and an interior node is any node not on a boundary of the solution space.

These derivative definitions are not applicable to nodes on the radial boundaries because they reference non-existent nodes outside the boundaries. On the inner radius, there is no value $T_{i-1,j}$, and on the outer radius there is no value $T_{i+1,j}$. By the problem definition, these boundaries are insulated, and therefore the first derivative of temperature at the radial boundaries is identically zero. Using this insulated condition and the central difference definitions for the derivatives implies that if there were "phantom" nodes immediately outside the boundary they would mirror nodes immediately inside the boundary. Under these considerations, the radial derivatives on the inner and outer radii boundaries become:

$$\left.\frac{\partial T}{\partial r}\right)_{r_i,j} = 0 \qquad (5.9)$$

$$\left.\frac{\partial T}{\partial r}\right)_{r_o,j} = 0 \qquad (5.10)$$

$$\left.\frac{\partial^2 T}{\partial r^2}\right)_{r_i,j} = \frac{2T_{i+1,j} - 2T_{i,j}}{(\Delta r)^2} \tag{5.11}$$

and,

$$\left.\frac{\partial^2 T}{\partial r^2}\right)_{r_o,j} = \frac{2T_{i-1,j} - 2T_{i,j}}{(\Delta r)^2} \tag{5.12}$$

where the subscripts $r_i$ and $r_o$ denote the inner and outer radii respectively.

The azimuthal direction has no physical boundary, but with a nodal numbering scheme that increases with angular position, there is a numerical boundary where all 360° of nodes have been sequentially defined. To ensure the temperature profile is continuous azimuthally, derivatives at the numeric boundary are evaluated *in modulo*, that is, if there are 100 azimuthal nodes numbered 1 to 100, for example, a derivative term index of 101 for $j$ would be replaced with an index of 1, and an index of 0 would be replaced with an index of 100.

### 5.1.6 Boundary Conditions

The solid and fluid energy balance equations represent five partial differential equations that must be solved simultaneously. Four equations represent the four fluid flow regions: flow from inner radius to outer radius, flow from outer radius to inner radius, and two no-flow regions. The last equation is the solid equation which does not change form with the local flow regime. In order to properly constrain the equations, the following boundary conditions were imposed:

- solid radial conduction on the inner radius is zero;
- solid radial conduction on the outer radius is zero;
- solid temperature is continuous azimuthally;
- fluid radial conduction on the inner radius is zero in the no-flow region;

- fluid radial conduction on the outer radius is zero in the no-flow region;
- fluid temperature is $T_c$ at the inlet to the cold blow (magnetized) region;
- fluid temperature is $T_h$ at the inlet to the hot blow (demagnetized) region;
- fluid radial conduction is continuous at the outlet of the cold blow region;
- fluid radial conduction is continuous at the outlet of the hot blow region.

### 5.1.7 Solution Algorithms

The AMRR energy balance equations are transformed from partial differential equations into finite difference equations by substitution of the above finite difference approximations for the temperature derivatives. The resulting simultaneous equations can be solved in several ways. In this study, three different solution algorithms were employed, all of which further simplified the AMRR fluid equation by assuming that the azimuthal fluid conductivity was negligible and could be ignored. Each of the solution algorithms employed is described in detail in subsequent chapters.

## 5.2 AMRR Model Computer Program

### 5.2.1 Program Overview

Once the solid and fluid energy equations have been discretized, a computer program is required to calculate the equation coefficients and solve the resulting system of equations. The complexity of the program required is increased significantly by the requirements of multiple materials and geometries in the regenerator bed. The requirement of modelling multiple active magnetic materials across the regenerator bed dictates proper management of transport properties to ensure that properties are coordinated with the specified materials in the specified proportions across the regenerator. The requirement of modelling multiple geometries (such as packed particles for one layer and wire screens for another) dictates proper management of the influence of geometry on the fluid properties such as enhanced effective fluid conduction due to eddy diffusivity, on the pressure drop of the fluid, and on the heat transfer coefficient between solid and fluid.

An object-oriented computer program using the C++ programming language was developed to solve the discretized energy balance equations. The object-oriented nature of C++, and the capacity for virtual object classes, was particularly useful to modularize the required solution operations. A thorough description of objects and virtual objects is beyond the scope of this thesis; however, a C++ object can be thought of as a self-contained, self-consistent group of data and functions that operate on that data. References [61], [62], and [63] together provide good coverage of the means and essence of programming in C++. In the program developed, each layer of material in the AMRR being modeled is an autonomous object in terms of determining thermal properties and fluid interaction for the layer. The layers in turn are polled by "manager" objects which coordinate each layer's contribution to give a global representation of the thermal properties.

A schematic diagram of the main elements of the AMRR computer program is given in Figure 5.1. The top row of the diagram gives the intent of the program, namely, to use a program to represent an AMRR model, and ultimately to give performance data for the model. The second and subsequent rows show the key components of the program and their hierarchy. The solid and fluid profiles are the independent variables being solved for in the energy equations. The "Iterator/Solver" algorithms are used to solve for the temperatures and are described in detail in the following chapters. All other boxes represent code used to specify the model and to calculate the energy balance coefficients.

### 5.2.2 Model Definition Input File

Each AMRR model is specified by means of an human-readable input file. The input file defines the basic elements of the discretization, such as mesh sizes for radial and azimuthal directions and the proportion of the mesh for each of the flow zones, as well as the more advanced elements such as model dimensions, field magnitude and profile, flow rates, flow directions, which property evaluation correlations apply, number of layers of materials, initial temperature profiles, and which results are of interest for output. A sample input file and a copy of the same input file with comments and descriptions are included in Appendix A.

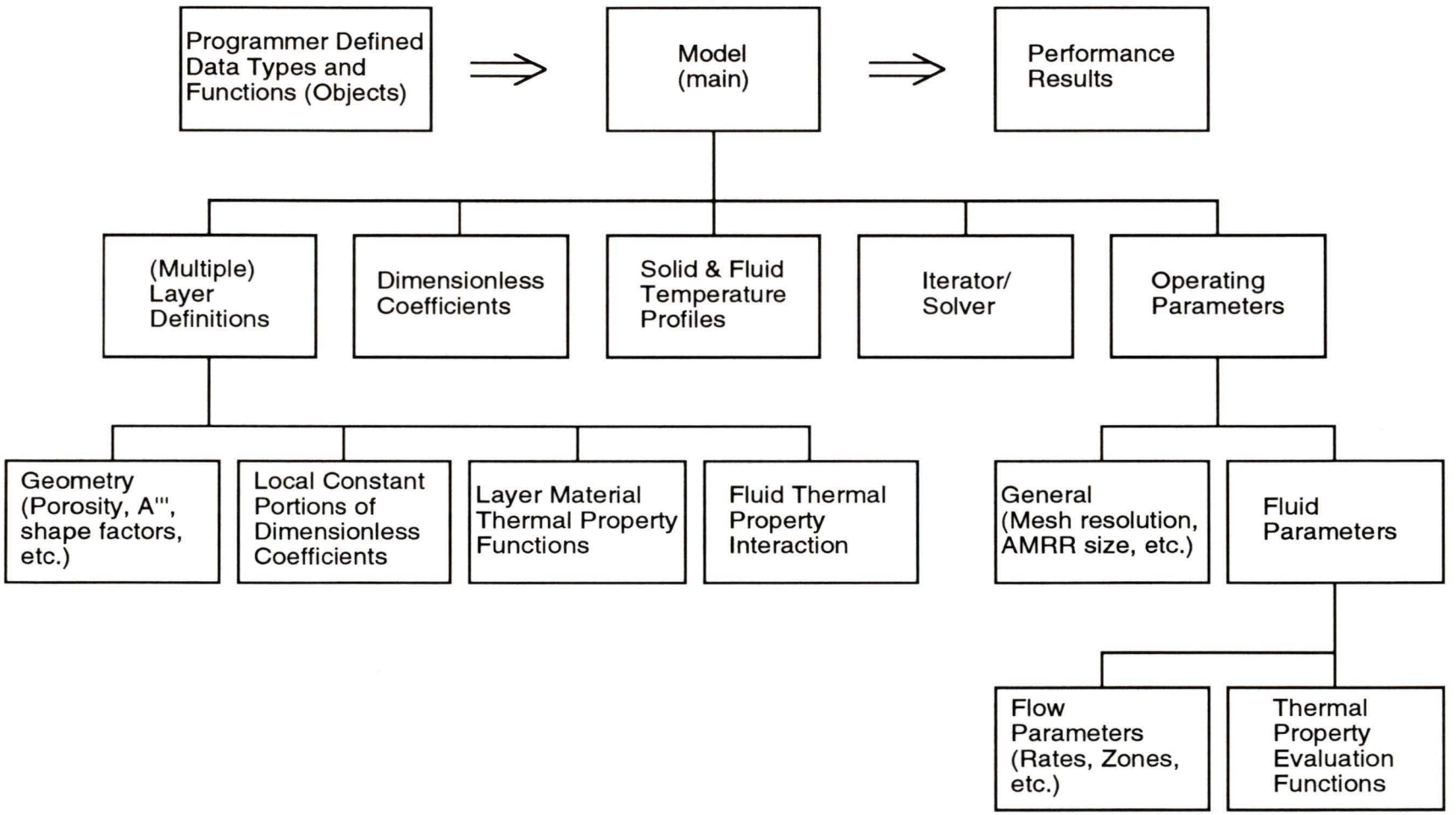


**Figure 5.1** Schematic diagram of the computer program used to solve the AMRR model.

### 5.2.3 Magnetic Field Profile

The quasi-steady-state rotary AMRR model has stricter requirements with respect to the application of the magnetic field to the magnetic matrix than transient linear reciprocating AMRR models. In the transient linear models, most researchers have modeled the application of the magnetic field by instantaneously adding the appropriate adiabatic temperature change to the regenerator solid. Effectively, this procedure models a step-function increase in the magnetic field from zero field to full field. In a practical device, magnetization of the solid will take some time, (when ramping up the current in the magnets, or when moving the magnetic solid into the magnetic field) and therefore the process for the porous magnetic regenerator won't be perfectly adiabatic.

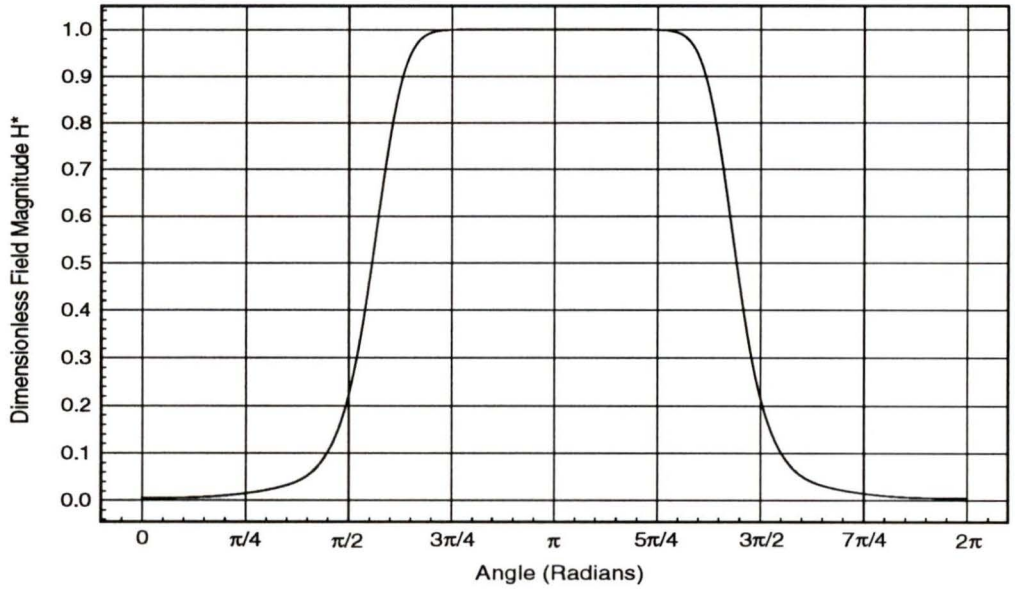


**Figure 5.2** Dimensionless magnetic field profile, $H^*$.

To more accurately describe a rotary device, the azimuthal magnetic field profile approximated a step function symmetrical about the centre of the magnetized flow region, but was smoothed to give bounded values for first and second derivatives. Further, a generic profile was used so that fields of different magnitudes could be modeled simply by specifying a scale factor for the profile.

Figure 5.2 gives the imposed dimensionless magnetic field profile as a function of angular position. In this profile, the field does not go to zero, but to a value fairly close to zero. This closely approximates real magnetic systems, where complete shielding of magnetic field is very difficult. Table C1 in Appendix C gives values for dimensionless field from 0° to 180°. Note that rotary AMR's pose a special problem for modelling efforts, in that the magnetic field profile must not be rotated out of phase with respect to the flow regimes, something that is much more easily done in the spatially defined system than in the transiently defined system.

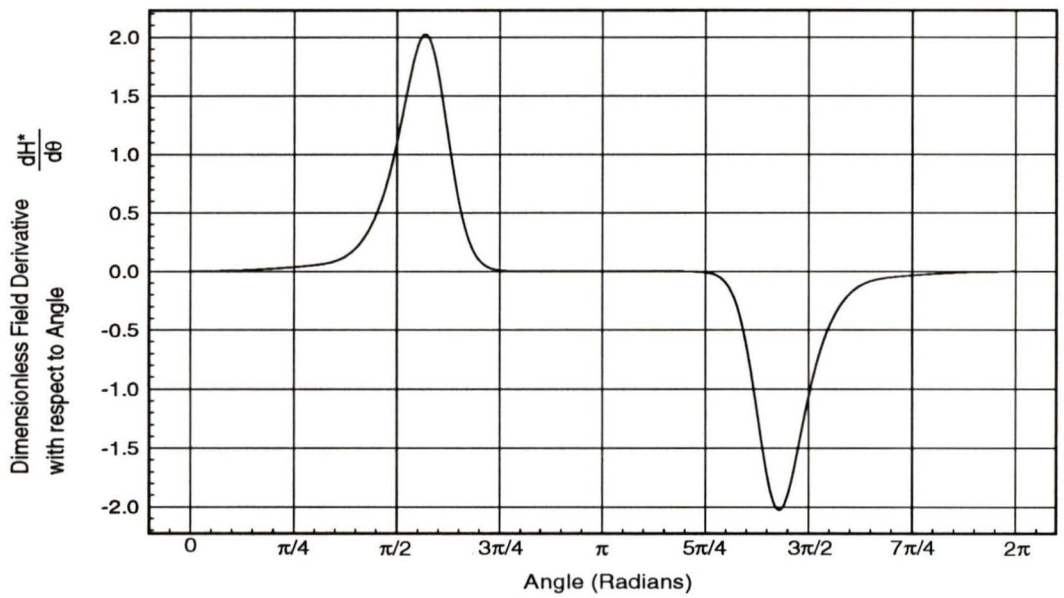


**Figure 5.3** 1st derivative of the dimensionless applied field, $dH^*/d\theta$.

The term representing the magnetocaloric effect in the solid equations shows that the magnetocaloric effect in the rotary system is dependent on both the local value of magnetic field and the local value of the derivative of the field. The field dependence comes about from the field dependence of the material properties, in particular, heat capacity and the change in magnetization with temperature at constant field. The field derivative dependence comes from the input of work of magnetizing the solid. Figure 5.3 gives the dimensionless field derivative with respect to angular position.

A standard field profile with no radial dependence was pre-calculated and stored as a lookup table and used for all models. When loading a model, the magnetic field profile was interpolated and coordinated to match the mesh size and relative positions of the flow and no-flow regions. Absolute field values were set by specifying the peak field value. From the interpolated field, the field derivative was calculated using a fourth-order accurate approximation. The computer model can accept any field profile, including those having a change in magnitude with radial position, as well as azimuthal position.

### 5.2.4 Active Magnetic Material

Any magnetic material can be modeled in an AMR, provided the appropriate thermodynamic properties for the material are given. The material properties required for this model for accurately representing magnetocaloric effect are heat capacity at constant applied field, $C_H$, change in magnetization with temperature at constant applied field, $\left(\frac{\partial M}{\partial T}\right)_H$, and change in magnetization with applied field at constant temperature, $\left(\frac{\partial M}{\partial H}\right)_T$. These values can be found experimentally, or, in some cases, numerically modeled. Other properties required are material density, $\rho_s$, electrical resistivity, $\rho_e$, and thermal conductivity, $k_s$.

The computer program developed to solve the AMRR energy equations is capable of modelling regenerators composed of multiple materials; however, this work employed only gadolinium as the working material, using magnetocaloric property data derived from a molecular field model and other property data taken from readily available literature. Thermodynamic properties of gadolinium that were used for modelling are given in Appendix D, where Figure D1 gives heat capacity, $C_H$, Figure D2 gives change in magnetization with temperature, $\left(\frac{\partial M}{\partial T}\right)_H$, and Figure D3 gives the change in magnetization with applied field, $\left(\frac{\partial M}{\partial H}\right)_T$, and Table D1 gives density, $\rho_s$, electrical resistivity, $\rho_e$, and thermal conductivity, $k_s$.

### 5.2.5 Heat Transfer Fluid

Almost any heat transfer fluid can be used in an AMRR; however, the energy balance equation for the fluid outlined previously includes the assumption that the change in fluid enthalpy with changes in pressure is negligible. This means that liquids and nearly ideal gases are most accurately modelled; whereas fluids with a strong pressure dependence on enthalpy, or that would experience a phase change within the AMRR are not suitable for this model.

All models in this thesis used 50 atm. helium as the heat transfer fluid. At this high pressure, helium acts as nearly an ideal gas. Properties were either evaluated as linearly varying with temperature, or constant with temperature. Constant properties were evaluated at a temperature given by the average of the inlet fluid temperatures, $T_c$ and $T_h$. Table D2 in Appendix D gives the fluid properties used for helium at 50 atm.

### 5.2.6 Heat Transfer Correlations

Numerous heat transfer correlations have been formulated by various researchers to represent the heat transfer coefficient, $h$, between fluids and solids of various shapes under different flow conditions. The modular design of the AMRR computer program allows for the easy addition of new correlations to a library of possible correlations that can be used for a given layer. Contained in the layer definition in each model input file is a specification of which correlation should be used to reflect the geometry of that layer. As a layer object in the program is constructed, the correct correlation as specified in the input file is also constructed and included as part of the layer object. There may be up to four different heat transfer correlations for a given layer, one for each of the four flow regimes. Usually, two correlations would be used, one for the two zones with fluid flow, and one for the two zones without fluid flow (but still having fluid entrainment). Each layer has its own independent heat transfer correlations, which are set to correspond to the geometry of the layer.

In this thesis, two heat transfer correlations were used, one for the zones with fluid flow, and one for the zones with no fluid flow. All layers consisted of randomly stacked spherical-particle packed beds. For the zones with fluid flow, the heat transfer coefficient was given by [64]:

Flow Zones Heat Transfer Coefficient Correlation:

$$h = 0.255\, C_p\, G(\alpha\, Re)^{-1/3}\, Pr^{-2/3} \tag{5.17}$$

where $h$ is the heat transfer coefficient, $C_P$ is the fluid heat capacity, $G=\dot{m}_f/A_c$ is the local fluid mass flow rate per unit free flow area, $Re=D_p \cdot G/\mu$ is the Reynolds number, $D_p$ is the particle diameter, and $\mu$ is the fluid viscosity. For the zones without fluid flow, the correlation for a single sphere in an infinite static medium was used:

No-Flow Zones Heat Transfer Coefficient Correlation:

$$Nu = 2 = \frac{h\, D_p}{k_f} \tag{5.18}$$

where $Nu$ is the Nusselt number, and $k_f$ is the fluid conductivity.

### 5.2.7 Fluid Conduction and Eddy Diffusivity

Several researchers have investigated the enhancement of thermal conductivity of the heat transfer fluid as a result of its flow conditions within packed particle beds [65], [66], [67], [68]. The effective conductivity is found to be composed of the static conductivity plus a component due to diffusion of the fluid within the solid. For the packed particle beds studied in this work, the effective conductivity of the fluid was given by:

$$\begin{aligned} k_{eff} &= k_f && Re < \frac{2\alpha}{Pr} \\ k_{eff} &= \frac{G\, D_p\, C_P}{2\alpha} && Re \geq \frac{2\alpha}{Pr} \end{aligned} \tag{5.19}$$

where $k_{eff}$ is the effective fluid thermal conductivity, $k_f$ is the "natural" fluid conductivity, $Pr=C_P \cdot \mu/k_f$ is the Prandtl number, $\alpha$ is the regenerator bed porosity, and all other terms are defined

as above. The effective fluid conductivity is used only for the purposes of calculating conduction within the fluid, and is not used in the calculation of heat transfer coefficient. The effective conductivity is further multiplied by the bed porosity and any geometrical factors to give the effective radial and azimuthal conductivities, $k_{fr}$ and $k_{f\theta}$.

### 5.2.8 Solution Algorithms

There are many algorithms that have been derived to solve PDE's. This work employed 3 different algorithms for solving the discretized energy balance equations. Each algorithm had its own benefits and drawbacks, and is described in turn in the following chapters.

# Chapter 6

# Fully Implicit Method

## 6.1 Description

One method employed to solve the solid and fluid energy balance equations was a fully implicit algorithm. In this algorithm, the complete set of solid and fluid equations are solved simultaneously for the entire problem domain. Iteration is required, but only as a result of the temperature dependence of the equation coefficients. In the simplified case where thermal properties are constant, only a single iteration is required. This algorithm has five steps:

1) Assume temperature profiles for the solid and fluid.
2) Evaluate the solid and fluid equation coefficients based on the current temperatures.
3) Represent the set of discretized equations in matrix form $[A]\{T\} = [B]$, where $[A]$ is the coefficient matrix, $\{T\}$ is the unknown solid and fluid temperatures, and $[B]$ is the equation residuals.
4) Solve for $\{T\}$.
5) Repeat from step 2) until converged.

## 6.2 Benefits and Drawbacks of the Fully Implicit Method

This algorithm has many benefits, most notably, quantifiable accuracy of the matrix solution set and minimum dependence of convergence time on regenerator reduced length. For a linear system of equations $[A]\{T\} = [B]$, the accuracy of the solution vector $\{T\}$ can be assessed by calculating the residual vector according to $\{r\} = [A]\{T\} - [B]$, where $\{r\}$ is the residual vector and $[A]$, $\{T\}$, and $[B]$ are as defined above. If $\{T\}$ can be solved exactly, $[r] = [0]$. In all solutions, the residual vector indicated the solution had less error than the uncertainty of the values of the

material thermal properties. In other words, the solution accuracy was limited by accuracy of thermal property data, not by the solution technique.

This method does have some drawbacks, however. Even though the coefficient matrix, *[A]*, is sparse and an optimized solver routine can be used to solve for the solid and fluid temperatures, *{T}*, the total memory storage requirements and solution time can be demanding. Memory storage for the coefficient matrix is given by:

$$S_M = K_M[8R^2(2C-3)+2R(C+4)] \tag{6.1}$$

where $S_M$ is the total memory required in bytes, $K_M$ is the memory required for one number in the matrix (typically 8 bytes for double precision numbers), $R$ is the number of nodes radially, and $C$ is the number of nodes azimuthally. Total memory required is larger, accounting for other variables and program storage itself, but for most meshes used, the coefficient matrix accounted for over 85 % of the total memory required. Figure 6.1 gives the form of the resulting system of equations for this method and the portion of the coefficient matrix for which memory storage is required. Note that the coefficient matrix has two "fringes"; one in the upper right corner and one in the lower left corner. These fringes provide the azimuthal self-consistency, coupling the start of the nodal numerical boundary with the end of the nodal numerical boundary. The fringes account for 50 % of the memory requirements of this method.

The matrix solution time per iteration is given by:

$$t = K_T R^3 C^2 \tag{6.2}$$

where $t$ is the total solution time per iteration, and $K_T$ is a proportionality constant dependent on the computer used. For a Sun Sparc 10, model 30, $K_T$ is approximately $9 \times 10^{-7}$ s, providing the entire problem fits in main memory and is not swapped to virtual memory on disk. Figure 6.2 gives the solution time per iteration on a Sun Sparc 10, model 30 for various model mesh sizes. Datapoints have been joined in this figure to distinguish the trends. Typically, a minimum of 8

**Figure 6.1** Form of system equations for the fully implicit solution technique with coefficient matrix memory storage requirements highlighted.

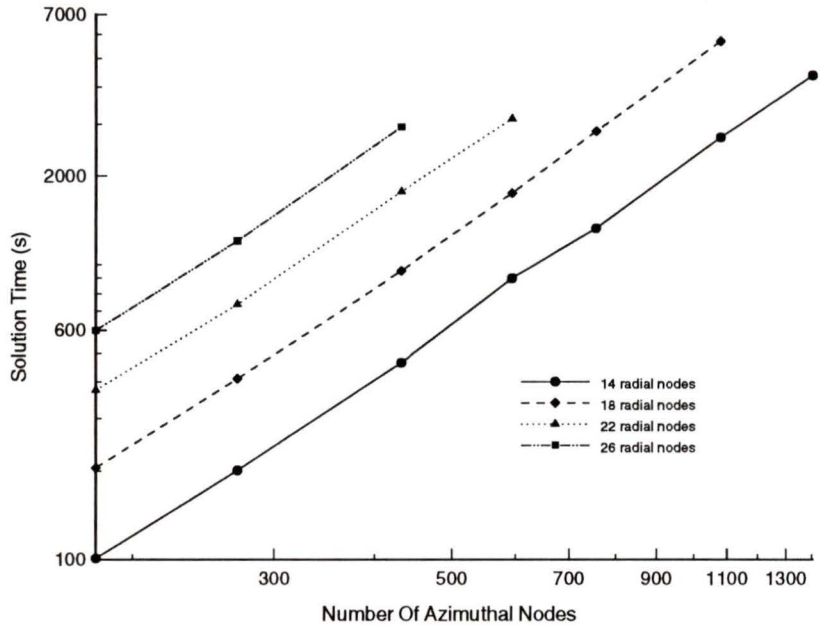


**Figure 6.2** Solution time per iteration vs. azimuthal mesh size for various radial mesh sizes for the fully implicit method (on a Sun Sparc 10, model 30).

matrix solution iterations were required when temperature-dependent physical properties were used.

One half of the memory storage requirement of this method is caused by the azimuthal continuity requirement where derivatives at the mesh numeric boundary are evaluated *in modulo*. The continuity requirement adds two fringes to the simple form of a pentadiagonal with two off-diagonals in the coefficient matrix, *[A]*. These fringes are responsible for the majority of the matrix solution time. For example, a simple test showed that for a mesh with 24 nodes radially and 180 nodes azimuthally, the matrix solution time could be reduced by a factor of 27 if the fringes could be eliminated. This incentive formed the basis for a second solution algorithm.

# Chapter 7

# Mostly Implicit Method

## 7.1 Description

The fully implicit method described in the previous chapter can be modified to help alleviate its memory and solution time requirements if the azimuthal continuity fringe elements are removed from the coefficient matrix. If reasonable approximations to the temperatures at the azimuthal numeric boundary are given, the fringes of the coefficient matrix can be pre-multiplied by the approximate temperatures and the result moved into the residual matrix as a "known" quantity. This reduces the coefficient matrix to the form of a pentadiagonal with two off diagonals, which can be solved many times faster than the full coefficient matrix with fringes. Further, the memory requirements of the coefficient matrix without fringes is half that of the full coefficient matrix.

This modified system of equations approximates the solution to the full coefficient matrix. The better the approximation of the temperatures at the numeric boundary, the closer the solution of the modified matrix is to the full matrix. If the coefficient matrix is LU decomposed (where the coefficient matrix is "decomposed" into an upper triangular matrix and a lower triangular matrix that can be quickly solved using back-substitution) using, for example, the skyline solution method [59], an iterative improvement of the solution matrix can be obtained using iterative improvements to the residual matrix and successive back substitutions. The successive back substitutions are computationally less intensive than the decompositions, so several iterative back substitutions can be performed to improve the overall solution before time is better spent on improving and re-decomposing the coefficient matrix to reflect any changes in the temperature dependent coefficients.

The modified implicit or "mostly" implicit method has eight steps:

1) Assume temperature profiles for the solid and fluid.
2) Evaluate the solid and fluid equation coefficients based on the current temperatures.
3) Represent the set of discretized equations in matrix form of $[A]\{T\} = [B]$, where $[A]$ is the coefficient matrix, $\{T\}$ is the unknown solid and fluid temperatures, and $[B]$ is the equation residuals.
4) Approximate the discretized equations by rewriting the equations in the form of $([A] - [F])\{T\} \approx [B] - [F]\{T'\}$, where $[F]$ is the fringe portion of the coefficient matrix and $\{T'\}$ is the current assumed solid and fluid temperature profiles.
5) Solve for $\{T\}$.
6) Improve the right hand side expression by using the new solution for $\{T\}$ determined in step 5).
7) Repeat from step 5) until iteration changes are "small".
8) Repeat from step 2) until converged.

## 7.2 Benefits and Drawbacks of the Mostly Implicit Method

This algorithm gave results consistent with the fully implicit method, but took longer to do so. While this method has a very rapid iteration cycle time, it requires too many iterations for a rapid overall solution. The iteration steps 5) and 6) result in only modest changes in the solution matrix on each iteration. There might be an opportunity to employ several acceleration techniques using the results from the iteration steps 5) and 6) to achieve a rapid solution, but that has been left for future work.

# Chapter 8

# Mixed Implicit/Explicit Method

## 8.1 Description

A third algorithm developed to solve the AMRR fluid and solid finite difference equations was a mixed implicit and explicit method. In this method, one radial row at a time, the fluid equation was solved implicitly, and then the solid equation solved explicitly. The fluid equation for a given radial row of nodes was represented as a matrix set of equations and solved simultaneously to give the fluid temperatures for the row. The solid equation for the same row was then calculated explicitly node by node for the solid temperature azimuthal derivative, taking every temperature in the row as known from previous iterations. The solid temperature for the next row was then approximated by a Taylor series expansion about the current row using the calculated derivative for the row.

The mixed implicit/explicit algorithm has nine steps:

1) Assume temperature profiles for the solid and fluid.
2) Consider the solid temperatures for a radial segment at the current row $\theta$ as known and the fluid temperatures as unknown.
3) Evaluate the fluid equation coefficients based on the current fluid temperatures.
4) Implicitly solve the set of fluid equations for the row. The fluid equations for the row generate a tri-diagonal matrix which is easily and quickly solved using the Thomas algorithm [60].
5) Evaluate the solid equation coefficients based on the current solid temperatures.

6) Explicitly evaluate the solid equation to give a value for the solid temperature derivative, $\frac{dT_s^*}{d\theta}$, for the row by expressing the solid equation in the form,

$$\frac{dT_{s_\theta}^*}{d\theta} = f\left(T_{s_\theta}^*, T_{f_\theta}^*, M_E, K_s, \Omega\right) \tag{8.2}$$

where the right hand side expression is given by the right hand side expression of Equation (3.25), a function of $T_{s\theta}^*$ and $T_{f\theta}^*$, the solid and fluid temperatures at the current node, respectively, $M_E$, the nodal magnetocaloric effect, $K_s$, the nodal radial and azimuthal conduction, and $\Omega$, the nodal eddy current power.

7) Approximate the temperature of the solid for the next row $\theta + \Delta\theta$ using a Taylor series expansion expression about the current row,

$$T_{s_{\theta+\Delta\theta}}^* = T_{s_\theta}^* + \frac{dT_{s_\theta}^*}{d\theta}\Delta\theta$$

8) Move to the next row and continue from step 2 until all rows azimuthally have been processed to complete one cycle.

9) Continue cycling until the temperatures converge and temperature cyclic continuity is achieved.

## 8.2 Benefits and Drawbacks of the Mixed Implicit/Explicit Method

This algorithm has many benefits, including, simplicity, very low memory storage requirements, rapid solution time per row, and a facility for extremely fine meshes. Unfortunately, this method has three significant drawbacks. First, for an explicit formulation of the regenerator equations, as the regenerator reduced length, $\Lambda$, is increased, the number of cycles to convergence increases [5]. This is caused by the slow propagation of boundary information into the interior of the solution space. In this work, for high reduced length, $\Lambda \geq 200$, the number of cycles to

convergence exceeded 50,000. This large number of cycles causes the total solution time to be quite long, negating the benefits of the short iteration cycle time.

A second drawback of this method is that convergence is nearly linear for the majority of the solution, hence it is not possible to employ common solution acceleration techniques. Reference [5] gives an example of an acceleration method used in passive regenerator studies (and applicable to this class of iterative problems). Acceleration was attempted with this algorithm, but it was found that the acceleration stability criterion was either violated or marginally satisfied, with a resultant divergence of the solution.

A third drawback of this technique was that for most of the AMRR designs of interest, a large number of cycles was required for convergence, and the accumulated integration error per cycle

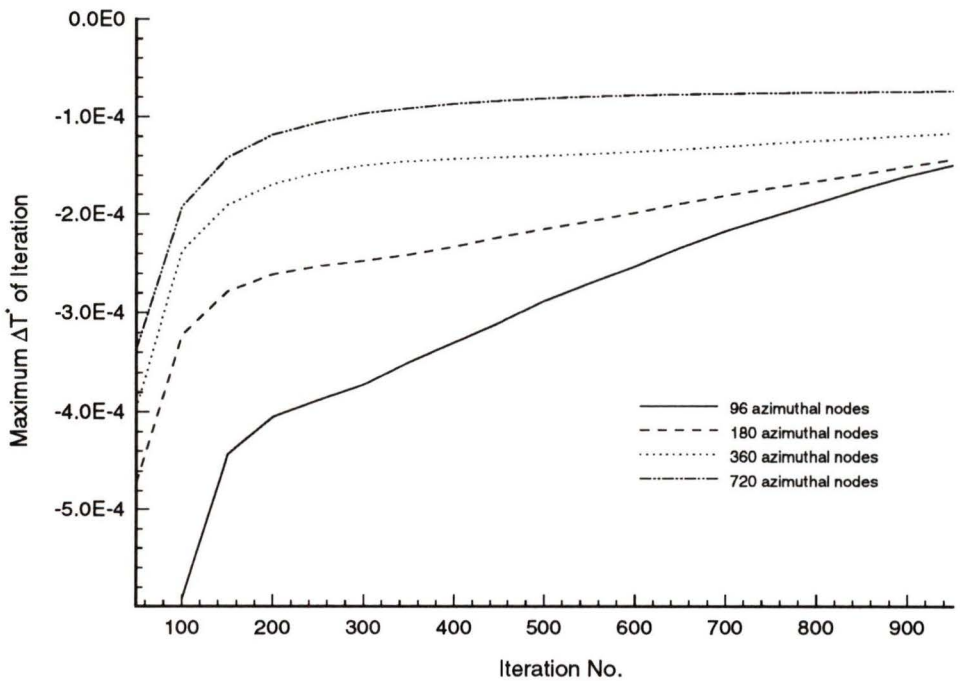


**Figure 8.1** Maximum change in reduced temperature, $\Delta T^*$, as a function of iteration number for the mixed implicit/explicit method.

became potentially comparable to the temperature convergence per cycle. This effect can be seen

in Figure 8.1. Beyond the first few hundred iterations, the convergence of the solution slows, and the solution steadily but slowly moves to a final temperature profile. As a result, the slow propagation of boundary information was in competition with the integration error to determine the final temperature profile. The profile therefore contains unquantifiable and inseparable integration error.

To help alleviate the integration error in this method, step 7) above was modified to include higher order derivatives calculated from the profiles of previous cycles. For the first few cycles, where higher order derivatives could not yet be evaluated, these terms were set to zero. This addition reduced the integration error per cycle, but did not affect the total number of cycle iterations required. It was still not possible to quantify the contribution of the integration error in the final temperature profiles, so the fully implicit algorithm was used.

# Chapter 9

# AMRR Model Results

## 9.1 Model Validation

The computer models developed consist of thousands of lines of object-oriented code in the C++ language, and were subjected to several levels of code validation and model validation. The primary level of code validation was subroutine validation, where every subroutine's output was compared to hand calculated values. Validated subroutines were organized into C++ objects, which were then validated in the same fashion. Finally, validated C++ objects were assembled into a complete code, which was subjected to the last level of validation.

There are no other models of a rotary AMRR, consequently, results for "standard cases" do not exist for use in comparisons. Further, published results for AMRR's have given insufficient details to approximate the work. For this reason, the model had to be evaluated in parts under different boundary conditions, and a presumption was made that the sum of the verified parts constitutes a verified whole. Several qualitative and quantitative tests were performed. For example, the magnetocaloric effect was independently tested by uncoupling the fluid equation from the solid equation by specifying zero heat transfer between solid and fluid, and imposing a radial temperature profile boundary condition for one row of nodes. The eddy current terms and conduction terms were turned off, leaving only the magnetocaloric term in Equation (3.25). When solved, this system gave the correct magnetocaloric adiabatic temperature change as a function of field and temperature, and gave an azimuthally consistent solution. In other cases, the magnetic field was specified as zero, giving in effect a passive rotary regenerator. These results were compared to results for passive regenerators and were found to be consistent. Further, effects of extremely high flow rates and low flow rates were compared qualitatively to expected profiles.

Finally, the model acts to solve energy balances on a local basis, and using the solid and fluid temperature solution profiles provides a means of verifying the energy balance on a global basis.

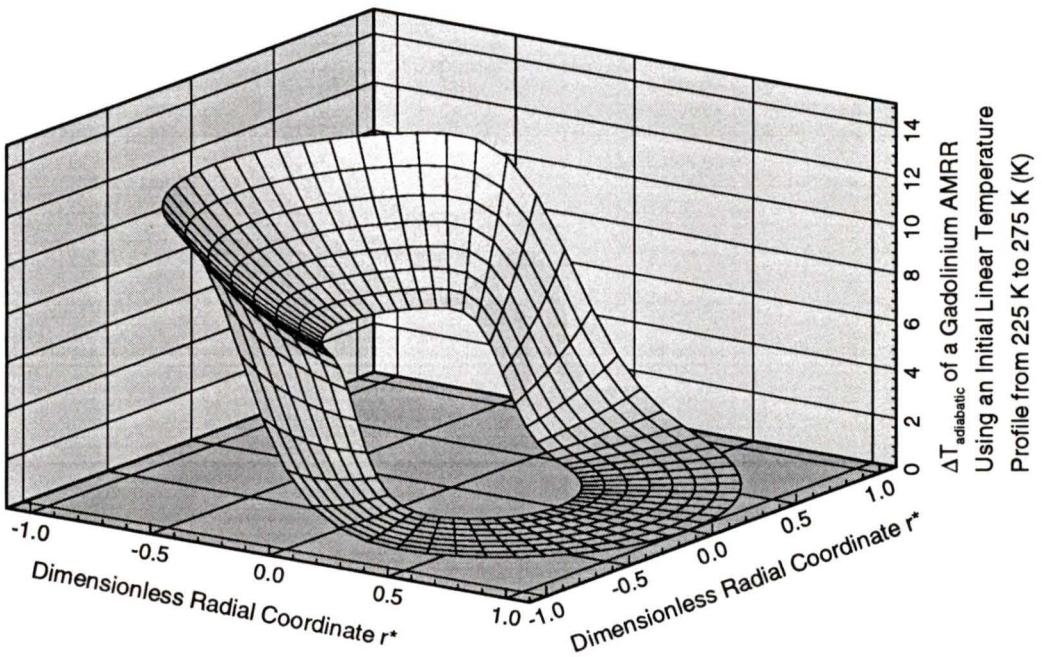


**Figure 9.1** $\Delta T_{adiabatic}$ of a Gadolinium AMRR subjected to a peak field $\mu_0 H$ = 7.5 Tesla starting from $Tc$ = 225 K and $T_h$ = 275 K.

Figure 9.1 gives the adiabatic temperature change for an AMRR with an initial temperature profile from 225 K at the inner radius to 275 K at the outer radius subjected to a peak applied field $\mu_0 H$ = 7.5 Tesla. The vertical axis gives the adiabatic temperature change, while the horizontal axes represent the position in the AMRR wheel. The overlaid mesh is used to show the concavity of the profile, consistent with the increasing adiabatic temperature change with increasing temperature for this temperature range.

## 9.2 Minimum Mesh Sizes

The global energy balance was found to be a good indicator of the required minimum sizes. As the mesh number increased (and mesh size therefore decreased), the energy balance improved. Further, the global energy balance indicated that more azimuthal nodes are needed for active regenerator cases than for passive cases. This can be explained in part by the limitations of the first-order azimuthal approximation and the effect on the temperature profile of the magnetocaloric effect. The explanation is given in two parts, first by considering the influence of the magnetic field on magnetocaloric effect, and second by considering the accuracy of the first-order approximation to the azimuthal derivatives.

Increasing magnetocaloric effect, by definition, increases the solid temperature change as the solid rotates into or out of the high field region. Outside the neighbourhood of the material's Curie point, the change in magnetization with temperature and the heat capacity are weak functions of field and temperature. In this case, magnetocaloric effect is closely approximated by a constant times the change in field. In the absence of heat transfer or with very limited heat transfer, the solid will assume a profile that approximates the shape of the applied magnetic field. If the solid

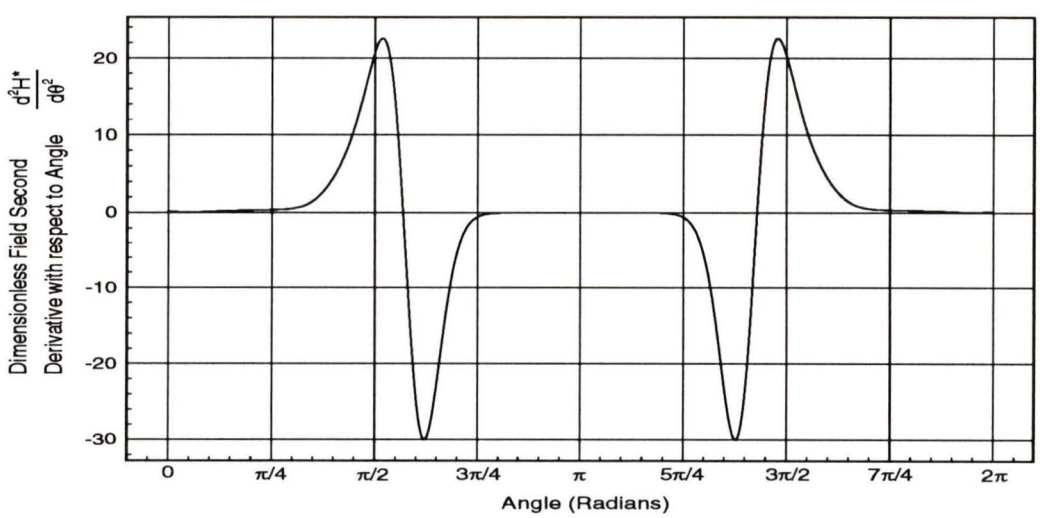


**Figure 9.2** 2nd derivative of the dimensionless applied field, $d^2H^*/d\theta^2$.

temperature profile very nearly approximates the profile of the magnetic field, then the derivatives of temperature will very nearly approximate the profiles of the derivatives of the field, where the field and temperature profiles differing only in magnitude and units. Figure 9.2 gives the second derivative with respect to azimuthal coordinate of the dimensionless applied magnetic field as a function of azimuthal coordinate.

In the first-order backwards difference scheme, the error from the truncation of higher order terms of the Taylor series expansion for the first derivative of some property $u$ with $\theta$ is given by:

$$T.E. = \left(\frac{d^2u}{d\theta^2}\right)\frac{\Delta\theta}{2!} - \left(\frac{d^3u}{d\theta^3}\right)\frac{(\Delta\theta)^2}{3!} + \left(\frac{d^4u}{d\theta^4}\right)\frac{(\Delta\theta)^3}{4!} - \ldots \qquad (9.1)$$

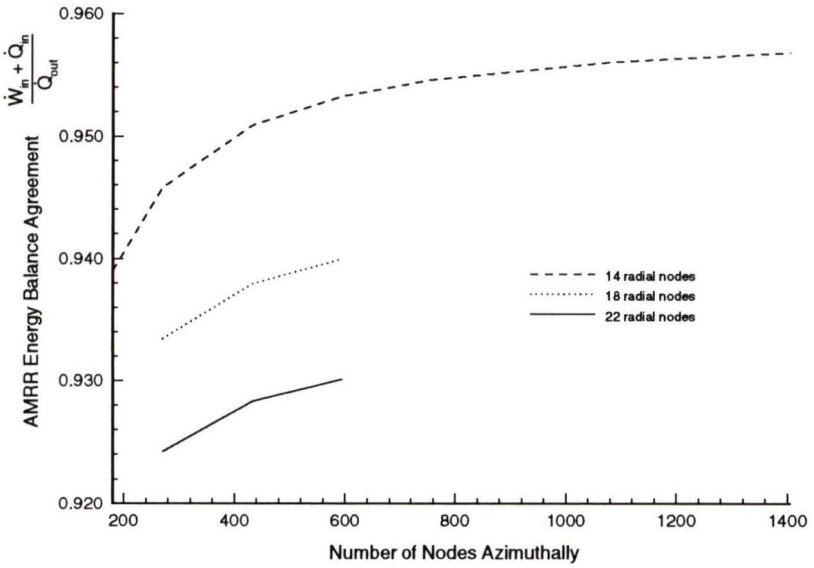


**Figure 9.3** AMRR global energy balance as a function of azimuthal mesh size.

As the solid assumes the profile with the large second order (and higher) derivatives, the truncation error increases, and consequently, the first order scheme requires more azimuthal mesh points to accurately represent the first derivative term. Figure 9.3 gives the dependence of global

energy balance as a function of azimuthal mesh size for a typical AMRR model. The vertical axis gives the sum of heat load in and work in divided by the heat load out. The closer this ratio is to 1, the better is the energy balance. In contrast to the active cases, the passive cases give a global energy balance in excess of 99.99 % at 720 azimuthal nodes (where work in was zero).

## 9.3 Selected Results

### 9.3.1 Passive Regenerators

The results for passive regenerators proved interesting because of the facility to visualize the transition of regenerator profiles with time. Traditionally, regenerator profiles have been "snapshots" in time, or sequences of discrete snapshots to represent the variation of temperature

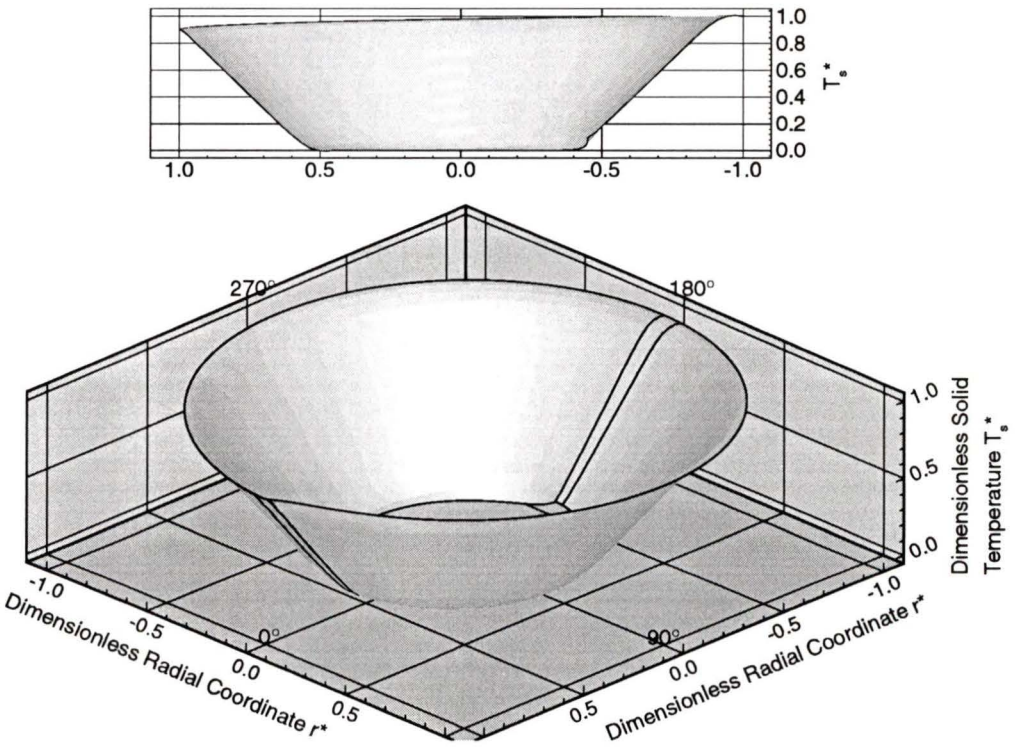


**Figure 9.4** Passive regenerator solid dimensionless temperature profile ($\Pi$ = 5, $\Lambda$ = 65, $T_h$ = 280 K, $T_c$ = 230 K).

with time. The polar geometry inspired a polar representation of regenerator temperature profile. In the polar geometry, an azimuthal coordinate is equivalent to a time coordinate. Figure 9.4 gives the polar representation of the solid dimensionless temperature in a passive regenerator model with $\Pi = 5$ and $\Lambda = 65$. The vertical axes on both the lower and upper figures give the dimensionless temperature of the solid corresponding to the position in the AMRR wheel as shown by the horizontal axes. The hot blow region is shown in the foreground, starting at 0° and ending at 170°. The two no-flow regions are shown on the left and right sides and are each 10° wide. The cold blow region is shown in the background. The boundaries of the flow zones are given by solid lines along the temperature profile. The regenerator rotates counter-clockwise.

A cutaway view showing the limits of the cold blow region is given in the upper portion of the figure and shows the radial temperature dependence at the ends of the hot and cold blow periods. Note the similarity between these profiles and those given in Figure 1.9 in chapter 1. The model input file for this passive regenerator is given in Appendix B.

### 9.3.2 Active Regenerators

The initial results from modelling active regenerators have already provided design guidelines. Figure 9.5 gives the polar representation of the solid temperature profile for an AMRR with $\Pi = 18$, $\Lambda = 700$, using a peak applied field of 6.5 Tesla. The flow zones for this model were 100° each for hot and cold blow regions, and 80° each for the no-flow regions. The start of the hot blow (demagnetized) region is at 0°, and the regenerator rotates counter-clockwise. The cold blow flow region was centred with the peak magnetic field. To a first approximation, the solution looks like that for the passive case, except for an increase in the solid temperature profile under the magnetic field region. A closer look reveals that the radial profile is more "bowl-shaped" than for the passive case. A thorough investigation of the nature of the radial profile is suggested for further work. The model input file for this active regenerator is given in Appendix B.

Figure 9.6 gives the solid temperature profile for an AMRR case identical to the above, except that the flow zones are not properly synchronized with the applied field so that flow starts and ends 20° too late. In effect, this allows flow during solid demagnetization, violating the adiabatic demagnetization criterion. From the diagram, a small temperature hook on the inner radius is

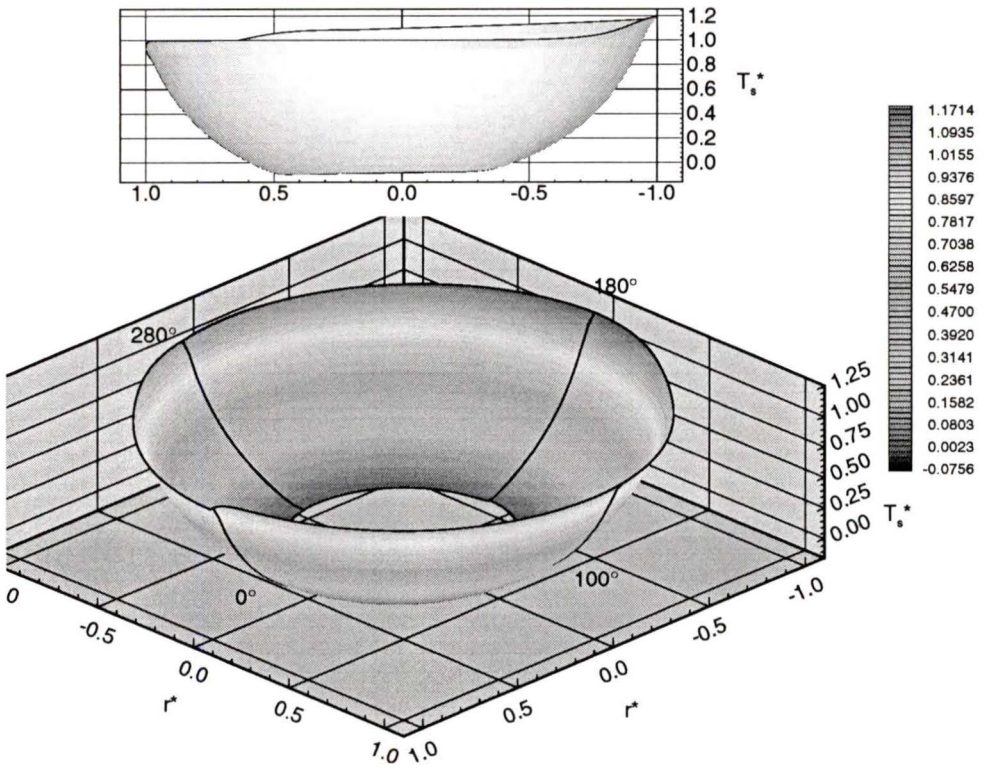


**Figure 9.5** AMRR solid dimensionless temperature profile ($\Pi$ = 18, $\Lambda$ = 700, $\mu_0 H_{max}$ = 6.5 T, $T_h$ = 275 K, $T_c$ = 225 K).

apparent. It is postulated that the hook is caused by isothermal demagnetization of the inner radius on exit from the high field region. For moderate flow rates, the solid at the inner radius equals the fluid temperature by the end of the high field region. Upon demagnetization, the solid temperature drops below that of the fluid, but if flow is continued, the fluid acts to warm the solid. There is not enough time for the fluid energy transfer to deeply penetrate the regenerator bed, but there is enough time to ensure that the inner radius is warmer than some point just inside the inner radius.

This last result was particularly unexpected and inspired some serious consideration of the required field profile for rotary systems. In particular, with high reduced length, $\Lambda$, the

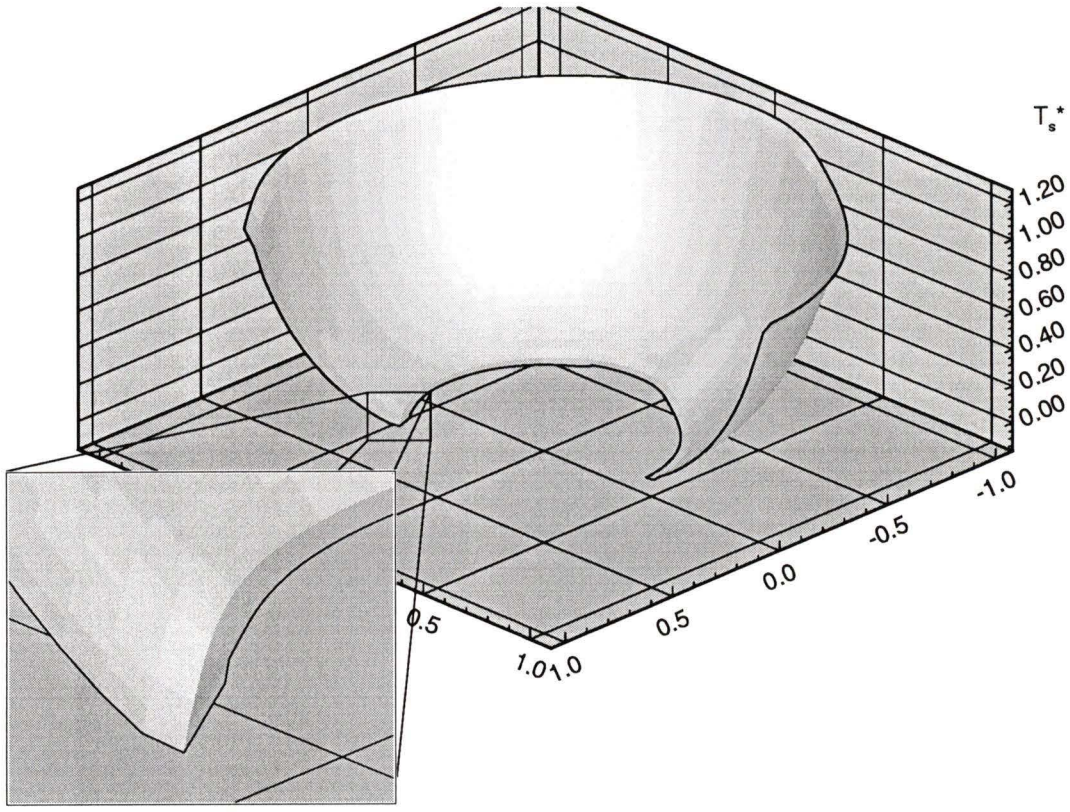


**Figure 9.6** AMRR solid dimensionless temperature profile, flow ending 20° too late and into demagnetization region ($\Pi$ = 18, $\Lambda$ = 700, $\mu_0 H_{max}$ = 6.5 T).

temperature difference between solid and fluid is approximately given by:

$$\Delta T \approx \frac{T_h - T_c}{\Lambda}$$

For a regenerator spanning 50 K, and having a reduced length of $\Lambda$ = 700, the approximate temperature difference between solid and fluid is 0.07 K. Under a 7 Tesla field, a drop in field of only 1 % will cause the solid temperature of the solid to drop to that of the fluid. A drop of 2 % in applied field would cause the solid to be colder than the local fluid, and the solid would warm. If the solid is warmed, it is not providing power input but is acting like a generator. There

is recovery of the work previously input to the solid, but the proportion of useful work to total work in the system is decreased. This increases the entropy production, increases the amount of working material required to give a particular cooling power, and lowers the cycle efficiency. An increase in magnet costs will be associated with increased field uniformity.

# Chapter 10

# Conclusions and Recommendations

## 10.1 Conclusions

The full solid and fluid energy equations were developed and solved for a rotary active magnetic regenerative refrigerator. Several solution algorithms were explored, namely, a fully implicit method, a "mostly implicit" method, and a mixed implicit/explicit method. Although each algorithm had its own advantages, the fully implicit algorithm was found to give the most accurate and reliable results in a reasonable time.

Global energy balance checks on the solutions from the fully implicit method indicate excellent accuracy for passive regenerators, but also indicate a need for better solution accuracy for active regenerator models. This accuracy can be achieved through refinement of the problem discretization mesh, but refinement dictates a significant increase of computation time and computer memory. Accuracy can also be improved if higher order discretization can be employed for azimuthal derivatives; however, the discretization method cannot be of second order because that would cause unconditional instability in the solution. Therefore, a third-order scheme or significantly more powerful computer equipment will be required if higher accuracy is to be obtained.

Initial solution results have provided insight into the design of AMRR's. Results have indicated that high performance regenerators will have small solid-fluid temperature differences, and consequently, very small deviations in the applied magnetic field profile could cause some sections of the AMRR to act as a generator, rather than as a refrigerator. From a theoretical standpoint, this will give a net reduction in the cooling power per unit mass of working material. This

phenomenon should be studied in detail to determine the required field uniformity on a AMRR for a given performance versus the total magnet cost.

Rotary AMRR temperature profiles are similar in some respects to temperature profiles of passive regenerators, but with two significant differences. First, the azimuthal variation in profile reflects the magnetocaloric effect of the material under the application of the applied field. Second, the radial variation in profile is more "bowled" than linear, and reflects to some degree the change in magnitude of material magnetocaloric effect with temperature. The complete ramifications of this result with respect to distribution of work in the system and cycle efficiency are not yet known, and therefore this area warrants future research.

## 10.2 Recommendations

The model described by this thesis should be further refined to overcome the limitations of the available computer hardware. There are many algorithms that have been proposed to solve simultaneous partial differential equations, while only three algorithms (with minor variations) were explored. Further, some techniques explored have potential for application of acceleration techniques. It is reasonable to expect that a better algorithm exists for solving these complicated equations; the task is then to find it.

The AMRR computer program developed has the capacity to model multiple layers of materials; however, this ability was not exploited in this work. Multiple materials could optimize the performance of an AMRR by maximizing the work capacity of the regenerator materials at their operating temperatures. The effects of multiple materials should be explored in future work.

Exploration of the many design parameters of rotary AMRR's has only just begun with the introduction of this computer model. Some interesting phenomena have been observed, and further research will undoubtedly reveal more. An investigation of proposed AMRR designs should be conducted concurrently with incremental improvements in the solution algorithm.

# References


1. Cross, C.R., J.A. Barclay, A.J. DeGregoria, S.R. Jaeger, J.W. Johnson, "Optimal temperature entropy curves for magnetic refrigeration", Advances in Cryogenic Engineering, Vol. 33, pp. 767-775 (1988).

2. Barclay, J.A., "A comparison of the efficiency of gas and magnetic refrigerators", Proceedings of the 22nd National Heat Transfer Conference, Niagara Falls, New York (1984).

3. Barclay, J.A., "A 4 K to 20 K Rotational-Cooling Magnetic Refrigerator Capable of 1-mW to >1-W Operation", Cryogenics, 20, 468-471 (1980).

4. Barclay, J.A., "The theory of an active magnetic regenerative refrigerator", NASA report NASA-Conference Publication-2287 (1983).

5. Schmidt, F.W. and J. John Willmott, *Thermal Energy Storage and Regeneration*, Hemisphere Publishing Corporation, Washington D.C. (1981).

6. DeGrogoria, A.J., "Modeling the Active Magnetic Regenerator", Advances in Cryogenic Engineering, 37, 867-873 (1991).

7. DeGrogoria, A.J., "Test Results of an Active Magnetic Regenerator", Advances in Cryogenic Engineering, 37, 875-882 (1991).

8. Green G.F., G. Patton, J. Stevens, J. Humphrey, "Magnetocaloric Refrigeration," DTNSRDC Report 87/032 (1987).

9. Walker, G., *Cryocoolers Part 1: Applications*, Plenum Press, New York (1983).

10. Walker, G., *Cryocoolers Part 2: Applications*, Plenum Press, New York (1983).

11. Hausen, H., *Heat Transfer in Counterflow, Parallel Flow and Cross Flow*, McGraw-Hill, New York, (1983).

12. Anderson, D.A., J.C. Tannehill, R.H. Pletcher, *Computational Fluid Mechanics and Heat Transfer*, Hemisphere Publishing Corporation, New York, (1984).

13. Shih, T.M., *Numerical Heat Transfer*, Hemisphere Publishing Corporation, New York, (1984).

14. Mitchell, A.R., D.F. Griffiths, *The Finite Difference Method in Partial Differential Equations*, John Wiley & Sons, New York (1980).

15. Patankar, S.V., *Numerical Heat Transfer and Fluid Flow*, W.J. Minkowycz and E.M. Sparrow, ed., Hemisphere Publishing Corporation, New York (1980).

16. Bejan, A., *Advanced Engineering Thermodynamics*, John Wiley & Sons, New York, (1988).

17. Callen, H.B., *Thermodynamics and an Introduction to Thermostatistics*, 2nd ed., John Wiley & Sons, New York, (1985).

18. Leyarovski, E., L. Leyarovska, Chr. Popov, "Techniques of the adiabatic experiments in high magnetic fields below 1 K", Proceedings of the 8th International Cryogenic Engineering Conference, pp. 466-470, Geneva (1980).

19. Kittel, P., "Refrigeration below 1 K in space", Physics 108(B), 1115-1118 (1981).

20. Kittel, P., "Eddy Current Heating in Magnetic Refrigerators", Advances in Cryogenic Engineering, 35, 1141-1148 (1990).

21. Yazawa, T., A. Sato, H. Ogiwara, J. Yamamoto, "Adiabatic demagnetization system for infrared detector", Proceedings of the 12th International Cryogenic Engineering Conference, pp. 621-625, Southampton (1988).

22. Serlemitsos, A.T., B.A. Warner, S. Castles, S.R. Breon, M. San Sebastion, T. Hait., "Adiabatic demagnetization refrigerator for space use", Proceedings of the 16th International Cryogenic Engineering Conference, (1989).

23. Zhang, L. S.A. Sherif, T.N. Veziroglu, J.W. Sheffield, "Performance analysis of reciprocating magnetic liquefiers", International Journal of Hydrogen Energy, 19, 945-956 (1994).

24. Steyert, W.A., "Magnetic refrigerator development", September 1 - November 30, 1977 Los Alamos Progress Report, No. LA-7165-PR (1978).

25. Barclay, J.A., J.C. Bronson, W.A. Steyert, "Magnetic regrigerator development, June 1 -August 31, 1979", Los Alamos Scientific Laboratory report, No. LA-8066-PR (1979).

26. Barclay, J.A., O. Moze, L. Paterson, "A reciprocating magnetic refrigerator for 2-4 K operation: initial results", Journal of Applied Physics, 50, 5870-5877 (1979).

27. Johnson, D.L., "Reciprocating magnetic refrigerator", Proceedings of the 3rd NBS Cryocooler Conference, pp. 33-41, Boulder, Colorodo (1984).

28. Nakagome, H., N. Tanji, O. Horigami, H. Ogiwar, T. Numazawa, Y. Wantanabe, T. Hasimoto, "The helium magnetic refrigerator I: development and experimental results", Advances in Cryogenic Engineering, 29, 581-587 (1984).

29. Seyfert, P., P. Bredy, G. Claudet, "Construction and testing of a magnetic refrigeration device for the temperature range of 5 to 15 K", Proceedings of the 12th International Cryogenic Engineering Conference, pp. 607-611, Southampton (1988).

30. Matsumoto, K, T. Ito, T. Numazawa, T. Hashinmoto, T. Kuriyawa, H. Nakagome, "A fundamental study of a regenerator for an Ericsson magnetic refrigerator", Proceedings of the 11th International Cryogenic Engineering Conference, pp. 256-261, Berlin-Weas (1986).

31. Matsumoto, K., T. Ito, T. Hashimoto, "An Ericsson magnetic refrigerator for low temperature", Advances in Cryogenic Engineering, 31, 743-750 (1988).

32. Barclay, J.A., "An analysis of magnetic refrigeration for air conditioning applications", Los Alomos National Laboratory report LA-7950-MS (1979).

33. Rogner, H-H., "Natural gas as the fuel of the future", Annual Review of Energy, 14, 14-73 (1989).

34. Intergovernmental Panel on Climate Change (IPPC) (1990), "Climate Change : the IPCC scientific assessment", Cambridge University Press, New York, 1990.

35. Scott, D.S., W. Häfele, "The coming hydroden age: Preventing world climatic disruption", International Journal of Hydrogen Energy, 15, 727-737.

36. Lee, T.H., H.R. Linden, D.A. Dreyfus, T. Vasko, *The Methane Age*, Kluwer Academic Publishers & IIASA, Dordrecht, 1988.

37. Costs, Inpacts, and Benefits of $CO_2$ Mitigation, Y. Kaya, N. Nakicenovic, W.D. Nordhaus, F.L. Toth, ed., Proceedings of a workshop at IIASA, Laxenburg, Austria, 1992.

38. Petsinger, R.E., "Natural gas quality in North America", Proceedings of Gaseous Fuels for Transportation Conference, pp. 529-571, Vancouver (1986).

39. Waynert, J.A., A.J. DeGregoria, R.W. Foster, A.J. Barclay, "Evaluation of Industrial Magnetic Heat Pump/Refrigerator Concepts that Utilize Superconducting Magnets", Argonne National Laboratory report ANL-89/23, June (1989).

40. Carpetis, C., "Numerical Study of Magnetic Refrigeration including Consideration of Magnetic Nanocomposites", Proceedings of the 18th International Congress of Refrigeration, Montreal (1991).

41. Barclay, J.A., "Prospects for Magnetic Liquefaction of Hydrogen", Proceedings of the 18th International Congress of Refrigeration, Montreal (1991).

42. Schroeder, E., "Performance predictions of a Magnetocaloric Refrigerator using a Finite Element Model", Advances in Cryogenic Engineering, 35, 1149-1155 (1990).

43. Green, G., G. Patton, J. Stevens, J. Humphrey, "Magnetocaloric Refrigeration", David Taylor Naval Ship Research and Development Center report DTNSRDC/87/032 (1987).

44. Carpetis, C., "An Assessment of the Efficiency and Refrigeration Power of Magnetic Refrigerators with Ferromagnetic Refrigerants", Advances in Cryogenic Engineering, 39 1407-1415 (1994).

45. Barclay, J.A., "A Review of Magnetic Heat Pump Technology", Preprint IECEC 1990.

46. Schuricht, S.R., A.J. DeGregoria, C.B. Zimm, "The effects of a layered bed on active magnetic regenerator performance", Proceedings of the 7th International Cryocooler Conference, 3, 614-620 (1992).

47. Jaefer, S.R., J.A. Barclay, "Analysis of magnetic refrigeration with external regeneration", Advances in Cryogenic Engineering, 29, 751-755 (1988).

48. Barclay, J.A., University of Victoria, personal communication, December 1994.

49. Wood, B.D., *Applications of Thermodynamics*, 2nd ed., Addison-Wesley Publishing Company, Reading, Massachusetts (1982).

50. Weiss, P., A. Piccard, "On a New Magnetocaloric Effect", C.R. Acad. Sci. (Paris), 166, 352 (1918).

51. Giauque, W.F., D.P. MacDougall, "Attainment of Temprature Below 1 Degree Absolute by Demagnetization of $Gd_2(SO_4)_3 \cdot 8H_2O$", Physics Review, 43, 768 (1933).

52. Daunt, J.G., C.V. Heer, Physics Review, 76, 985 (1949).

53. Heer, C.V., C.B. Barnes, J.G. Daunt, "The Design and Operation of a Magnetic Refrigerator for Maintaining Temperatures below 1 K", Review of Scientific Instruments, 25, 1088-1098 (1954).

54. Barclay, J.A., "Magnetic Refrigeration for Efficient Cryogen Liquefaction", Los Alamos National Laboratory Progress Report to Department of Energy, October 1, 1983 to September 30, 1984.

55. Steyert, W.A., "Rotating Carnot-Cycle Magnetic Refrigerators for Use Near 2 K", Journal of Applied Physics, 49, 1227-1231 (1978).

56. Kral, S.F., J.A. Barclay, "Magnetic Refrigeration: A Large Cooling Power Cryogenic Refrigeration Technology", Applications of Cryogenic Technology, 10 (1991).

57. Barclay, J.A., "Wheel-Type Magnetic Refrigerator", United States Patent #4,408,463 (1983).

58. Brown, G.V., "Magnetic heat pumping near room temperature", Journal of Applied Physics, 47, 3673-3680 (1976).

59. James, M.L., G.M. Smith, J.C. Wolford, *Applied Numerical Methods for Digital Computation*, 3rd. ed., Harper & Row, New York (1985).

60. Press, W.H, B.P. Flannery, S.A. Teukolsky, W.T. Vetterling, *Numerical Recipes: The Art of Scientific Computing*, Cambridge University Press, Cambridge (1989).

61. Prata, S., *C++ Primer Plus: Teach yourself object-oriented programming*, Waite Group Press, Corte Madera (1991).

62. Coplien, J.O., *Advanced C++: Programming Styles and Idioms*, Addison-Wesley Publishing Company, Reading (1992).

63. Stroustrup, B., *The C++ Programming Language*, 2nd ed., Addison-Wesley Publishing Company, Reading (1991).

64. Timmerhaus, K.D., T.M. Flynn, *Cryogenic Process Engineering*, K.D. Timmerhaus, A.F. Clark, C. Rizzuto, ed., Plenum Press, New York (1989).

65. Tsotsas, E., H. Martin, "Thermal Conductivity of Packed Beds: A Review", Chemical Engineering Processing, 22 (1987).

66. Vortmeyer, D., W. Adam, "Steady-state measurements and analytical correlations of axial effective thermal conductivities in packed beds at low gas flow rates", International Journal of Heat and Mass Transfer, 27, (1984).

67. Edwards, M.F., J.F. Richardson, "Gas dispersion in packed beds", Chemical Engineering Science, 23 (1968).

68. Duncan, A.B., G.P. Peterson, L.S. Fletcher, "Effective thermal conductivity within packed beds of spherical particles", ASME Publication HTD V104, Pt. 3 (1988).

# Appendix A

## - AMRR Computer Program Sample Input File

The AMRR computer program reads ascii input files to define each AMRR model to be solved. The input file for the fully implicit solver method is defined in six sections:

- Comments
- Operating Parameters
- Results Output
- Layer Definitions
- Fluid Properties
- Magnetic Field, Fluid and Solid Temperatures, and Pressure Profiles

Some lines are optional in the results and profiles sections. In the results section, there are several options for when results are to be printed. These options are: 1) never, 2) begin (beginning of the program, after profiles have been initialized, but before any iteration has started) 3) before (after an iteration has completed but before the temperature profiles have been updated by the iteration solution), 4) after (after the temperature profiles have been updated by an iteration solution), and 5) end (at the end of the program after all iterations have been completed). These options proved helpful in program debugging to ensure that each solution stage was operating as expected.

In the profiles section, a magnetic field profile is mandatory; however, fluid and solid temperature profiles are optional. If initial temperature profiles are not specified, a linear profile between dimensionless limits zero and one is assumed based on the flow directions specified. That is, the "hot end" is the magnetized region, and the zone for which fluid of dimensionless temperature zero is provided to the inlet. If the flow direction for that zone is from inner radius to outer radius, then the temperature profile increases from inner radius to outer radius. Likewise, if the flow direction is from outer radius to inner radius, the profile increases from outer radius to inner radius.

In the profiles section, a fluid pressure profile is also optional. The program is capable of inclusion of pressure dependent correlations and properties, but to date no pressure dependent correlations have been added. Addition of such correlations will require this optional profile to become a mandatory profile.

The input file reflects the interactions and hierarchy within the AMRR program. An understanding of the input file will aid in understanding the structure of the program.

Following is a sample input file, then that same file with the inclusion of comments.

Active Regenerator Model #25
December 31, 1994

[start]

[operating parameters]

[T hot] 275
[T cold] 225
[T environment] 315
[mu0Hmax] 6.5
[zero offset angle] 50.3030303030
[frequency w] 1.570796327
[inner radius] 0.35
[outer radius] 0.5
[z thickness] 0.06
[# layers] 1
[radial row size] 22
[total azimuthal rows] 594
[cold end azimuthal rows] 5
[no-flow #1 azimuthal rows] 4
[hot end azimuthal rows] 5
[no-flow #2 azimuthal rows] 4
[fluid flow conditions]
  [cold end flow] 0.3
  [no-flow #1 flow] 0.3
  [hot end flow] 0.3
  [no-flow #2 flow] 0.3
  [cold end flow direction] out2in
  [no-flow #1 flow direction] noflow
  [hot end flow direction] in2out
  [no-flow #2 flow direction] noflow
[solver iterations] 10
[T update damping iterations] 0
[T update damping factor] 1
[ramp field iterations] 0
[ramp field iteration skip] 1

[end operating parameters]

[results output]

[Tecplot style output] on
[Output description labels] on
[Scientific format output] on
[Extra precise numbers] off

[Magnetic Field Profile] [start list] never [end list]

[Magnetic Field Derivative Profile] [start list] end [end list]
[Fluid Pressure Profile] [start list] never [end list]
[Solid Temperature Profile] [start list] end [end list]
[Solid Temperature Profile Derivative wrt Theta] [start list] never [end list]
[Fluid Temperature Profile] [start list] end [end list]
[Solid Thermal Conductivity Profile] [start list] never [end list]
[Fluid Modified Thermal Conductivity Profile] [start list] never [end list]
[Solid Heat Capacity Profile] [start list] never [end list]
[Solid dM/dT Profile] [start list] never [end list]
[Solid dM/dH Profile] [start list] never [end list]
[Solid Magnetization Profile] [start list] never [end list]
[Solid Electrical Resistivity Profile] [start list] never [end list]
[Fluid Heat Capacity Profile] [start list] never [end list]
[Fluid Thermal Conductivity Profile] [start list] never [end list]
[Fluid Density Profile] [start list] never [end list]
[Fluid Viscosity Profile] [start list] never [end list]
[Fluid Heat Transfer Coefficient] [start list] never [end list]
[Solid Dimensionless Coefficient PI] [start list] never [end list]
[Solid Dimensionless Coefficient ZETA] [start list] never [end list]
[Solid Dimensionless Coefficient RAD_LAMBDA] [start list] never [end list]
[Solid Dimensionless Coefficient AZ_LAMBDA] [start list] never [end list]
[Solid Dimensionless Coefficient OMEGA] [start list] never [end list]
[Fluid Dimensionless Coefficient LAMBDA_F] [start list] never [end list]
[Fluid Dimensionless Coefficient CAP_LAMBDA] [start list] never [end list]
[Fluid Dimensionless Coefficient BETA] [start list] never [end list]
[Power per unit volume] [start list] end [end list]
[Average Refrigeration Temperature] [start list] end [end list]
[Average Rejection Temperature] [start list] end [end list]
[Maximum Solid Temperature Change for Iteration] [start list] before end [end list]
[Maximum Fluid Temperature Change for Iteration] [start list] before end [end list]
[Net Motor Power] [start list] before end [end list]
[Net Averaged Qdot Load] [start list] before end [end list]
[Net Averaged Qdot Rejected] [start list] before end [end list]
[Residual] [start list] never [end list]

[end results output]

[layer definitions]

[layer]
[# nodes] 22
[radial conduction on/off] on
[azimuthal conduction on/off] on
[eddy currents on/off] off
[material density] fromfile Properties/Soliddata Gadolinium_95_325K
[bed porosity]
  (22) [0.35 #]

```
[heat transfer area/unit volume]
  (22) [4333.3333333 #]

[eddy current shape factor]
  (22)  [1.018591636 #]

[eddy current cross sectional area]
  (22) [6.361725124e-7 #]

[eddy current particle contact fudge factor]
  (22) [1.0 #]

[radial thermal conductivity geometry factor]
   (22) [0.65 #]

[azimuthal thermal conductivity geometry factor]
   (22) [0.65 #]

[thermal conductivity temperature variation function]
  fromfile Properties/Soliddata Gadolinium_95_325K linear
[electrial resistivity temperature variation function]
  fromfile Properties/Soliddata Gadolinium_95_325K linear
[heat capacity group]
 fromfile Properties/Gd_multi Gadolinium CHmultitable
[fluid conduction modifiers]
   [cold end flow zone] immediate adjust4Re_particles
    [particle diameters] (22) [0.9e-3 #]
   [no-flow #1 flow zone] immediate adjust4porosity
   [hot end flow zone] immediate adjust4Re_particles
    [particle diameters] (22) [0.9e-3 #]
   [no-flow #2 flow zone] immediate adjust4porosity
[heat transfer correlations]
   [cold end flow zone] immediate Timmerhaus_and_Flynn_particles
    [particle diameters] (22) [0.9e-3 #]
   [no-flow #1 flow zone] immediate No_flow_particles_Nu=2
    [particle diameters] (22) [0.9e-3 #]
   [hot end flow zone] immediate Timmerhaus_and_Flynn_particles
    [particle diameters] (22) [0.9e-3 #]
   [no-flow #2 flow zone] immediate No_flow_particles_Nu=2
    [particle diameters] (22) [0.9e-3 #]

[end layer]
[end layer definitions]

[fluid properties functions]
  fromfile Properties/mixedfluidcombos Helium_50_atm mixed linear_mix_1
[end fluid properties functions]
```

```
[magnetic field profile]
  fromfile Field/SmoothedFields smooth7_flat
[end magnetic field profile]

[initial solid temperature profile]
  fromfile TProfiles/Ts_and_Tf solid
[end initial solid temperature profile]

[initial fluid temperature profile]
  fromfile TProfiles/Ts_and_Tf fluid
[end initial fluid temperature profile]

[end]
```

Active Regenerator Model #25
December 31, 1994

{All lines above the keyword "[start]" are considered comments and are ignored. Following all words or phrases within square brackets are keywords, while what follows the keywords is the data requested. All comments will be enclosed in braces, like this comment.}
[start]

[operating parameters]

{Regenerator inlet fluid temperatures, and environmental temperature for irreversible entropy production calculations.}
[T hot] 275
[T cold] 225
[T environment] 315

{Maximum value of the applied field. The dimensionless field profile is scaled by this factor to give the absolute field magnitude in Tesla.}
[mu0Hmax] 6.5

{All profiles must be coordinated so that they are in phase with each other. If all meshes were the same size, this would not be a problem. With different angular widths of the flow zones possible, and initial profiles of varying angular size, the "zero offset angle" provides a reference of an angular displacement between a standard "zero" position, and the location of the first row of nodes in the hot blow (demagnetized) region.}
[zero offset angle] 50.3030303030

{Rotational frequency of the AMRR solid, in radians/s}
[frequency w] 1.570796327

{Physical dimensions of the AMRR}
[inner radius] 0.35
[outer radius] 0.5
[z thickness] 0.06

{AMRR's can be composed of multiple layers of materials, differing in magnetic materials or geometry between layers. This specifies how many layers will be in this model.}
[# layers] 1

{Mesh discretization dimensions.}
[radial row size] 22
[total azimuthal rows] 594

{Proportions of the azimuthal rows devoted to each of the flow regimes.}
[cold end azimuthal rows] 5
[no-flow #1 azimuthal rows] 4
[hot end azimuthal rows] 5
[no-flow #2 azimuthal rows] 4

{Flow rate of the heat transfer fluid for each of the flow regimes. It is possible to describe a model where the two no-flow regimes are transformed into flow regimes. This can be used to eliminate the no-flow regions, so the model effectively consists of two flow regimes.}
[fluid flow conditions]
  [cold end flow] 0.3
  [no-flow #1 flow] 0
  [hot end flow] 0.3
  [no-flow #2 flow] 0

{For a regenerator, alternating flow is required. The alternating flow has typically been shown as radially inward in the demagnetized region and radially outward in the magnetized region. It is possible to switch the flow directions for the magnetized and demagnetized regions. The no-flow regions can be specified as flow regions by specifying a flow direction (a flow rate must be correspondingly given above).}
  [cold end flow direction] out2in
  [no-flow #1 flow direction] noflow
  [hot end flow direction] in2out
  [no-flow #2 flow direction] noflow

{Maximum number of iterations to perform in the solver routine.}
[solver iterations] 10

{Artificial solution update damping can be imposed, where $T_{new}=(T_{solution}+A*T_{old})/(A+1)$ for the first "T update damping iterations", where $A$="T update damping factor".}
[T update damping iterations] 0
[T update damping factor] 1

{The applied field can be ramped from zero up to its final value in "ramp field iterations" steps, increased by equal increments every "ramp field iteration skip"'th iteration.}
[ramp field iterations] 0
[ramp field iteration skip] 1

[end operating parameters]

{The model is solved to get an understanding of the operation of AMRR's. Several aspects of the model can be of interest. Each item is optional, and if omitted from this list is considered "off" or not given in the results output.}
[results output]

{Labels and formatting of output to facilitate processing in other packages.}
[Tecplot style output] on
[Output description labels] on
[Scientific format output] on
[Extra precise numbers] off

{Current output options.}
[Magnetic Field Profile] [start list] never [end list]
[Magnetic Field Derivative Profile] [start list] end [end list]

[Fluid Pressure Profile] [start list] never [end list]
[Solid Temperature Profile] [start list] end [end list]
[Solid Temperature Profile Derivative wrt Theta] [start list] never [end list]
[Fluid Temperature Profile] [start list] end [end list]
[Solid Thermal Conductivity Profile] [start list] never [end list]
[Fluid Modified Thermal Conductivity Profile] [start list] never [end list]
[Solid Heat Capacity Profile] [start list] never [end list]
[Solid dM/dT Profile] [start list] never [end list]
[Solid dM/dH Profile] [start list] never [end list]
[Solid Magnetization Profile] [start list] never [end list]
[Solid Electrical Resistivity Profile] [start list] never [end list]
[Fluid Heat Capacity Profile] [start list] never [end list]
[Fluid Thermal Conductivity Profile] [start list] never [end list]
[Fluid Density Profile] [start list] never [end list]
[Fluid Viscosity Profile] [start list] never [end list]
[Fluid Heat Transfer Coefficient] [start list] never [end list]
[Solid Dimensionless Coefficient PI] [start list] never [end list]
[Solid Dimensionless Coefficient ZETA] [start list] never [end list]
[Solid Dimensionless Coefficient RAD_LAMBDA] [start list] never [end list]
[Solid Dimensionless Coefficient AZ_LAMBDA] [start list] never [end list]
[Solid Dimensionless Coefficient OMEGA] [start list] never [end list]
[Fluid Dimensionless Coefficient LAMBDA_F] [start list] never [end list]
[Fluid Dimensionless Coefficient CAP_LAMBDA] [start list] never [end list]
[Fluid Dimensionless Coefficient BETA] [start list] never [end list]
[Power per unit volume] [start list] end [end list]
[Average Refrigeration Temperature] [start list] end [end list]
[Average Rejection Temperature] [start list] end [end list]
[Maximum Solid Temperature Change for Iteration] [start list] before end [end list]
[Maximum Fluid Temperature Change for Iteration] [start list] before end [end list]
[Net Motor Power] [start list] before end [end list]
[Net Averaged Qdot Load] [start list] before end [end list]
[Net Averaged Qdot Rejected] [start list] before end [end list]

{LU-decomposed matrix solution residual}
[Residual] [start list] never [end list]

[end results output]

{As many layers as specified in "operating parameters" are specified here. The first layer is considered to be at the inner radius, and each layer is added concentrically outward.}
[layer definitions]

[layer]

{Number of nodes for the layer, out of the total radial nodes specified.}
[# nodes] 22

{Optional effects can be turned on and off to determine their influence on the model solution. In effect, turning these off reduces the solid energy balance equation to include only the heat transfer with the fluid and the magnetocaloric effect.}
[radial conduction on/off] on
[azimuthal conduction on/off] on
[eddy currents on/off] off

{$\rho_s$ - The notation "(22) [0.35 #]" signifies two things: 1) 22 values are specified, which serves mainly as an error detection device, and 2) the first element has a value of 0.35 and subsequent elements have the same value. This compact notation simplifies the model when some properties are constant across the layer. The properties need not be constant, though, and all 22 values could be specified uniquely by replacing the "#" symbol with the missing values.}
[material density] fromfile Properties/Soliddata Gadolinium_95_325K
[bed porosity]
(22) [0.35 #]

{$A'''$}
[heat transfer area/unit volume]
(22) [4333.3333333 #]

{$\Gamma$}
[eddy current shape factor]
(22) [1.018591636 #]

{$A_x$}
[eddy current cross sectional area]
(22) [6.361725124e-7 #]

{Scale factor to include the influence of oxide coatings on regenerator material but considering projected area to be larger than the particles themselves.}
[eddy current particle contact fudge factor]
(22) [1.0 #]

{The radial conductivity of the solid is adjusted by this amount to account for geometrical effects including porosity, or material anisotropy.}
[radial thermal conductivity geometry factor]
(22) [0.65 #]

[azimuthal thermal conductivity geometry factor]
(22) [0.65 #]

{Thermal conductivity of the solid is a function of temperature. This specifies the material data to use and the type of approximation to use from the library of approximation methods. Two input modes exist, "immediate" and "fromfile". This allows data to be specified in the file (immediate mode) or to be stored in a separate file (fromfile mode). Fromfile mode ensures that similar models use the same data, and the input files are more compact.}
[thermal conductivity temperature variation function]
fromfile Properties/Soliddata Gadolinium_95_325K linear

{Electrical resistivity of the solid is a function of temperature. This specifies the material data to use and the type of approximation to use from the library of approximation methods.}
[electrial resistivity temperature variation function]
  fromfile Properties/Soliddata Gadolinium_95_325K linear

{Heat capacity of the solid is a function of temperature and applied field. This specifies the material data to use and the type of approximation to use from the library of approximation methods.}
[heat capacity group]
 fromfile Properties/Gd_multi Gadolinium CHmultitable

{The effective thermal conductivity can be enhanced by material geometry and eddy diffusivity. This specifies which correlations should be used to adjust the fluid conductivity to give the effective fluid conductivity. In the absence of fluid flow, the fluid conductivity must be adjusted to account for the porosity of the layer. Any information required by the modifier is included after its specification.}
[fluid conduction modifiers]
  [cold end flow zone] immediate adjust4Re_particles
   [particle diameters] (22) [0.9e-3 #]
  [no-flow #1 flow zone] immediate adjust4porosity
  [hot end flow zone] immediate adjust4Re_particles
   [particle diameters] (22) [0.9e-3 #]
  [no-flow #2 flow zone] immediate adjust4porosity

{The correct heat transfer correlation depends on material geometry and flow conditions. This section sets the correct correlation to use from the library of possible correlations. A layer composed of wire screens will use different correlations from a layer composed of packed particles. Any information required by the correlation beyond porosity and heat transfer area per unit volume, and fluid flow conditions, are included after the correlation specification.}
[heat transfer correlations]
  [cold end flow zone] immediate Timmerhaus_and_Flynn_particles
   [particle diameters] (22) [0.9e-3 #]
  [no-flow #1 flow zone] immediate No_flow_particles_Nu=2
   [particle diameters] (22) [0.9e-3 #]
  [hot end flow zone] immediate Timmerhaus_and_Flynn_particles
   [particle diameters] (22) [0.9e-3 #]
  [no-flow #2 flow zone] immediate No_flow_particles_Nu=2
   [particle diameters] (22) [0.9e-3 #]

[end layer]

{More layers could be specified following for other models.}
[end layer definitions]

{Fluid properties are evaluated over the entire AMRR. These properties can be pressure and temperature dependent, and are specified from the library of available evaluation functions. The properties required are: heat capacity, density, viscosity, and "natural" thermal conductivity.

Typically, corresponding evaluation functions would be used, such as all linear, or all constant, and each for the exact same fluid, however, this is not enforced.}
[fluid properties functions]
  fromfile Properties/mixedfluidcombos Helium_50_atm mixed linear_mix_1
[end fluid properties functions]

{The magnetic field profile is standardized and pre-calculated. It is interpolated to fit the current mesh conditions. The field profile can vary in the radial direction, as well as the azimuthal direction. The profile itself specifies its relative angular orientation with respect to the "zero" position. The position of minimum field is considered the "zero" and all other angular measurements are considered relative to this position.
[magnetic field profile]
  fromfile Field/SmoothedFields smooth7_flat
[end magnetic field profile]

{Optional fluid pressure profile omitted, since there is no pressure dependence considered in this model.}

{Optional initial profiles.}
[initial solid temperature profile]
  fromfile TProfiles/Ts_and_Tf solid
[end initial solid temperature profile]

[initial fluid temperature profile]
  fromfile TProfiles/Ts_and_Tf fluid
[end initial fluid temperature profile]

{All lines after the keyword "[end]" are considered comments and are ignored.}
[end]

# Appendix B

## - Regenerator Model Input Files

**Passive Regenerator Model**

Passive Regenerator Case #10.

[start]

[operating parameters]

[T hot] 280
[T cold] 230
[T environment] 315
[mu0Hmax] 10.0
[zero offset angle] 87.75
[frequency w] 0.157079633
[inner radius] 1.95
[outer radius] 2.05
[z thickness] 0.05
[# layers] 1
[radial row size] 20
[total azimuthal rows] 720
[cold end azimuthal rows] 35
[no-flow #1 azimuthal rows] 1
[hot end azimuthal rows] 35
[no-flow #2 azimuthal rows] 1
[fluid flow conditions]
  [cold end flow] 0.1
  [no-flow #1 flow] 0
  [hot end flow] 0.1
  [no-flow #2 flow] 0
  [cold end flow direction] out2in
  [no-flow #1 flow direction] noflow
  [hot end flow direction] in2out
  [no-flow #2 flow direction] noflow
[solver iterations] 1
[T update damping iterations] 0
[T update damping factor] 1
[ramp field iterations] 0
[ramp field iteration skip] 1

[end operating parameters]

[results output]

[Tecplot style output] on
[Output description labels] on
[Scientific format output] on
[Extra precise numbers] off

[Solid Temperature Profile] [start list] end [end list]
[Fluid Temperature Profile] [start list] end [end list]
[Solid Dimensionless Coefficient PI] [start list] end [end list]
[Fluid Dimensionless Coefficient CAP_LAMBDA] [start list] end [end list]
[Fluid Dimensionless Coefficient BETA] [start list] end [end list]
[Average Refrigeration Temperature] [start list] end [end list]
[Average Rejection Temperature] [start list] end [end list]
[Maximum Solid Temperature Change for Iteration] [start list] before end [end list]
[Maximum Fluid Temperature Change for Iteration] [start list] before end [end list]
[Net Averaged Qdot Load] [start list] before end [end list]
[Net Averaged Qdot Rejected] [start list] before end [end list]

[end results output]

[layer definitions]

[layer]
[# nodes] 20
[radial conduction on/off] off
[azimuthal conduction on/off] off
[eddy currents on/off] off
[material density]
 fromfile Properties/Soliddata Gadolinium_95_325K
[bed porosity]
  (20) [0.4 #]

[heat transfer area/unit volume]
  (20) [2400 #]

[eddy current shape factor]
  (20)  [1.018591636 #]

[eddy current cross sectional area]
  (20) [1.767145E-6 #]

[eddy current particle contact fudge factor]
  (20) [1.0 #]

[radial thermal conductivity geometry factor]
   (20) [0.6 #]

[azimuthal thermal conductivity geometry factor]
   (20) [0.6 #]

[thermal conductivity temperature variation function]
  fromfile Properties/Soliddata Gadolinium_95_325K linear
[electrial resistivity temperature variation function]

```
  fromfile Properties/Soliddata Gadolinium_95_325K linear
[heat capacity group]
 fromfile Properties/Gd_const Gadolinium_constprops CHtable
[fluid conduction modifiers]
   [cold end flow zone] immediate adjust4porosity
   [no-flow #1 flow zone] immediate adjust4porosity
   [hot end flow zone] immediate adjust4porosity
   [no-flow #2 flow zone] immediate adjust4porosity
[heat transfer correlations]
   [cold end flow zone] immediate Timmerhaus_and_Flynn_particles
    [particle diameters] (20) [1.5e-3 #]
   [no-flow #1 flow zone] immediate No_flow_particles_Nu=2
    [particle diameters] (20) [1.5e-3 #]
   [hot end flow zone] immediate Timmerhaus_and_Flynn_particles
    [particle diameters] (20) [1.5e-3 #]
   [no-flow #2 flow zone] immediate No_flow_particles_Nu=2
    [particle diameters] (20) [1.5e-3 #]

[end layer]
[end layer definitions]

[fluid properties functions]
  fromfile Properties/mixedfluidcombos Helium_constprops mixed linear_mix_1
[end fluid properties functions]

[magnetic field profile]
  fromfile Field/Smooth2 zero_field
[end magnetic field profile]

[initial solid temperature profile]
  fromfile TProfiles/Ts_and_Tf solid
[end initial solid temperature profile]

[initial fluid temperature profile]
  fromfile TProfiles/Ts_and_Tf fluid
[end initial fluid temperature profile]

[end]
```

**Active Regenerator Model**

Active Regenerator Case #16.
[start]

[operating parameters]

[T hot] 275
[T cold] 225
[T environment] 315
[mu0Hmax] 6.5
[zero offset angle] 50.2
[frequency w] 25.13274123
[inner radius] 0.2725
[outer radius] 0.3275
[z thickness] 0.05
[# layers] 1
[radial row size] 36
[total azimuthal rows] 900
[cold end azimuthal rows] 5
[no-flow #1 azimuthal rows] 4
[hot end azimuthal rows] 5
[no-flow #2 azimuthal rows] 4
[fluid flow conditions]
  [cold end flow] 0.1
  [no-flow #1 flow] 0
  [hot end flow] 0.1
  [no-flow #2 flow] 0
  [cold end flow direction] out2in
  [no-flow #1 flow direction] noflow
  [hot end flow direction] in2out
  [no-flow #2 flow direction] noflow
[solver iterations] 0
[T update damping iterations] 0
[T update damping factor] 1
[ramp field iterations] 0
[ramp field iteration skip] 1

[end operating parameters]

[results output]

[Tecplot style output] on
[Output description labels] on
[Scientific format output] on
[Extra precise numbers] off

[Solid Temperature Profile] [start list] end [end list]

[Fluid Temperature Profile] [start list] end [end list]
[Solid Dimensionless Coefficient PI] [start list] end [end list]
[Fluid Dimensionless Coefficient CAP_LAMBDA] [start list] end [end list]
[Fluid Dimensionless Coefficient BETA] [start list] end [end list]
[Power per unit volume] [start list] end [end list]
[Average Refrigeration Temperature] [start list] end [end list]
[Average Rejection Temperature] [start list] end [end list]
[Maximum Solid Temperature Change for Iteration] [start list] before [end list]
[Maximum Fluid Temperature Change for Iteration] [start list] before [end list]
[Net Motor Power] [start list] end [end list]
[Net Averaged Qdot Load] [start list] end [end list]
[Net Averaged Qdot Rejected] [start list] end [end list]

[end results output]

[layer definitions]

[layer]
[# nodes] 36
[radial conduction on/off] on
[azimuthal conduction on/off] on
[eddy currents on/off] off
[material density]
 fromfile Properties/Soliddata Gadolinium_95_325K
[bed porosity]
  (36) [0.4 #]

[heat transfer area/unit volume]
  (36) [36000 #]

[eddy current shape factor]
  (36)  [1.018591636 #]

[eddy current cross sectional area]
  (36) [7.85398164E-9 #]

[eddy current particle contact fudge factor]
  (36) [1.0 #]

[radial thermal conductivity geometry factor]
   (36) [0.6 #]

[azimuthal thermal conductivity geometry factor]
   (36) [0.6 #]

[thermal conductivity temperature variation function]
  fromfile Properties/Soliddata Gadolinium_95_325K linear

```
[electrial resistivity temperature variation function]
  fromfile Properties/Soliddata Gadolinium_95_325K linear
[heat capacity group]
 fromfile Properties/Gd_multi Gadolinium CHmultitable
[fluid conduction modifiers]
   [cold end flow zone] immediate adjust4Re_particles
    [particle diameters] (36) [100e-6 #]
   [no-flow #1 flow zone] immediate adjust4porosity
   [hot end flow zone] immediate adjust4Re_particles
    [particle diameters] (36) [100e-6 #]
   [no-flow #2 flow zone] immediate adjust4porosity
[heat transfer correlations]
   [cold end flow zone] immediate Timmerhaus_and_Flynn_particles
    [particle diameters] (36) [100e-6 #]
   [no-flow #1 flow zone] immediate No_flow_particles_Nu=2
    [particle diameters] (36) [100e-6 #]
   [hot end flow zone] immediate Timmerhaus_and_Flynn_particles
    [particle diameters] (36) [100e-6 #]
   [no-flow #2 flow zone] immediate No_flow_particles_Nu=2
    [particle diameters] (36) [100e-6 #]

[end layer]
[end layer definitions]

[fluid properties functions]
  fromfile Properties/mixedfluidcombos Helium_50_atm mixed linear_mix_1
[end fluid properties functions]

[magnetic field profile]
  fromfile Field/Smooth2 smooth7_flat
[end magnetic field profile]

[initial solid temperature profile]
  fromfile TProfiles/Working solid15
[end initial solid temperature profile]

[initial fluid temperature profile]
  fromfile TProfiles/Working fluid15
[end initial fluid temperature profile]

[end]
```

# Appendix C
## - Magnetic Field Profile

| Dimensionless Field Magnitude, $H^*$ vs. Angle in Degrees | | | | | |
|---|---|---|---|---|---|
| Angle | $H^*$ | Angle | $H^*$ | Angle | $H^*$ |
| 0 | 4.6466E-3 | 63 | 3.1998E-2 | 123 | 9.9035E-1 |
| 3 | 4.7369E-3 | 66 | 3.6751E-2 | 126 | 9.9561E-1 |
| 6 | 4.8577E-3 | 69 | 4.2896E-2 | 129 | 9.9797E-1 |
| 9 | 5.0175E-3 | 72 | 5.1158E-2 | 132 | 9.9905E-1 |
| 12 | 5.2195E-3 | 75 | 6.2434E-2 | 135 | 9.9957E-1 |
| 15 | 5.4667E-3 | 78 | 7.7788E-2 | 138 | 9.9982E-1 |
| 18 | 5.7703E-3 | 81 | 9.8539E-2 | 141 | 9.9993E-1 |
| 21 | 6.1555E-3 | 84 | 1.2638E-1 | 144 | 9.9997E-1 |
| 24 | 6.6578E-3 | 87 | 1.6346E-1 | 147 | 9.9999E-1 |
| 27 | 7.3093E-3 | 90 | 2.1232E-1 | 150 | 1.0000E+0 |
| 30 | 8.1293E-3 | 93 | 2.7574E-1 | 153 | 1.0000E+0 |
| 33 | 9.1262E-3 | 96 | 3.5601E-1 | 156 | 1.0000E+0 |
| 36 | 1.0305E-2 | 99 | 4.5323E-1 | 159 | 1.0000E+0 |
| 39 | 1.1676E-2 | 102 | 5.6310E-1 | 162 | 1.0000E+0 |
| 42 | 1.3253E-2 | 105 | 6.7584E-1 | 165 | 1.0000E+0 |
| 45 | 1.5054E-2 | 108 | 7.7870E-1 | 168 | 1.0000E+0 |
| 48 | 1.7093E-2 | 111 | 8.6141E-1 | 171 | 1.0000E+0 |
| 51 | 1.9385E-2 | 114 | 9.2027E-1 | 174 | 1.0000E+0 |
| 54 | 2.1949E-2 | 117 | 9.5774E-1 | 177 | 1.0000E+0 |
| 57 | 2.4833E-2 | 120 | 9.7922E-1 | 180 | 1.0000E+0 |
| 60 | 2.8127E-2 | | | | |

**Table C1** Dimensionless Field Magnitude, $H^*$ vs. Angular Position in Degrees.

# Appendix D
## - Material Properties

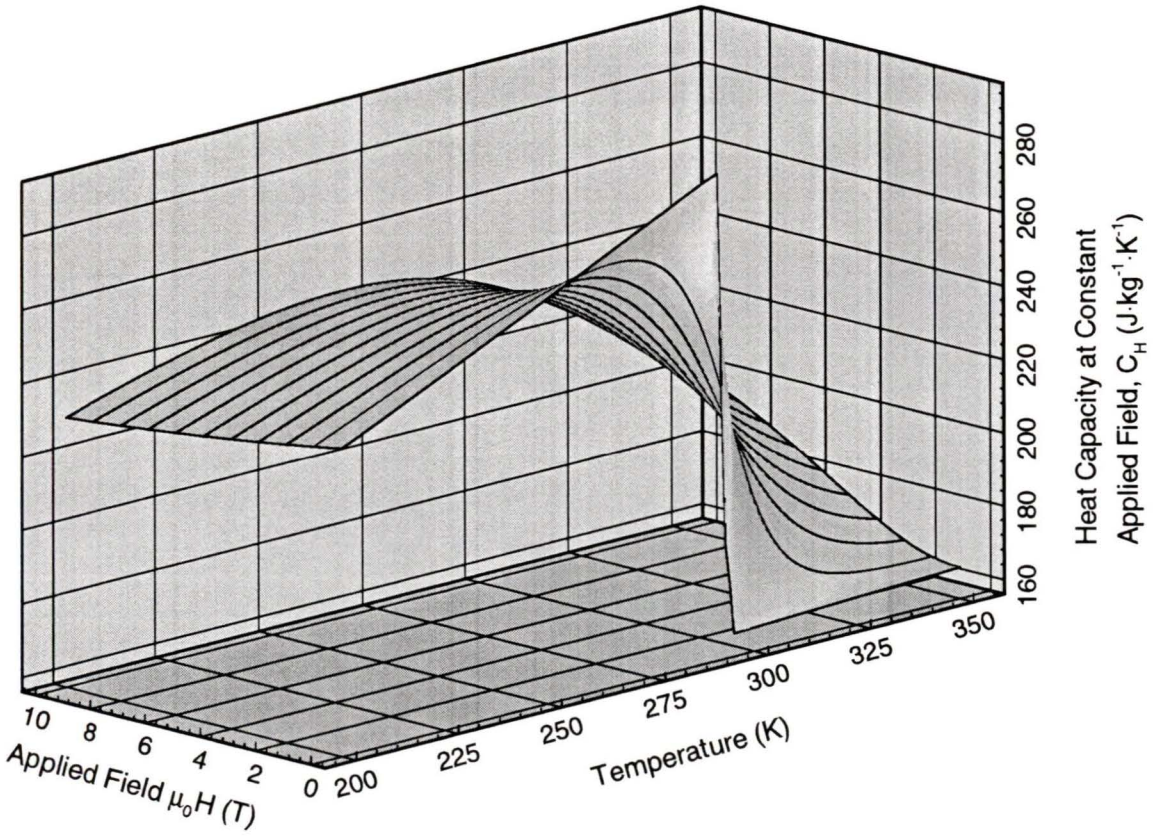


**Figure D1** Heat capacity of gadolinium at constant applied field as a function of field and temperature (calculated using a molecular field model).

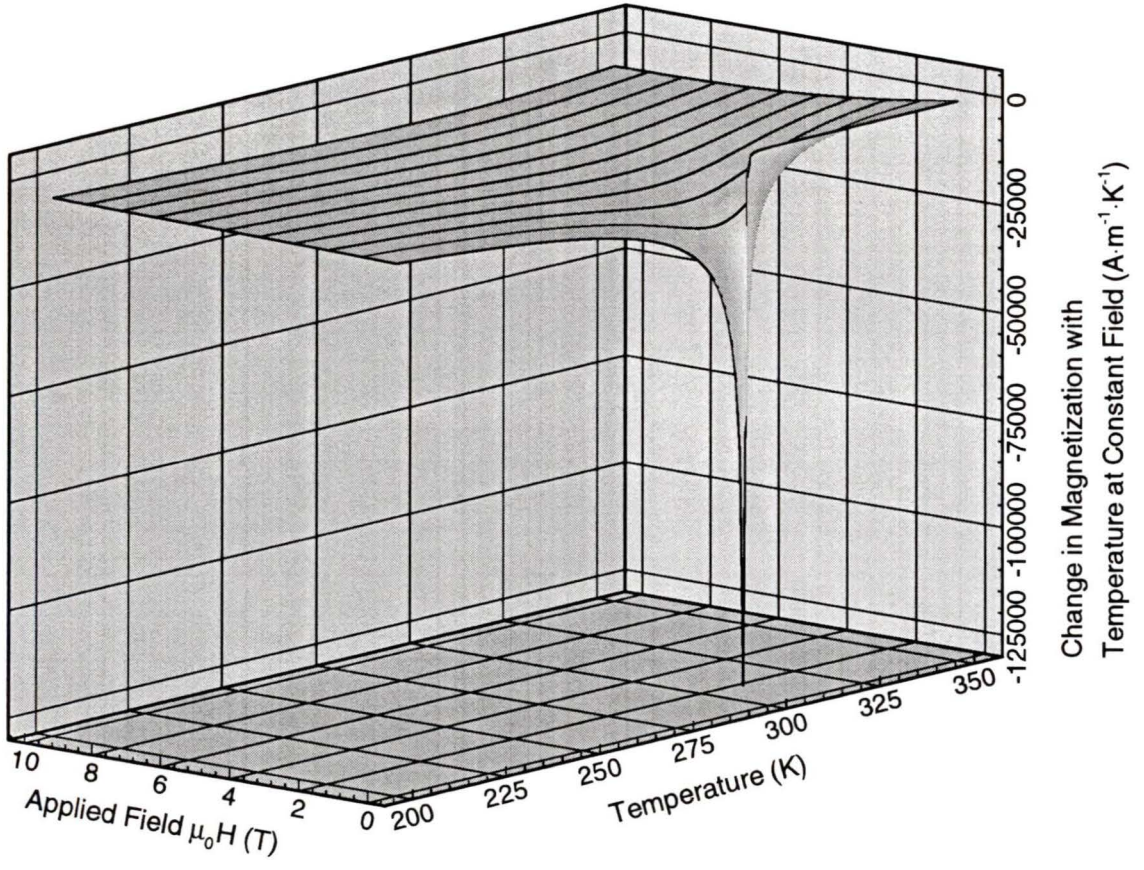


**Figure D2** Change in magnetization with temperature at constant applied field for gadolinium (calculated using a molecular field model).

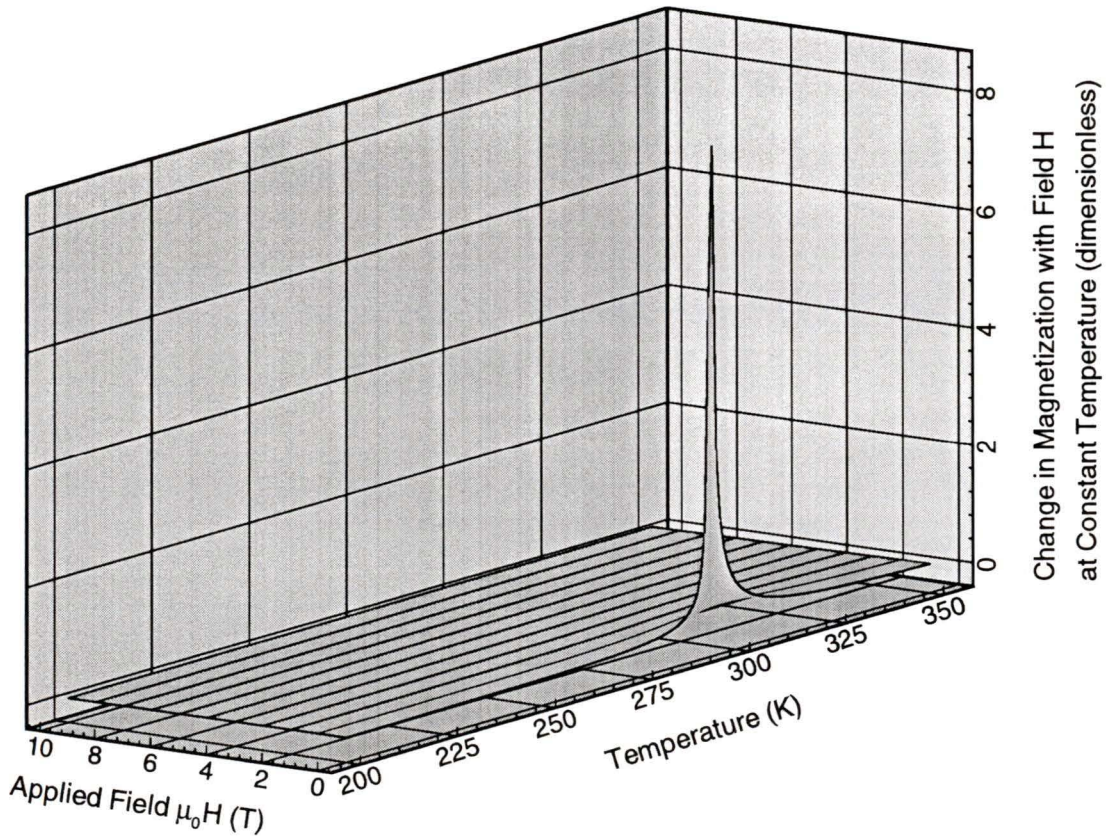


**Figure D3** Change in magnetization with applied field at constant temperature for gadolinium (as calculated using a molecular field model).

| Properties for Gadolinium at 95 and 325 K | | | |
|---|---|---|---|
| Property | 95 K | 325 K | Units |
| Density density, $\rho_s$ | 7910.0 | 7910.0 | $kg \cdot m^{-3}$ |
| Electrical resistivity, $\rho_e$ | 0.443e-6 | 1.493e-6 | $\Omega \cdot m$ |
| Thermal conductivity, $k_s$ | 14.400 | 8.8000 | $W \cdot m^{-1} \cdot K^{-1}$ |

**Table D1** Transport properties of Gadolinium at 95 and 325 K.

| Properties for 50 atm. Helium at 95 and 325 K | | | |
|---|---|---|---|
| Property | 95 K | 325 K | Units |
| Heat capacity at constant pressure, $C_P$ | 5264.0 | 5189.0 | $J \cdot kg^{-1} \cdot K^{-1}$ |
| Thermal conductivity, $k_f$ | 0.074 | 0.160 | $W \cdot m^{-1} \cdot K^{-1}$ |
| Density, $\rho_f$ | 23.830 | 7.349 | $kg \cdot m^{-3}$ |
| Viscosity, $\mu$ | 9.60e-6 | 20.80e-6 | $kg \cdot m^{-1} \cdot s^{-1}$ |

**Table D2** Transport properties of 50 atm. Helium at 95 and 325 K.

# VITA

Surname: Spearing Given Names: Ian Gregory

Place of Birth: Toronto, Ontario, Canada

Educational Institutions Attended:

| | |
|---|---|
| University of Victoria | 1992 to 1994 |
| University of Toronto | 1989 to 1990 |
| University of Toronto | 1984 to 1987 |

Degrees Awarded:

| | | |
|---|---|---|
| B.A.Sc. | University of Toronto | 1990 |

Honours and Awards:

| | |
|---|---|
| J. Edgar McAllister Foundation Award | 1984 |

## PARTIAL COPYRIGHT LICENSE

I hereby grant the right to lend my thesis to users of the University of Victoria Library, and to make single copies only for such users or in response to a request from the Library of any other university, or similar institution, on its behalf or for one of its users. I further agree that permission for extensive copying of this thesis for scholarly purposes may be granted by me or a member of the University designated by me. It is understood that copying or publication of this thesis for financial gain shall not be allowed without my express written permission.

Title of Thesis:

A Numerical Model for a Rotary Active Magnetic Regenerative Refrigerator

Author: [redacted]

Ian Gregory Spearing
December 31, 1994